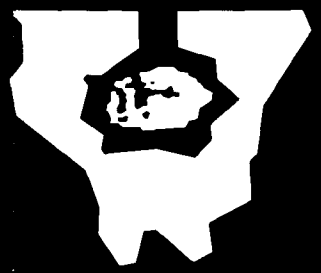

Coal Extraction and Utilization Research Center

Southern Illinois University at Carbondale

SIU

Reactivity of Whole Coals, Selected Pure Maceral Fractions, and Cleaned Coal Products

J. C. Crelling
E. J. Hippo

FINAL REPORT
January 1 - December 31, 1988

Southern Illinois University at Carbondale
Carbondale, Illinois 62901

Submitted to:
U.S. Department of Energy

Contract No. DE-FC22-88PC88861

Reactivity of Whole Coals, Selected Pure Maceral Fractions, and Cleaned Coal Products

by

DOE/PC/88861--T15

DE89 010730

John C. Crelling
Department of Geology

Edwin J. Hippo
Department of Mechanical Engineering and Energy Processes

Southern Illinois University at Carbondale
Carbondale, Illinois 62901

Final Report
January 1 - December 31, 1988

Submitted to
U.S. Department of Energy
Contract Number DE-FC22-88PC88861

March 1989

DISCLAIMER

ABSTRACT

A long-term program is currently underway at SIUC to determine the process response properties of pure single coal maceral fractions in order to predict the behavior of various whole coals of different maceral compositions and rank. The primary objectives of the study are to: (1) evaluate the reactivity of whole coals and macerals from other seams, covering the same broad rank range studied in the first phase of the program; (2) assess the degree of applicability of predictive equations for coals in general; and (3) evaluate the combustion characteristics of cleaned coals. The program has been conducted for 2 years and is being continued for one additional year. During the first year of the program eight Hartshorne coals and macerals were investigated. The results indicated that: combustion profile parameters varied with rank; rank trends were best observed with pure macerals; data was more reproducible when pure macerals were used; rank relationships were more linear with pure macerals; range of variation was smaller for the pure macerals; variations due to maceral properties are as great as rank variations; and macerals interact during combustion tests. This year, Argonne Premium samples were examined, as well as a number of coals obtained from various points throughout the U.S. and the world (SIU coals). The coals were examined to determine if the relationships developed last year could be extrapolated to a wider rank range and maceral composition than the Hartshorne coals used in the last year's study. Efforts continued on modeling of the data obtained last year. Three cleaned and feed samples were obtained from OTISCA, Inc. Besides the OTISCA coals, three feed and cleaned coals were obtained from the U.S. Department of Energy Pittsburgh Energy Technology Center and prepared. These coals will also be tested in the coming year's test matrix. A series of supercritical extraction (SCE) products, as well as the feeds, have also been tested. These samples were used to examine the effect of thermal desulfurization processing on combustion properties. A set of 50 samples has been obtained from The Pennsylvania State University. Twenty-five of these samples are of a rank series from the Lower Kittaning seam and will be used to further test and develop previously defined relationships. A second series is a set of high-sulfur coals. This year's results confirm what was found last year. In addition, the following was found: the OTISCA T-process may be a suitable candidate for preparing samples for liquefaction feedstocks; macerals can be remixed to give matrix interactions; combustion profile parameters are rank related; not all coals follow the same rank relationships; vitrinite and liptinite behaviors are more predictable than inertinite behavior; techniques to identify macerals in small particle assemblages need to be developed; physical cleaning has positive or little effect on combustion profile behavior; SCE has some negative impacts on combustion profiles, but these negative effects are partially negated by potassium addition and physical precleaning; if SCE is used to prepare combustion feedstocks, deep physical cleaning is recommend to enhance desulfurization and combustion properties; the combustion profiles can be modeled as apparent first ordered reactions; activation energy is independent of rank, but not maceral composition or rank type (the rank band the coal belongs to); combustion curves can be normalized; burnoff curves can be fitted to a polynomial-log equation; and best predictions are obtained when curves are fitted to the the individual macerals obtained from the whole coal being modeled.

INTRODUCTION

The overall objective of this project is to determine the chemical reactivity properties of pure single coal maceral fractions in order to predict the behavior of various whole coals of different maceral compositions and rank.

This is a long-range program ending its second year. A third year's effort is currently underway. The primary objectives of the study were to: (1) evaluate the reactivity of whole coals and macerals from other seams, covering the same broad rank range studied in the first phase of the program; (2) assess the degree of applicability of predictive equations for coals in general; and (3) evaluate the combustion characteristics of cleaned coals.

The primary purpose of coal characterization is to characterize a given coal sample well enough to predict its behavior in any process of interest, such as pyrolysis, gasification, liquefaction, or coking. Currently, chemical analysis and optical microscopy are used in defining predictive properties such as coal rank and type. However, the present predictive capability is somewhat imperfect, due in part to the fact that most work has been carried out on heterogeneous samples.

In general, the heterogeneity of coal is recognized as the bane of all coal scientists and the reason for their existence. Neavel (1981) likens the heterogeneity of coal to a fruitcake. Like different fruitcakes, no two coal samples are exactly alike.

The heterogeneity of coal causes analytical difficulties. First, the heterogeneity makes it difficult to obtain representative samples. Second, chemical and physical properties of the various sub-components vary widely. It is therefore difficult to standardize and calibrate a particular test in order to accurately measure the properties of all the sub-components within the sample. Third, some components interfere with the measurements of others. For example, moisture will

interfere with IR measurements for OH groups. Variation in components can cause variation in reactivity, multiplexity of reactions, multiple reaction pathways, and complexity of resultant products.

Accounting for coal's heterogeneity has proven to be an intractable problem in the past. Several attempts have been made to laboriously hand-pick sub-components with the aid of a microscope. Vitrinite concentrates have been obtained by selective sampling (Fenton and Smith 1959). These methods have failed to produce sufficient quantities of pure maceral samples to adequately characterize and develop predictive behavior. The recent use of micronization and the medical technique of density gradient centrifugation (DGC) described by Dyrkacz and Horwitz (1982), Dyrkacz et al. (1984a,b,c,d and 1987), Karas et al. (1985), Chai et al. (1987), Crelling et al. (1987), Hippo et al. (1987), Stock (1987), and Tseng et al. (1987) have resulted in the successful separation of coal into its constituent maceral groups: liptinite, vitrinite, and inertinite. The outstanding efficiency of the DGC technique for separating coal macerals has been well demonstrated by these researchers. In addition, the annual Coal Technology Laboratory (CTL) reports for the last five years of the coal maceral separation work by Dr. John C. Crelling, Department of Geology, have shown that individual macerals are cleanly separated at different densities (Miller and Crelling 1984, Crelling and Miller 1985, Crelling 1986, Jobling and Crelling 1987). These results have been verified by both petrographic and fluorescence spectral analyses, as well as SEM analysis. These results have been presented at various national professional meetings and have been published (Crelling et al. 1987).

METHODS

Samples

In this study, Argonne Premium samples were examined, as well as a number of coals obtained from various points throughout the U.S. and the world (SIU coals). These coals were selected on the basis of rank and maceral content. The coals were examined to determine if the relationships developed last year could be extrapolated to a wider rank range and maceral composition than the Hartshorne coals used in the previous year's study. In addition to testing these coals, efforts continued on modeling of the data obtained last year. Three cleaned and feed samples were obtained from OTISCA, Inc. Combustion profiles were run on these samples. In addition, DGC density profiles of the feed and products were obtained. The fractions from the DGC tests have been selected for testing in next year's program. Using these and several other fractionated samples, we hope to obtain variation in the combustion profile parameters as a function of separation density, and at the same time establish a washability curve for fine particles.

Besides the OTISCA coals, three feed and cleaned coals were obtained from the U.S. Department of Energy Pittsburgh Energy Technology Center and prepared. These coals will also be tested in the coming year's test matrix. A series of SCE products, as well as the feeds, have also been tested. These samples were used to examine the effect of thermal desulfurization processing on combustion properties. A set of 50 samples has been obtained from The Pennsylvania State University. Twenty-five of these samples are of a rank series from the Lower Kittaning seam and will be used to further test and develop previously defined relationships. A second set of high-sulfur coals in the The Pennsylvania State University sample bank has been extensively studied by Neil et al. (1987). Using DGC, these samples will be separated into various fractions and combusted. The variation between combustion

profiles of whole coal and the separated fractions should yield information on the effects of advanced physical beneficiation on coal combustion properties.

Separation

The approach being used to separate the macerals is the density gradient centrifugation (DGC) technique in which the samples are broken up in a planetary ball mill to about –200 mesh (40 μm) and then fed to a fluid energy mill (FEM). This is powered by dry nitrogen gas and reduces the particles to the micron range. Demineralization of the ground samples is accomplished by standard acid leaching techniques using HCl and HF. The sample is suspended in water by means of an ultrasonicator and is then layered on the top of a density gradient which is formed by using a commercial gradient maker. The gradient is then centrifuged in a Beckman, J2-21M centrifuge using a JCF-Z zonal rotor. Running time is approximately 1.5 hr, at 10,000 rpm (16,000 x G). The gradient is then pumped into a fraction collector using a dense chase solution (Fluorinert FC-43). The aqueous cesium chloride density of each fraction is determined with a refractometer and/or a density meter. In addition, the weight of each fraction is measured after it is dried and collected.

Following separation, the maceral fraction is washed in hot water and HCl in a procedure which has been developed to remove CsCl to a level of less than 0.1%. We have found that this level of cesium has no detectable effect on oxidation reactivity.

Reactivity Testing

The principal apparatus that was used in charring combustion and gasification tests was a standard TGA, in which the raw, demineralized micronized samples were heated under nitrogen at a constant heating rate of 50° C/min to a maximum

temperature of 1000° C and held at that temperature for 1 hr (Jenkins et al. 1973, Hippo and Walker 1975, Ashu et al. 1978, Hippo et al. 1979, Jones et al. 1985).

Two types of combustion tests were conducted. In the first, the sample was heated in air at a constant rate. The weight loss of the sample was followed as a function of temperature and time. The objective was to determine the amount of moisture in the sample, the initial temperature of oxygen chemisorption, the ignition temperature, the temperature of peak reactivities (consisting of two peaks for low-rank coals and one for high-rank coals), and the temperature of carbon burnout (Smith et al. 1981, Cumming 1984, Saayman 1985, Tsai and Scaroni 1984, Wagoner and Duyz 1967, Wagoner and Winegarther 1973).

The other combustion test was conducted on char samples pyrolyzed at 700° C in nitrogen. They were reacted in 5% oxygen at 500° C, as described by Jenkins et al. (1973), Linares-Solano et al. (1979), Mahajan and Walker (1978a,b), and Majahan et al. (1978). The reactivity was calculated based on the maximum rate of reaction of the rectilinear portion of the burnoff curve.

The gasification tests were run on the samples produced in the charring tests. The reactions were measured at 900° C in carbon dioxide gas, as described by Hippo et al. (1979) and Radovic et al. (1983a,b,c) and were measured by the rectilinear portion of the burnoff curve.

A literature survey of combustion profiles is attached as Appendix A.

RESULTS AND DISCUSSION

Basic Characterization

The results of the chemical analyses of the samples being studied are given in Table 1. These results are unusual in that the relationship between carbon content and volatile matter is not systematic, as is expected of coals in this rank range. This is shown in Figure B.1 (See Appendix B). For the Hartshorne samples studied last

Table 1

Results of Ultimate and Proximate Analysis on Coals Studied

SIU Sample Number	Carbon DMMF	Hydrogen DMMF	Nitrogen DMMF	Sulfur DMMF	Oxygen by Diff DMMF	Moisture as Rec	Ash Dry	Volatile Matter DMMF	Fixed Carbon DMMF	% Vit Reflect
647	78.01	5.62	1.64	0.78	13.95	4.08	11.59	40.30	59.70	0.57
1307						1.40	12.40	40.30	59.70	0.80
1468						2.92	2.91	37.90	62.10	0.80
1469							25.10	48.90	51.10	
1681										
1794										0.97
1795							16.00	52.05	47.95	
561										
OTISCA Coals										
Product 1						1.56	2.83	26.67	73.33	
Product 2						1.99	1.98	24.75	75.25	
Product 3						1.14	1.23	25.03	74.97	
Feed 1						1.33	23.70	23.23	76.77	
Feed 2						4.75	2.05	24.19	75.81	
Feed 3						4.16	6.68	25.11	74.89	
Hartshorne Coals										
1310	80.16	5.07	2.15		12.62	2.65	5.88	39.09	60.91	0.80
1311	88.69	4.91	1.78		4.62	0.83	7.06	26.57	73.43	1.19
1312	89.96	4.50	1.88		3.66	0.69	5.90	22.92	77.08	1.42
1332	81.55	5.38	2.06		11.02	2.38	4.30	40.61	59.39	0.71
1356	87.06	4.18	1.97		6.79	2.21	14.10	19.52	80.48	1.68
1365	86.19	4.61	1.86		7.35	1.19	14.79	24.95	75.05	1.28
1366	86.92	4.28	1.95		6.85	1.59	14.13	19.51	80.49	1.78
1367	87.34	3.83	1.83		6.99	1.61	9.10	17.78	82.22	2.08

Table 1

Results of Ultimate and Proximate Analysis on Coals Studied

SIU Sample Number	Carbon DMMF	Hydrogen DMMF	Nitrogen DMMF	Sulfur DMMF	Oxygen by Diff DMMF	Moisture as Rec	Ash Dry	Volatile Matter DMMF	Fixed Carbon DMMF	% Vit Reflect
Argonne Coals										
1	88.08	4.84	1.60	0.76	4.72	1.13	13.18	32.56	67.44	
2	76.04	5.42	1.13	0.48	16.90	28.09	8.77	49.75	50.25	
3	80.73	5.20	1.43	2.47	10.11	7.97	15.48	49.23	50.77	
4	84.95	5.43	1.68	0.91	6.90	1.65	9.25	42.53	57.47	
5	91.81	4.48	1.34	0.51	1.66	0.65	4.77	19.60	80.40	
6	81.32	5.81	1.59	0.37	10.88	4.63	4.71	48.61	51.39	
7	85.47	5.44	1.61	0.67	6.68	2.42	19.84	34.47	63.53	
8	74.05	4.90	1.17	0.71	19.13	32.24	9.72	50.52	49.48	

year and the Argonne samples studied this year, the Hartshorne coals tend to be lower in volatile matter for a given content than the Argonne or SIU coals. As is seen later, this affects TGA results in a consistent manner.

The results of the petrographic analyses of these samples are given in Table 2. As can be seen, petrography varies widely as do the rank parameters listed in Table 1. A list of seams from which the SIU samples were obtained is given in Table 3. Additional characterization of some samples is in progress.

Combustion Profiles

The combustion profiles developed for this study consisted essentially of a continuous measurement of the mass of a coal sample heated in air at a constant rate. A typical profile is given in Figure 1. The figure consists of a weight loss curve and the first derivative of that curve. From these curves, a number of parameters are derived. These parameters include:

1. moisture content – this shows up as a weight loss between the starting temperature and 130° C;
2. percentage of oxygen chemisorption – this is the weight gain between 130° C and the temperature of combustion onset;
3. ash yield – this is the weight remaining at a temperature of about 800° C; and
4. maximum rate of weight loss – this is the value of the peak of the derivative curve.

In addition to these values, there are eight temperatures of interest:

1. initial chemisorption,
2. maximum rate of chemisorption,
3. combustion onset,

Table 2

Results of Petrographic Analysis

Sample (SIU) No.	Macerals									Reflectance f_o
	Vitrinite	Pseudo-vitrinite	Semi-fusinite	Semi-macri-nite	Fusinite	Macri-nite	Micrinite	Exinite	Resinite	
647	65.9	10.3	5.7	-	4.0	6.5	6.3	6.3	1.3	0.58
647J	56.3	8.7	4.0	-	3.4	-	5.5	21.2	-	0.58
1307	65.5	18.7	8.3	0.6	2.0	-	1.0	3.6	0.3	0.80
1468	45.7	37.2	3.3	0.3	1.4	-	0.3	9.5	0.5	0.80
1469	23.0	-	44.9	-	17.9	4.0	5.4	5.0	0.5	0.64
1497	45.7	37.2	3.3	0.3	1.4	-	0.3	9.5	0.5	0.80
1795	74.4	-	0.7	-	-	-	0.2	24.7	-	0.40
1681	67.0	1.9	1.5	2.4	-	-	1.2	25.2	0.7	0.51

Table 3

Identification of SIU Coals

SIU No.	Description	Seam	Region	Country
561	Resin Concentrate		Utah	U.S.A.
647		Indiana No. 5	Indiana	U.S.A.
647J	Paper Concentrate	Indiana No. 5	Indiana	U.S.A.
1307	Banded Lithotypes	Pittsburgh No. 8	Pennsylvania	U.S.A.
1468	Banded Lithotypes	Elkhorn No. 3	Kentucky	U.S.A.
1469	High Inert	Matla		South Africa
1497	Banded Lithotypes	Elkhorn No. 3	Kentucky	U.S.A.
1681	Paper Coal		Texas	U.S.A.
1794	High Lipid	Black Creek	Alabama	U.S.A.
1795		Shovel Creek	Alaska	U.S.A.

4. first ignition (volatile combustion),
5. second ignition (char combustion),
6. maximum reactivity,
7. 50% burnoff of organic material, and
8. char burnout.

The effects of sample weight, heating rate, and air flow rate were standardized last year. Reproducibility of the test was also established. Two coals were used for the establishment of standard deviations for each parameter of the combustion profiles, and are periodically rerun to check the calibration of the test. Whenever test results fall outside two standard deviations of the previously determined mean, furnace temperature and flow rates are recalibrated. Thus far, this approach has been sufficient to maintain reproducible results for SIU 1310 and 1367 samples.

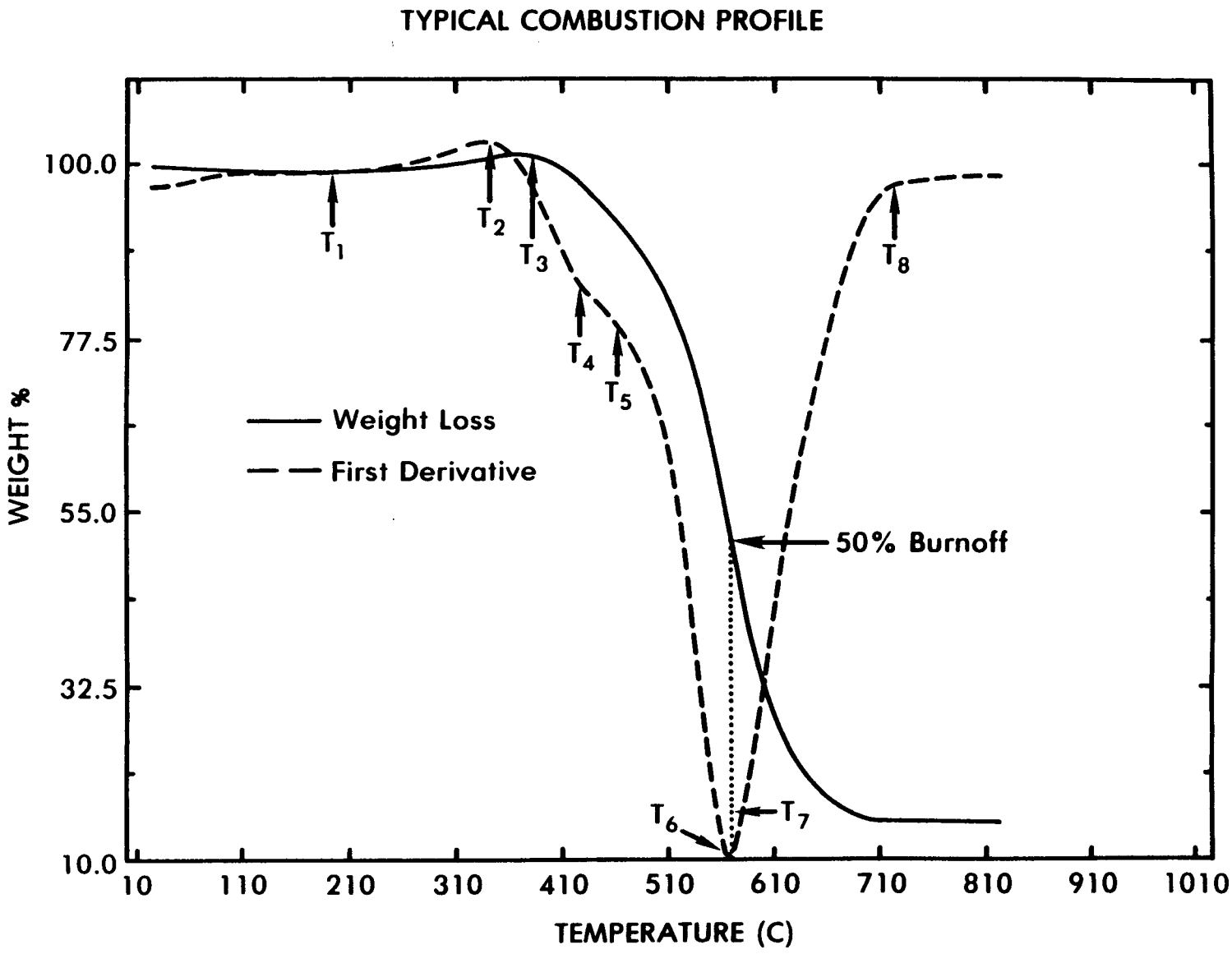

Figure 1. Typical combustion profile showing the parameters measured.

Reconstruction

To further substantiate that DGC separation and CsCl do not have a catalytic effect, raw coal and coal reconstructed from DGC separated macerals were compared. Results of comparing an original –200-mesh demineralized SIU 1311, a Hartshorne sample, and a coal reconstructed in proper proportions are illustrated by Figure 2, which shows a comparison of burnoff curves for coal No. 1311. The curves overlap almost exactly until the very end of the combustion process. This small discrepancy between the curves may be a result of using only maceral peaks from the DGC separation process and is not considered to be significant. The inertinites may not be totally represented by a single fraction. This is discussed in a later section of the report. In addition, the close proximity of these curves shows that CsCl does not catalyze combustion in air.

Rank effects/whole coals. The data from the combustion profiles for the Argonne coal samples, as received, ground for 30 min, and demineralized, are given in Table B1 (Appendix B). Data for the separated macerals obtained from the demineralized Argonne coals are listed in Table B2. Results for the OTISCA coals and the bottom residue fractions for DGC separators are shown in Table B3, while results from a group of SIU coals are listed in Table B4. Results from coals and supercritical extraction (SCE) products of these coals are listed in Table B5.

In last year's report we presented data and graphs that demonstrated clear relationships between rank parameters such as carbon content, volatile matter yield, and vitrinite reflectance and key combustion profile temperatures and weights. One of the objectives of this year's program was to determine the applicability of these relationships to other coals. As a first approach, Argonne premium samples were obtained. The samples were tested in their as received state, and aliquots were ground to a nominal 200-mesh size. A portion of the

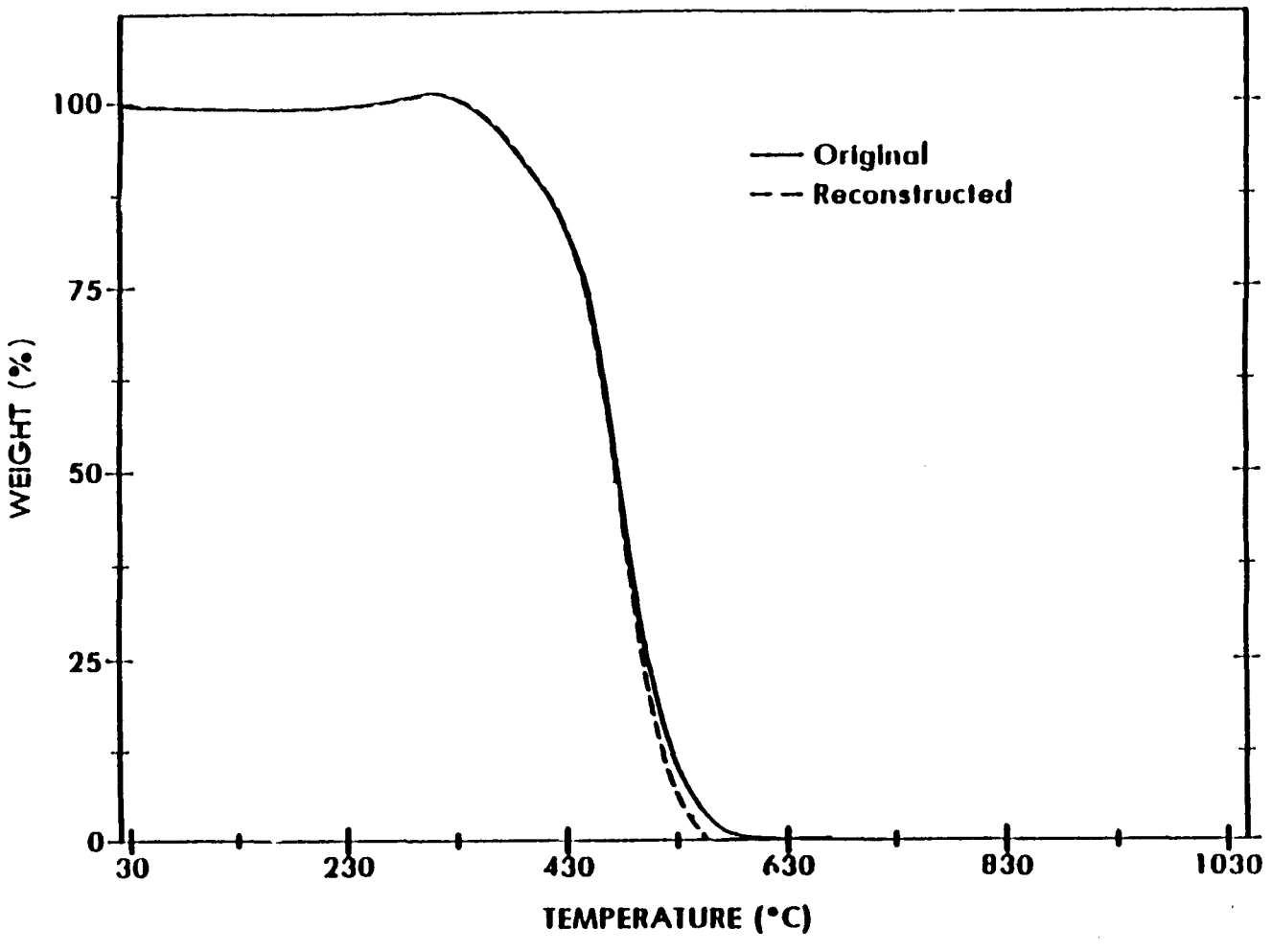

Figure 2. Comparison of burnoff curves for original coal (No. 1311) and coal reconstructed from coal macerals.

ground sample was tested and another portion demineralized. Some of the demineralized coals were also tested. The results are listed in Table B1. Figures can be found in the appendix from which comparisons between the Argonne coals and the Hartshorne coals can be made.

Figure B.2 gives the TGA ash yield for the Argonne samples and Figure B.3 gives the ash yields for the Hartshorne coals. The figures show that most of the samples are low-mineral coals to begin with and that demineralization sharply reduces, but does not eliminate, ash yields. The demineralized coals vary in ash yield from 0 to 4%.

Figures B.4 through B.9 are plots of key combustion temperatures as a function of carbon content. Some of the Argonne coals did not produce the same shape burnoff coals as the Hartshorne coals. In particular, lower rank coals yielded double peaked derivative curves that closely resembled those reported by Smith et al. (1981) for low rank coals. As rank increased, the two derivative peaks gradually converged to yield a single peak. This will necessitate the development of models with added parameters for the multipeak curves.

Despite the problem of varying curve shapes, the Argonne coals do give linear relationships versus carbon content. In fact, the relationships appear to be better for the Argonne coals than for the Hartshorne coals. In general, decreasing the particle size decreases the key combustion temperatures of the Argonne coals, and demineralization tends to increase them. The lignite in the sample bank gave a slightly different pattern for T2 and T3. This might be expected because of the large carboxyl group concentration in this coal.

The demineralization effects are opposite of those observed in the Hartshorne coals. Although both sets of coals give linear relationships between carbon content and key combustion parameters, the relationships form two different bands. T8 gives the most scatter in the relationships, and T3 the least scatter. The difference in

the whole coal profiles means that a better rank parameter must be found or that the coals vary because the macerals are not alike in various seams. At this point a distinction can not be made. However, in light of the findings of Niel et al. (1987), it appears that there may be multiple rank bands. The number of those identified by Niel (5) may be insufficient to account for the variations seen in all coals. The number required is yet to be established. However, if there are a number of rank bands, then a method must be developed to classify coals into the proper band. Although this will require a lot of effort, it may be necessary in order to develop a complete understanding of coal behavior. We will be testing the samples employed by Niel and those of another rank series to determine if there are indeed multiple bands. It should be noted that the range in scatter reported by Smith et al. (1981) is greater than that reported here. Thus, the inability to develop better predictive tools than those published by Neavel et al. (1986) may be due to this inability to distinguish rank type. It also means that molecular structure parameters are important to coal behavior, which is in contrast to the concepts published earlier by Neavel et al. (1986).

The maximum amount of chemisorbed oxygen is observed at T3 and can be seen in Figure B.10. Data scatter blurs the distinction between the Hartshorne and Argonne coals. In general, the trends are the same as those reported last year. Since the amount adsorbed at T2 is a linear function of the amount adsorbed at T3 this parameter is not further discussed. As reported last year, demineralization increases chemisorption in some coals and decreases it in others. As with the profile temperatures, less scatter is observed in the demineralized sample than in the raw samples. As expected, decreased particle size increases chemisorption.

The profile temperatures and chemisorption are plotted as function of volatile matter in Figures B.11 through B.17. Volatile matter gives slightly tighter bands and blurs the differences between the Hartshorne and Argonne coals for some

parameters. It was reported last year that vitrinite reflectance and volatile matter yields were stronger correlative factors for some parameters. Vitrinite reflectance data are not available for the Argonne coals because they have been ground too fine during preparation for the sample bank. Also, as was found last year, no parameter appears to be be a good predictor of maximum combustion rate.

Rank effects/macerals. Figure B.18 lists the ash yields for the macerals derived from the demineralized Argonne coals. The ash yields indicate that some macerals hold more minerals than others during the DGC separation. However, the selectivity appears to be coal dependent. Data on macerals obtained from raw Hartshorne coals showed a similar response pattern. Thus, the selectivity does not seem to be affected by demineralization. Some of the ash yields in the macerals may be due to residual cesium chloride left after DGC separation. Thus the differences in ash may also be due to the affinity of different macerals for cesium.

Figures B.19 through B.24 show the relationships between combustion profile temperatures of the separated macerals and carbon content of the whole Argonne coals. The results of combustion profiles obtained on the raw and demineralized coals are also reported. As reported last year, the vitrinite data give a tighter band than the data for the raw or demineralized whole coal. Data for inertinites are scattered and do not show a consistent trend. Although the data for the inertinite does not show a consistent trend, the liptinite data does. The change in combustion profile temperature with changes in carbon content seems to be greater with the liptinite data than with the vitrinite data. This is a new observation made possible by increased numbers of coals containing liptinites as compared to the Hartshorne coals. Again the data shows clear evidence of matrix effects, but these effects appear to be variable, and caused by different phenomena. Thus, no clear pattern emerges when examining the data for the whole coals relative to the data for the macerals.

Figure B.25 shows that the maximum amount of chemisorption for the macerals increases linearly with carbon content. Again, matrix effects are obvious but variable. However, the trends are more clearly seen in the demineralized whole coals and macerals than in the raw whole coal. Thus, minerals appear to play a part in the chemisorption process. The vitrinites have a tendency to chemisorb the same or less than the whole coal. The inertinites tend to chemisorb less than the vitrinites, and the liptinites even less than the inertinites. Some data in the graph are plotted as negative adsorption. This phenomena is the result of volatile loses at the same time chemisorption is occurring. The chemisorption can be followed by monitoring changes in the first and second derivatives of the weight loss curves.

Figures B.26 through B.31 show that combustion profile temperatures are related to volatile matter as well as to carbon content. However, the relationship is nonlinear. It is flatter at high ranks and loses resolution at low ranks. Again, nonconsistent trends were observed for temperatures of the macerals relative to each other or to the whole coals. Data scatter is greatest for the inertinites. Stronger trends are observed for T2, T3,and T4 than were observed for T5, T6, and T8. Figure B.32 shows similar trends for the amount chemisorbed.

Figures B.33 through B.74 give a comparison of combustion profile parameters for individual macerals obtained from Argonne and Hartshorne coals. Figures B.33 through B.46 show relationships for vitrinites; Figures B.47 through B.60 show relationships for inertinites; and Figures B.61 through B.74 show relationships for the liptinites. The data are plotted against whole coal rank parameters of carbon content and volatile matter. In Figures B.33 through B.39 combustion profile parameters for the vitrinites obtained from the Argonne coals are clearly linearly related to rank. T2, T3, and T4 show tighter relationships than T5, T6, and T8. As with the whole coals, the vitrinites from the Argonne coals give lower temperature parameters than the vitrinites from the Hartshorne coals. This adds further

evidence that more than one rank band exists. The DGC run of the Upper Freeport coal yielded two vitrinites. The higher density (1.28 g/cc) fraction yields data that is closer to the Hartshorne band than the rest of the Argonne samples. This could mean that there are at least two types of vitrinite that are difficult to differentiate by optical microscopy, but whose density and chemical properties are divergent. The relationships with volatile matter shown in Figures B.40 through B.46 show similar but more nonlinear trends. In the latter stages of the burnout curve, the differences between the Hartshorne and Argonne samples become smaller.

The DGC run on the low rank Argonne coals gave no clear distinction as to where the densities of the inertinites fall. We have been further hampered in obtaining inertinite fractions from the low-rank coals because of the lack of reliable petrography data. To obtain verified maceral separation in low-rank coals, flouresence or other techniques must be developed that can differentiate between fine vitrinite and fine inertinite particles. The inertinites from the six other Argonne coals cover the same carbon content range and yield combustion profile temperatures that are in general lower than those obtained for the Hartshorne coals. Again, linear relationships are tight and more separated in the earlier stages of burnoff than in the latter stages of burnoff. Not all of the inertinites show a first ignition temperature. Again, the Upper Freeport coal (Argonne No. 1) shows behavior more similar to the Hartshorne coals than to the rest of the Argonne coals, and the behavior of the inertinites from the Argonne coals is markedly different than that of the inertinites from the Hartshorne coals. Argonne coal No. 7 (Lewiston-Stockton seam) yielded an odd DGC weight recovery curve with four high density fractions showing a substantial, relatively constant weight recovery of material. These four fractions were combusted separately and gave widely different combustion profiles. Both the shape and temperature of the profiles varied. The data for these four fractions are included in Figures B.47 through B.60.

The range in these four fractions is almost as great as the range found in the rest of the Argonne samples. These results demonstrate that not all inertinites behave in the same manner and that a better inertinite classification scheme is required. It may also mean that rank parameters used in the classification of whole coals do not reflect changes in some inertinites. In other words, some inertinites might change drastically as rank increases while other inertinites are not affected by the metamorphic conditions that affect other macerals. It certainly implies that all inertinites are not entirely alike.

Because of the high rank, not many of the Hartshorne coals contained identifiable liptinites. All of the Argonne coals did. The relationships between combustion profile temperatures of the liptinite macerals and rank parameters of the whole coals are demonstrated in Figures B.61 through B.74. Like the vitrinites and the inertinites, the relationships are tighter for the earlier stages of burnoff. Also, the data give lower temperatures for the liptinites derived from the Argonne coals than those derived from the Hartshorne coals. The separation in data is not as evident when volatile matter is used as the predictor. However, the relationships with volatile matter are not as clearly defined as they are with carbon content.

Miscellaneous coals. Several coals in the SIU sample bank have also been tested, but characterization has not been completed. Those having adequate characterization are discussed below and the remainder will be discussed when characterization is completed. SIU 1468 was obtained from the Elkhorn No. 3 seam and separated into a vitrain and clarain by hand picking. The whole sample has a volatile matter and a vitrinite reflectance similar to that of one of the Hartshorne coals (SIU 1310). The combustion profile temperatures for the raw and demineralized vitrain, clarain, and SIU 1310 coals are presented in a bar graph (Figure B.75). Temperatures are clearly lower for the Elkhorn sample, as compared to the Hartshorne sample. Curve shape for the clarain and vitrain were markedly

different. The clarain showed evidence of three peaks in the derivative curve and the vitrain showed a curve similar in shape to the Hartshorne coal. Profile temperatures of the raw clarain are lower than those for the raw vitrain. Demineralization increases the profile temperatures of both the clarain and vitrain. But the effect is so much more pronounced in the clarain that the demineralized vitrain gave lower temperatures than the demineralized clarain. A similar pattern is observed for a Pittsburgh clarain and vitrain hand picked from SIU 1307. Again, SIU 1307 has a similar volatile and the same vitrinite reflectance. The data for the Pittsburgh clarain and vitrain are very close to those obtained from the Argonne No. 4 coal, which is a Pittsburgh seam coal. The pattern is shown in Figure B.76. The burnoff curve is similar in shape for the clarain and vitrain of the Pittsburgh sample, and it is closer to the Hartshorne shape than the Elkhorn samples. No evidence of split peaks were observed in any of the Pittsburgh samples. This shows that both the mineral and maceral compositions are important to the combustion profile of these lithotypes.

Vitrinite and inertinite macerals separated from the Elkhorn coal give higher T2 and T3s than the whole lithotypes and the Hartshorne coal. The liptinite gave slightly lower values (Figure B.77). Figure B.78 demonstrates that T4 for the vitrinite and inertinite macerals are similar to the Hartshorne coal and higher than the lithotypes. The liptinite gave the lowest T4. T5 was higher for the vitrinite and inertinite macerals than for the lithotypes or the Hartshorne coal, but the liptinite gave the lowest T5 value. However, T6 and T8 (Figure B.79) are lower for all the macerals than for the Hartshorne coal. The lithotypes gave lower values than the vitrinites and the inertinites. The liptinite again gave the lowest values. The curve shape for all the macerals is similar and is close to that of the Hartshorne coal. The vitrinites and inertinites appear to delay ignition longer than the whole coal, but burn more intensely in the latter stages of the combustion profile. Again from this

data there appears to be a matrix effect that allows the lithotypes to ignite and burn more quickly than the individual macerals.

Coal cleaning effects/physical. To test the effect of advanced physical coal cleaning on combustion profiles, a set of samples was obtained from OTISCA, Inc. The set consisted of an as-mined sample of Pocahontas No. 3 coal and two precleaned samples of that coal. These samples were similar in properties to the Argonne No. 5 sample. The details of the precleaning are unavailable at this time. The samples are referred to as F1, F2, and F3. These three samples were fed to OTISCA's T-process to obtain products P1, P2, and P3. DGC profiles were run on these coals. The cumulative and incremental recovery for the six samples are shown in Figures B.80 and B.81, respectively. The weight data does not include the 1.5 sink material. The data indicate that the high ash in the original feed does not affect the density profile below 1.2 g/cc. However, the first feed contains higher density material than feeds 2 and 3. This may be because of high ashes in association with organics. However, the curve for feed 3 is displaced to lower density than that for feed 2 even though it contains a higher ash content. We conclude from this that the precleaning has preferentially selected out high density inertinites and selectively concentrated the other macerals. The precleaning did not increase the lipid concentration. After processing, the ash yield for P1 is substantially lower than for F1 (see Table 1). Feed 2, which was already fairly low in ash yield, was cleaned only a small amount, from 3 to 2% ash yield. The third feed gave the product with the lowest ash yield (1.23%). All three of the products show marked increases in the low density materials. Since product 2 contains a small amount of minerals to begin with, and because the ash yield changes little during processing, the increase of low density material must be the result of selective rejection of inertinites. This is an extremely important finding. It means that liquefaction feeds can be prepared with lower amounts of unconvertable and hard-to-convert carbon. This in turn should

allow increased throughput and conversions. Since the Wilsonville Plant (Southern Research Services, Wilsonville, Alabama) is currently operating in a mode that is limited by the amount of inertinites in the feed, this may prove to be the correct process to try on Wilsonville feeds.

Outside of burning at a slightly higher reaction rate, the combustion profiles of the product and the feeds are nearly identical. Feed 2 and feed 3 produce a slightly different curve shape. The profile temperatures are represented in bar graph form in Figure B.82. The figure includes data for Argonne sample No. 5 as well as the feed and the products of the T-process and the bottom residue from DGC of the feeds and products. The temperatures are extremely close for each pair (i.e., F1 and P1). There appear to be some differences related to the precleaning with F2, P2 and F3, P3. Combustion profiles are displaced to slightly higher temperatures than the F1 and P1 profiles. From these results it appears that the OTISCA T-process has little or no negative effect on combustion properties, and may even improve the combustion because of increased burning intensity. The bottom residue gave similar curves slightly displaced to a higher temperature. In the case of F1 the intensity of the combustion was significantly reduced due to the presence of approximately 60% mineral content. Combustion profiles of the other density fraction are currently being conducted. Chemisorption, as shown in Figure B.83, is only slightly affected by processing. The precleaning steps to obtain feed 3 seems to reduce the chemisorption slightly, but this was recovered after T-processing. The bottom residues show little chemisorption, which would be expected if they are mostly mineral and inertinites. Mass balance would indicate that they are high in inertinites and in minerals.

Effects of coal cleaning/thermal-chemical. SIU has been studying the super-critical extraction (SCE) of coals with alcohol to selectively remove sulfur from the coals. One of the concerns of the process is that combustion of the solid residue

may be adversely affected by SCE. A series of samples were prepared to study the kinetics of the desulfurization. The combustion profiles of theses samples were obtained and the results can be found in Figures B.84, B.85, and B.86. The raw coal, SIU 647, was selected for the SCE study because of its high sulfur and liptinite contents. As expected, micronization of the –60-mesh raw coal resulted in an increase in chemisorption and a decrease in all of the combustion profile temperatures. Demineralization decreased chemisorption, T2, T4, and T8, but increased T3, T5, and T6. This essentially meant that the demineralization changed the profile curve shape and delayed ignition, but intensified the combustion reaction rate. The flotation process removed some heavy inertinites and pyrite. It had a profound effect on the combustion profile. It intensified the combustion further and allowed the volatile combustion to be resolved from the char combustion. Flotation lowered all the combustion profile temperatures and reduced the chemisorption phenomena. The chemisorption reduction in the combustion profile may be the result of chemisorption during flotation or the blocking of pore or chemisorption sites with cesium. The profile for the separated vitrinite showed a similar result, but the profiles for two pseudovitrinite macerals did show some signs of chemisorption, which could be attributed to different types of chemisorption sites or different pore volume distributions that do not trap as much cesium. The separated macerals yielded combustion profile temperatures that were greater than the floated coal. This is another indication that a matrix effect exists during combustion profile tests.

The effect of SCE of the raw coal for 60 min at various temperatures on combustion profiles can be seen in Figures B.87 and B.88. The first ignition temperature is not apparent, indicting some loss of volatiles. T2 increases with increasing SCE temperatures up to 450° C and is greater than T2 of the profile for the raw coal, except for the lowest SCE temperature of 350° C. T3 shows a similar

increase with increased SCE temperatures but is lower than that of the raw coal, except for the residue prepared at 450° C. T5, T6, and T7 are slightly increased after SCE but are relatively independent of SCE temperature. T8 appears to go through a minimum range as SCE temperature is increased, but is lower than T8 obtained on the raw coal. Thus, the tendency of SCE of raw coals is to broaden the combustion profile. This suggests that the SCE residues of raw coals will be more difficult to combust.

To see if mineral removal might affect this finding, combustion profiles were obtained for SCE residues originating from demineralized and floated samples. The results of the combustion profiles are seen in Figures B.89, B.90, and B.91. For the residues from the demineralized coals, T2, T3, T5, T6, and T8 are constant for varying SCE temperatures and lower than the equivalent temperature obtained from the demineralized coal. T4 increases with increasing SCE and becomes larger than T4 of the demineralized coal at a reaction temperature of 400° C. Thus, after mineral removal, SCE does not adversely impact combustion profiles.

A series of samples prepared at 400° C at various reaction times from both the raw and the floated coal showed very little change in the combustion profile as a function of extraction time. This data can be found in Table B4 but is not depicted graphically. From this data, it can be seen that SCE does remove volatile material, but the residue burns intensely and should present little problem in terms of burner design. However, burners presently burning coals would need to be retrofitted or derated if SCE residue were to be used as a feedstock. With physical precleaning, the residues may be very reactive and only present a small problem with flame stability. With increased loading of potassium in the residue, the raw coals might present slagging problems, but the precleaned samples may not. The physical removal of the mineral matter enhances the ultimate amount of sulfur removed. Thus deep physical cleaning has positive effects on the desulfurization and requires

less severe conditions for sulfur removal. Lower extraction temperatures should enhance combustion properties.

Modeling

The combustion profiles of the Hartshorne coals have been modeled using an empirical approach. The details of the model are described in Appendix C. The model results indicate that strong matrix interactions occur during the combustion profile test. Also, the model indicates that the interactions are coal dependent. It is not known if these interactions are intensified or mitigated by actual combustion conditions which probably have greater heat and mass transport effects than the combustion profile. Also, the demineralized whole coals can be modeled more accurately than raw coal samples. Thus, for the model to become fully predictive, a model that incorporates mineral effect needs to be developed and the organic interactions need to be modeled. Also, because some coals contain more peaks in the derivative curve, the numbers of parameters used to describe the burnoff curve need to be increased for some coals. Finally, T50 predictions for individual macerals need to be developed and the combustion profile parameters must be related to crucial large scale combustion parameters. Obviously this chore goes beyond the scope of this project, but the knowledge gained thus far has further defined what is required to develop a truly predictive model.

SUMMARY AND CONCLUSIONS

The following is a brief list of important conclusions drawn as a result of this project:

1. The OTISCA T-process may be a suitable candidate for preparing samples for liquefaction feedstocks.
2. Maceral interactions occur during combustion profile tests.

3. Macerals can be remixed to give matrix interactions.
4. Combustion profile parameters are rank related.
5. Not all coals follow the same rank relationships.
6. Pure macerals more clearly define the rank relationships.
7. Vitrinite and liptinite behavior is more predictable than inertinite behavior (for combustion profiles).
8. Techniques to identify macerals in small particle assemblages need to be developed.
9. Physical cleaning has positive or little effect on combustion profile behavior.
10. SCE has some negative impacts on combustion profiles.
11. The negative effects of SCE are partially negated by potassium addition and physical precleaning.
12. If SCE is to be used to prepare combustion feedstocks, then deep physical cleaning is recommend to enhance desulfurization and combustion properties.
13. The combustion profiles can be modeled as apparent first ordered reactions.
14. Activation energy is independent of rank but not maceral composition or rank type (the rank band the coal belongs to).
15. Combustion curves can be normalized.
16. Burnoff curves can be fitted to a polynomial-log equation.
17. The best predictions are obtained when curves are fitted to the individual macerals obtained from the whole coal being modeled.

PUBLICATIONS AND PRESENTATIONS

Crelling, J. C. 1988. Separation and characterization of coal macerals including pseudovitrinite. In Ironmaking Proceedings, pp. 351-356. American Institute of Mining Engineers.

Crelling, J. C., N. M. Skorupska, and H. Marsh. 1988. Reactivity of coal macerals and lithotypes. Fuel 67:781-785.

Crelling, J. C., and E. H. Hippo. 1988. Reactivity of whole coals and selected pure maceral fractions. In Proceedings of the International Conference on Carbon, pp. 107-109. American Carbon Society.

Crelling, J. C. 1988. Separation and characterization of coal macerals including pseudovitrinite. Paper presented at The Annual Meeting of the Iron and Steel Society, April, Toronto, Canada.

Crelling, J. C., and E. J. Hippo. 1988. Reactivity of whole coals and selected pure maceral fractions. Paper presented at The International Conference on Carbon, September 1988, American Carbon Society, Newcastle-upon-Tyne, England.

Woerner, B. A. 1988. Masters Thesis, Department of Mechanical Engineering and Energy Processes, Southern Illinois University at Carbondale.

REFERENCES

Ashu, J. T., N. Y. Sakala, O. P. Mahajan, and P. L. Walker, Jr. 1978. Fuel 57:250-251.

Chai, C., G. R. Dyrkacz, and L. M. Stock. 1987. Base catalyzed maceral separation. Paper presented at 21st Great Lakes Regional Meeting of the American Chemical Society, June, Evanston Illinois.

Crelling, J. C., N. M. Skorupska, and H. Marsh. 1987. Reactivity of coal macerals and lithotypes. Extended Abstracts from 18th Biannual Conference on Carbon, Worcester, Massachusetts: Elsevier.

Crelling, J. C. 1986. Separation and fluorescence characterization of coal macerals. Coal Technology Laboratory Final Report. Carbondale: Southern Illinois University at Carbondale, Coal Research Center.

Crelling, J. C., and D. M. Miller. 1985. Separation and fluorescence characterization of coal macerals. Coal Technology Laboratory Final Report. Carbondale: Southern Illinois University at Carbondale, Coal Research Center.

Cumming, J. W. 1984. Reactivity assessment of coals via a weighted mean activation energy. Fuel 63(10):1436-1440.

Dyrkacz, G. R., C. Chai, and K. C. Hsieck. 1987. DGC separation of coal macerals. In 202nd National Meeting of ACS, Fuel Div. Preprints, vol. 32(1).

Dyrkacz, G. R., C. A. A. Bloomquist, and L. Ruscic. 1984a. High-resolution density variations of coal macerals. Fuel 63:1367-1374.

Dyrkacz, G. R., C. A. A. Bloomquist, and L. Ruscic. 1984b. Chemical variations in coal macerals separated by density gradient centrifugation. Fuel 63:1166-1174.

Dyrkacz, G. R., C. A. Bloomquist, L. Ruscic, and E. P. Horwitz. 1984c. Variations in properties macerals elucidated by density gradient separation. In Chemistry and characterization of coal macerals, American Chemical Society Symposium Series 252, eds. E. W. Randall and J. C. Crelling, pp. 65-77. Washington, D.C.: American Chemistry Society.

Dyrkacz, G. R., C. A. A. Bloomquist, and P. R. Solomon. 1984d. Fuel 63:536-542.

Dyrkacz, G. R. and E. P. Horwitz. 1982. Separation of coal macerals. Fuel 61(1):3-12.

Fenton, G. W., and A. V. H. Smith. 1959. Gas World (Coking Section) 149:81-87.

Hippo, E. J., J. C. Crelling, D. P. Sarvela, and J. Mukherjee. 1987. Organic sulfur distribution and desulfurization of maceral fractions. In Proceedings of the 2nd International Conference on Utilization and Processing of High Sulfur Coals, eds. Y. P. Chugh and R. D. Caudle. New York: Elsivere.

Smith, S. E., R. C. Neavel, E. J. Hippo, and R. N. Miller. 1981. DTGA combustion of coals in the Exxon coal library. Fuel 60(6):458-462.

Stock, L. M., G. R. Dyrkacz, and C. Chai. 1987. The base catalyst maceral separations. In 202nd National Meeting of ACS, Fuel Division Preprint 32(1).

Tsai, C. Y., and A. W. Scaroni. 1984. Roles of various constituents in pulverized coal combustion. SME-AIME Preprints No. 336. Society of Mining Engineers.

Tseng, B. H., M. Buckenting, K. C. Hsiek, C. A. Wert, and G. R. Dyrkacz. 1987. Organic sulfur in coal macerals. Fuel 65.

Wagoner, C. L., and A. F. Duyz. 1967. Burning profiles of solid fuels. In Proceedings, Annual Winter Meeting of ASME, Pittsburgh, Pennsylvania.

Wagoner, C. L., and Winegarther, E. C. 1973. Further development of burning profile. Journal of Engineering for Power (April):119-123.

APPENDICES

APPENDIX A

LITERATURE SURVEY OF COMBUSTION PROFILES

TGA has been used extensively to study the thermal properties of coal. A review by Kneller (1986) lists 156 references for the thermal analysis of coal. Thermal analysis using TGA can be divided into four major categories: pyrolysis, char combustion, char gasification, and coal combustion in air. Combustion studies of chars prepared in nitrogen or other inert gas [Jenkins et al. 1973, Rubak et al. 1984, Hippo et al. 1979, Elder and Harris 1984, Kopp and Harris 1984, Schouten et al. 1987, and Skorupska et al. 1987] and gasification studies [Hippo and Walker 1975, Kayembe et al. 1976, Mahajan et al. 1977, Linares-Salano et al. 1979, Young and Smith 1987, and Chatwani et al. 1987] are numerous. The above references demonstrate the acceptance of TGA for the study of coal in various environments.

Combustion analysis of coal in air using TGA is more limited in the literature. Wagoner and Duzy [1967] were the first to establish TGA and DTGA technique for use in the study of combustion in air. They identified the portion of the burning profiles representing oxidation. This fundamental work showed TGA analysis as superior to ASTM methods in avoiding false ignition points. False ignition points were observed in 20% of the fuels studied. This work showed the peak of the TGA derivative curve as proportional to the peak reactivity of the fuel. Also observed was that the area under the oxidation curve was found to be proportional to the heat liberated during combustion. This study included various solid fuels including coals, cokes, and chars. Results were implemented in subsequent boiler design by Babcock and Wilcox.

Wagoner and Winegartner [1973] expanded the work of Wagoner and Duzy [1967] in a sequel article which lists the precautions in using burning profile techniques. The techniques of TGA used at Babcock and Wilcox were run in conjunction

Cumming [1984a] expanded this concept in his thesis on the application of thermoanalytical techniques to routine coal analysis. His work involved two phases. Phase I compared standard proximate analysis data with TGA proximate analysis data for 14 widely varying samples of coal. Results were comparable. Phase II involved the determining of calorific values by using burning profiles. Area under the derivative of the weight loss curve is an indication of the calorific value of the coal. Calorific values were found by conventional methods for 36 coals. TGA methods were compared to conventional methods and found to be similar. This work illustrated the use of TGA burning profiles as a viable alternative to conventional methods of calorific value determination.

Ghetti [1985] also investigated the use of TGA data for routine coal analysis. He found correlation of TGA data with proximate and ultimate analyses of coal. Data showed good correlations between the volatile matter/fixed carbon ratio (VM/FC), carbon/hydrogen ratio (C/H), and carbon plus hydrogen/oxygen ratio (C + H/O) and rate of weight loss data and temperatures deduced from burning profiles. VM/FC was considered indicative of coal rank. C/H was related to aromaticity. C + H/O gave an indication of the extent of oxidation of the fuel. They found rank and aromaticity to decrease as the extent of oxidation of coals increased. Temperature of combustion onset, temperature of peak combustion, temperature of volatiles release, and temperature of peak volatiles release were noted and found to correlate non - linearly with VM/FC, C/H, and C + H/O. Rate of maximum combustion and rate of maximum volatile release were also similarly correlated. Direct correlation between ignition temperature and volatile matter present was also observed. It was also noted that the height of the burning profile is related to the peak reactivity of the coal. The higher the burning profile, the more reactive the coal.

Saayman [1985] continued the concept of using TGA data to characterize coal. His work reported the use of TGA in a computerized data set which uses burning profiles as a method of identifying and categorizing the combustion qualities of various coals.

Smith et al. [1981] performed combustion analysis which has become a basis for subsequent researchers in coal combustion utilizing TGA. This work standardized many of the experimental parameters for studying whole coals. A wide range of whole coals of varying rank from the Exxon coal library were analyzed. They found the greatest value of TGA in "determining relative properties of different samples run under specified standard conditions." Smith developed a concept of fitting burning profile data to Arrhenius plots to determine "activation energies" for coal burn off. When data was fitted to this kinetic model, four regions of combustion were found. Region 1 resulted from light volatile evolution and combustion so this region is chemical reaction controlled. In region 2, higher molecular weight volatile components diffuse from pores and combust. Region 3 was a smaller region, believed to be the transition between chemical and diffusion controlled reaction. In region 4, reaction is diffusion controlled as chemical reaction rates become faster than oxygen diffusion. Mineral matter contributions were neglected. This work gave activation energies based on slopes for each of the four regions of linearity noted on the Arrhenius plots.

Cumming [1984b] expanded work done by Smith on finding activation energies for whole coals of various seams and varying coal rank. Cumming modified Smith's procedure of finding activation energies by proposing a weighted mean activation energy to characterize the primary burn off region. This involved using the activation energies found as per Smith, weighting them by the fractional percentage in each region, and adding them to provide weighted mean activation energy for each coal. These combined weighted activation energies were thought

to provide an easier method of categorizing the combustion quality of coal. A combined activation energy, E_m, is easier to use than the multiple activation energies calculated by Smith and was used to rank reactivities. Tests of 22 solid fuels ranking from lignites to anthracites, showed E_m values ranging from 153 kJ/mole for higher ranked coals (anthracites) to 56 kJ/mole for the lowest ranked lignites. E_m values thus gave an indication of reactivity for coals spanning the rank range to which other coals could be compared.

Related research into burning profiles for whole coals has been done by Ghetti et al. [1985]. Ghetti investigated correlations between thermal analysis data and surface area measurements. Strong correlations were found. By plotting surface area data vs. heating temperature, a surface area curve was obtained whose profile very closely resembled the relevant burning profile. This was done for 12 coal samples of varying rank and illustrated the strict correlation that exists between the burning profile and the development of the surface area of coal during combustion. Also noted was a well defined shoulder of variable intensity on the burning profiles, which had not been previously modeled. They found the height of this shoulder related to the (volatile matter/fixed carbon) ratio. Lower ranked coals had a more pronounced shoulder.

Other related work investigating TGA combustion of whole coals in air was performed by Sarageldin and Pan [1983, 1984a,b]. Their work stressed the effects of catalysts on combustion profiles. Addition of alkali salts (K_2CO_3, Na_2CO_3, and Li_2CO_3) each progressively lowered the activation energies of coal burning in air. Alkali salts increased overall coal decomposition. They also suggested that changing the heating rate of the gas will change the activation energy so a standard heating rate should be used to gain consistent values. Li_2CO_3 was the most effective catalyst. Mixed catalysts were more effective than single catalysts. A decrease in activation energy did not always reflect an increase in coal reactivity. Correlations

between activation energy and heat of reaction were developed. A r^2 = .55 correlation was observed for combustion in air.

The literature reviewed thus far has not included any investigation of coal macerals. TGA combustion of pure maceral fractions in air has been limited due to the unavailability of pure macerals. Bengtsson [1987] has investigated comparative thermal analysis methods for whole coals (of various origins and petrographic compositions) and for a few maceral fractions. She used Smith's procedure to analyze activation energies. The goal of this work was not to focus on TGA, but to compare the various thermal techniques for coal analysis. TGA portion of this work was limited. This work stressed the effects of combustion on coals and chars. The limited maceral data was to support the comparative analysis.

The work most related to TGA maceral analysis of coal was performed by Morgan et al. [1986]. Their study of coal oxidation using TGA included the analysis of some lithotypes. Noted in this work were maceral effects, rank effects, reaction kinetics, and reactivity characteristics of whole coals and lithotypes. Maceral effects were evidenced by the resolution of vitrinite and inertinite peaks. Lower burnout temperatures were observed for lithotypes with high vitrinites than those with high inertinites. Rate effects illustrated that as rank increases, peak temperature and burnout temperature increase for both vitrinite and inertinite lithotypes, while reactivity differences decrease. Reaction kinetics involved plotting activation energies and resolving curves into regions. Avoidance of over interpretation was stressed. Reactivity characteristics revealed superior burnout performance with coals having lower burnout temperatures and that higher rank coals burn with higher unburnt fuel loss. Burning profiles were seen as a viable ranking tool for whole coals and lithotypes. Pure maceral separates were not studied.

LITERATURE CITED

Bengtsson, M., "Combustion Behavior for a Range of Coals of Various Origins and Petrographic Compositions," 1987 International Conference on Coal Science, Elsevier Science Publishers B.V., Amsterdam, 893-896 (1987).

Bryers, R. W., B. K. Biswas, and T. E. Taylor, "Fuel Evaluation Using Differential Thermal Techniques", Paper presented at Coal Technology '74, International Coal Utilization Conference and Exhibition, Houston, Texas, October 17-19, 1974, 583-623 (1974).

Chatwani, A., A. Turan, and F. Hals, "Fundamental Modelling of Pulverized Coal and Coal Water Slurry Combustion in a Gas Turbine Combustor", Prepared Paper American Chemical Society Division Fuel Chemistry, 165-170. (1987).

Cumming, J. W., "Reactivity Assessment of Coals via a Weighted Mean Activation Energy", Fuel, 63 (10), 1436-1440 (1984a).

Cumming, J. W., "The Application of Thermoanalytical Techniques to Routine Coal Analysis". Masters Thesis University of Salford, Scotland (1984b).

Elder, J. P., and M. B. Harris, "Thermogravimetry and Differential Scanning Calorimetry of Kentucky Bituminous Coals", Fuel, 63 (2), 262-267 (1984).

Ghetti, P., "DTG Combustion Behavior of Coal", Fuel, 64 (1985).

Ghetti, P., U. De Robertis, S. D'Antone, M. Villani, and E. Chiellini, "Coal Combustion - Correlation Between Surface Area and Thermogravimetric Analysis Data", Fuel, 64 (7), 950-955 (1985).

Hippo, E. J., and P. L. Walker, Jr., "Reactivity of Heat Treated Coals in Carbon Dioxide at 900 C", Fuel, 54 (10), 245-248 (1975).

Hippo, E. J., R. G. Jenkins, and P. L. Walker, Jr., "Enhancement of Lignite Char Reactivity to Steam by Cation Addition", Fuel, 58, 338-344 (1979).

Jenkins, R. G., S. P. Nandi, and P. L. Walker, Jr., "Reactivity of Heat Treated Coals in Air at 500#C", Fuel, 52 (10), 288-293 (1973).

Kayembe, N. and A. H. Pulsifer, "Kinetics and Catalysts of the Reaction of Coal Char and Steam", Fuel, 55 (7), 211-216 (1976).

Kneller, W. A., "Physiochemical Characterization of Coal and Coal Reactivity: A Review", Thermochemica Acta, 1e08 Elsevier Science Publishers, 357-388 (1986).

Kopp, O. C. and L. A. Harris, "Initial Volatilization Temperatures and Average Volatilization Rates of Coal - Their Relationship to Coal Rank and other Characteristics", International Journal of Coal Geology, 3,333-348 (1984).

Linares-Salano, A., O. P. Mahajan, and P. L. Walker, Jr., "Reactivity of Heat Treated Coals in Steam", Fuel, 58 (5), 327-332 (1979).

Mahajan, O. P., R. Yarzab, and P. L. Walker, Jr., "Unifaction of Coal Char Gasification Reaction Mechanisms", Fuel, 57 (10), 643-646 (1977).

Morgan, P. A., S. D. Robertson, and J. F. Unsworth, "Combustion Studies by Thermogravimetric Analysis", Fuel, 65 (11), 1546-1549 (1986).

Rubak, W., H. Karcz, and M. Zembrzski, "Evaluation of Intrinsic Kinetic Parameters of Coal Combustion", Fuel, 63 (4), 488-493 (1984).

Saayman, C. H., "Thermogravimetric Analysis and its Application for Estimating the Combustion Properties of Coal from the Study of Small Samples", Thermochemica Acta, 93, 369-372 (1985).

Sarageldin, M. A. and W. Pan, "Coal Analysis Using Thermogravimetry", Thermochemica Acta, 76 Elsevier Science Publishers, 145-160 (1984a).

Sarageldin, M. A., and W. Pan, "Coal: Kinetic Analysis of Thermogravimetric Data", Thermochemica Acta, 71 Elsevier Science Publishers, 1-14 (1983).

Sarageldin, M. A. and W. P. Pan, "Coal: Kinetic Analysis of Thermogravimetric Data (II)" Prepared Paper American Chemical Society Division Fuel Chemistry, 29 (2), 112-118 (1984b).

Schouten, J. C. et al, "Thermoanalytical Study on the Release of Sulfur During Coal Combustion", 1987 International Conference on Coal Science, Elsevier Science Publishers B.V., Amsterdam, 837-840 (1987).

Skorupska, N. M. et al, "The Use of an Entrained Flow Reactor to Assess the Reactivity of Coals of High Inertinite Content", 1987 International Conference on Coal Science, Elsevier Science Publishers B.V., Amsterdam 827-831 (1987).

Smith, S. E., R. C. Neavel, E. J. Hippo, and R. N. Miller, "DTGA Combustion of Coals in the Exxon Coal Library", Fuel, 61(5), 458-462 (1981).

Vecci, S. J., C. L. Wagoner, and G. B. Olson, "Fuel and Ash Characterization and Its Effect on the Design of Industrial Boilers", Proceedings of the American Power Conference Volume 40, 850-864 (1978).

Wagoner, C. L. and A. F. Duzy, "Burning Profiles for Solid Fuels", Paper presented at Winter Annual Meeting, ASME, Pittsburgh, PA, November 12-16, 1967.

Wagoner, C. L. and E. C. Winegartner, "Further Development of the Burning Profile", Journal Engineering Power, April 1973, 119-123.

Young, B. C. and I. W. Smith, "Carbon Combustion: The Order of Reaction in Oxygen", 1987 International Conference on Coal Science, Elsevier Science Publishers B.V., 793-796 (1987).

APPENDIX B

Table B1. Results of TGA Combustion Profiles of Argonne Premium Coals.

COAL SAMPLES ARGONNE IDENT. NO.	TGA % MOIST	WT % AT MAX CHEM-ISORPTION	% DRY ASH	TEMP. C INITIAL C. A.	TEMP MAX C. A.	TEMP. C COMB ONSET	TEMP. C IGNITION I	TEMP. C IGNITION II	TEMP. C MAXIMUM REACTIVIT	TEMP. C CHAR BURNOUT	TEMP. C 50 % BURNOUT	MAXIMUM RATE (%/min)
AS RECIEVED												
1	0.13	2.56	12.94	112	369	406	438	515	550	678	565	16
2	20.17	0.00	6.59	132	240	254	314	370	398	653	401	15
3	3.04	1.18	15.26	126	273	318	351	426	496	660	504	11
4	0.79	1.83	9.09	133	300	332	378	446	517	683	518	12
5	0.25	3.15	4.55	112	343	369	406	473	547	697	548	14
6	0.58	0.97	4.25	112	250	259	315	406	478	628	468	13
7	1.62	1.58	19.42	135	305	337	0	450	504	712	542	9
8	12.72	0.00	8.32	130	240	265	0	352	401	586	402	10
GROUND												
1	0.38	2.66	13.02	123	276	308	371	423	485	639	498	14
2	7.35	0.00	10.64	95	165	225	291	331	348	441	346	32
3	0.85	1.76	15.13	106	216	248	0	387	449	596	455	13
4	0.70	2.27	7.88	130	269	302	0	426	467	602	473	16
5	0.12	3.71	4.37	107	294	325	369	438	476	586	490	20
6	0.92	1.17	3.38	112	222	240	311	393	441	553	436	17
7	0.61	1.72	18.51	112	262	279	0	400	456	615	490	11
8	12.89	0.00	6.96	118	222	230	0	314	461	525	395	10
DEMINERALIZED												
1	0.06	1.44	0.92	103	328	357	407	484	571	678	545	14
3	2.08	0.31	4.08	112	245	273	331	398	470	617	460	12
4	1.16	1.29	2.51	112	277	305	0	439	482	628	482	16
5	0.19	2.70	0.20	112	300	332	366	426	510	669	503	14
6	2.25	0.09	0.16	112	250	259	322	426	490	614	474	14
7	1.28	1.33	0.74	121	268	299	335	410	476	651	478	12
8	6.89	0.00	0.00	112	149	167	320	429	502	641	468	9

Table B2. Results of TGA Combustion Profiles of Macerals Produced from Argonne Coals.

COAL SAMPLES ARGONNE IDENT. NO.	MACERAL	TGA % MOIST	WT % AT MAX CHEM-ISORPTION	% DRY ASH	TEMP. C INITIAL C. A.	TEMP. C MAX RATE C. A.	TEMP. C COMB ONSET	TEMP. C IGNITION I	TEMP. C IGNITION II	TEMP. C MAXIMUM REACTIVIT	TEMP. C CHAR BURNOUT	TEMP. C 50 % BURNOUT	MAXIMUM RATE (%/min)
1	VIT.	0.31	2.47	0.04	121	292	332	383	442	510	651	503	15
1	INT. 1	0.39	1.12	2.10	112	314	360	421	479	568	718	561	12
1	INT. 2	0.49	1.23	1.47	112	320	351	412	482	556	697	552	13
1	LIP. 1	0.47	1.91	0.00	112	323	370	413	476	557	707	550	13
1	LIP. 2	0.68	0.67	0.00	130	309	332	407	479	577	686	561	13
2	VIT.	0.25	2.50	0.00	112	332	351	412	476	563	715	554	13
2	LIP.	1.75	0.00	1.77	121	167	171	265	312	420	605	418	15
2	INT.	5.70	0.00	0.18	121	204	204	305	412	485	605	453	10
3	INT.	1.19	0.00	2.57	121	231	236		421	514	646	494	10
3	LIP.	1.39	0.00	0.74	121	213	222	322	401	487	625	470	12
3	VIT.	1.59	0.19	1.32	126	250	250	320	403	464	605	454	14
4	INT.	0.90	0.00	0.00	110	250	273	323	393	472	530		12
4	LIP.	0.90	0.00	0.00	103	257	277	323	395	481	560		13
4	VIT.	0.80	0.80	0.00	112	243	277	332	387	473	560		11
5	INT.	0.30	0.00	2.91	112	332	335	389	453	547	689	539	13
5	LIP.	0.38	0.00	4.16	121	320	332	378	455	504	642	506	16
5	VIT.	0.28	2.80	0.00	112	306	332	383	438	521	678	513	14
6	INT.	1.43	0.00	0.66	130	222	227	328	413	490	606	478	12
6	LIP.	1.11	0.00	1.10	112	222	250	311	384	470	594	444	12
6	VIT.	1.58	0.00	0.10	112	254	277	311	423	491	573	478	13
7	INT. 1	0.72	1.32	0.03	112	268	286		412	436	577	432	34
7	INT. 2	0.93	1.23	0.00	130	277	314		441	473	586	468	34
7	INT. 3	0.60	0.63	0.22	112	222	259	299	378	446	623	443	11
7	INT. 4	0.79	0.00	5.07	116	254	282		430	504	641	501	14
7	LIP.	0.65	0.76	1.89	121	277	314	351	447	491	648	500	23
7	VIT.	1.24	1.16	1.73	130	259	295		410	459	641	460	14
8	VIT	3.10	0.00	0.00	112	185	204	271	309	337	470		14
8	LIP. 1	1.00	0.00	0.00	109	188	220	301	355	444	510		10
8	LIP. 2	1.10	0.00	0.00	112	185	213	280	338	404	460		29

Table B3. Results of TGA Combustion Profiles of OTISCA Coals.

COAL SAMPLES SIU IDENT. NO.	TGA % MOIST	WT % AT MAX CHEM-ISORPTION	% DRY ASH	TEMP. C INITIAL C. A.	TEMP. C MAX RATE C. A.	TEMP. C COMB ONSET	TEMP. C IGNITION I	TEMP. C IGNITION II	TEMP. C MAXIMUM REACTIVIT	TEMP. C CHAR BURNOUT	TEMP. C 50 % BURNOUT	MAXIMUM RATE (%/min)
OTISCA COALS												
T3-P1	1.08	2.88	2.28	130	272	295	351	420	493	641	483	14
T3-P2	1.42	2.92	1.68	130	268	295	341	370	442	614	463	16
T3-P3	1.27	2.40	0.89	112	272	295	351	420	491	623	475	14
F1	1.20	2.88	23.51	130	277	295	344	420	493	641	520	10
F2	2.81	3.23	6.46	112	268	291	332	390	447	641	472	16
F3	5.20	1.33	2.20	112	272	286	341	370	413	620	445	13
DGC BOTTOM RESIDUE FROM OTISCA COALS												
T3-P1	0.40	0.59	15.00	141	318	335	378	450	530	697	522	10
T3-P2	0.80	0.82	13.80	158	312	338	387	440	501	683	508	14
T3-P3	0.50	1.18	6.20	167	318	335	397	440	533	657	521	13
F1	0.50	0.00	55.10	112	325	343	401	470	550	683	528	5
F2	0.70	0.18	42.80	126	328	351	397	470	556	720	537	7
F3	1.60	1.12	9.20	236	323	338	392	470	537	687	523	12

Table B4. Results of TGA Combustion Profiles of Various Coals.

COAL SAMPLES SIU IDENT. NO.	TGA % MOIST	WT % AT MAX CHEM-ISORPTION	% DRY ASH	TEMP. C INITIAL C. A.	TEMP. C MAX RATE C. A.	TEMP. C COMB ONSET	TEMP. C IGNITION I	TEMP. C IGNITION II	TEMP. C MAXIMUM REACTIVIT	TEMP. C CHAR BURNOUT	TEMP. C 50 % BURNOUT	MAXIMUM RATE (%/min)
647	1.69	0.65	10.70	139	250	300	330	392	465	614	489	11
647	1.03	0.57	0.45	168	237	250	297	413	452	550	445	29
647	1.06	0.78	10.48	152	250	270	320	387	426	577	424	27
647	0.84	0.00	3.82	112	194	230	270	320	395	462	289	29
647	3.68	0.55	2.16	158	225	239	305	415	449	522	445	22
647J	3.78	0.00	0.59	112	259	277	280	400	416	599	413	24
647J	5.15	0.18	2.36	130	286	320	370	410	513	568	493	11
1307	2.55	0.00	1.98	112	286	314	401	440	507	563	490	14
1307	1.48	0.00	4.15	121	245	268	371	390	488	596	469	14
1307	2.03	0.29	0.68	130	291	314	400	450	513	602	499	15
1307	1.17	0.07	0.00	112	268	295	371	400	495	586	463	16
1307	1.52	2.04	1.93	130	337	361	416	500	559	669	552	24
1307	1.78	1.95	2.27	144	323	357	421	470	570	666	551	14
1468	3.14	0.31	2.03	121	277	305	375	430	513	556	490	13
1468	2.17	0.85	2.57	112	268	282	299	370	452	542	449	32
1468	2.24	0.00	0.93	112	295	308	395	440	534	577	505	14
1468	1.92	0.25	2.48	116	240	259	288	430	465	522	454	35
1468	1.22	2.05	1.27	130	317	341	378	430	499	586	497	18
1468	2.75	2.56	1.14	130	328	358	430	500	563	637	560	19
1469	4.34	0.00	24.96	130	314	338	410	460	539	638	570	24
1497	3.56	0.33	0.54	139	320	346	401	490	586	608	541	14
1497	2.66	0.85	1.70	130	323	341	406	530	586	600	548	17
1497	0.68	0.00	2.84	93	300	326	380	400	537	611	525	13
1497	1.21	0.00	22.55	112	309	332	412	420	516	680	539	8
1497	0.92	0.00	0.60	116	286	305	360	410	516	582	507	21
1497	1.62	0.49	2.69	116	283	309	380	350	488	547	484	18
1681	3.18	0.00	7.91	130	277	292	351	370	453	574	448	24
1794	2.88	2.05	1.56	130	314	329	485	520	542	585	518	21
1794	0.00	2.55	1.80	121	286	302	351	420	505	619	493	15
1795	1.84	1.05	2.14	121	259	279	311	400	438	525	437	20
1795	0.00	0.00	21.63	130	273	283	329	350	455	596	483	11
561	0.00	0.00	0.77	130	231	260	318	360	410	565	398	21
561	2.88	0.00	8.17	130	277	283	337	410	467	548	462	18

Table B5. Results of TGA Combustion Profiles of SCE Feeds and Products.

COAL SAMPLES	TGA % MOIST	% CHEMI-SORPTION	% ASH	TEMP. C INITIAL C. A.	TEMP. C MAX RATE C. A.	TEMP. C COMB ONSET	TEMP. C IGNITION I	TEMP. C IGNITION II	TEMP. C MAXIMUM REACTIVIT	TEMP. C CHAR BURNOUT	TEMP. C 50 % BURNOUT	MAXIMUM RATE (%/min)
RAW	1.69	0.65	10.70	139	250	300	330	392	465	614	489	11
DEMINERALIZED	1.03	0.57	0.45	168	237	250	297	413	452	550	445	29
MICRONIZED	1.06	0.78	10.48	152	250	270	320	387	426	577	424	27
FLOATED	0.84	0.00	3.82	112	194	230	270	320	395	462	289	29
PSEUDO-VITRINITE(2)	3.68	0.55	2.16	158	225	239	305	415	449	522	445	22
VITRINITE	3.78	0.00	0.59	112	259	277	280	400	416	599	413	24
PSEUDO-VITRINITE(1)	5.15	0.18	2.36	130	286	320	370	410	513	568	493	11
SUPERCRITCALLY EXTRACTED COALS												
FROM DEMINERALIZED COAL												
EXTRACTION												
TEMPERATURE TIME												
350 60	1.30	0.07	6.40	130	222	224	265	351	398	516	394	30
375 60	1.77	0.06	8.41	155	222	227	295	354	375	507	373	32
400 60	0.83	1.73	3.22	126	242	254	308	364	389	488	385	32
450 60	1.56	0.33	9.02	127	222	236	340	360	370	519	370	31
FROM RAW COAL												
350 60	1.67	0.00	17.04	150	213	228	390	415	458	612	468	9
375 60	1.02	0.00	16.12	129	245	250	315	410	447	596	450	7
400 60	1.87	0.00	15.02	130	253	256		415	464	559	463	12
425 60	1.51	0.00	18.84	145	236	254		418	468	582	478	8
450 60	0.50	0.00	18.77	150	291	311		421	455	623	504	14
500 60	3.19	0.79	16.41	129	259	300		424	499	619	502	13
400 30	1.02	-0.41	15.11	130	259	268		363	479	619	487	10
400 60	1.31	-0.63	15.02	130	253	256		352	464	559	463	12
400 120	4.69	-0.36	16.88	138	256	292		346	461	623	475	10
FROM FLOATED COAL												
400 30	1.94	-1.26	11.75	112	199	194	268	320	334	539	363	17
400 60	100.00	-0.83	25.41	158	240	222	341	351	427	545	447	12
400 120	100.00	-4.47	12.85	112	222	250		335	361	611	415	12

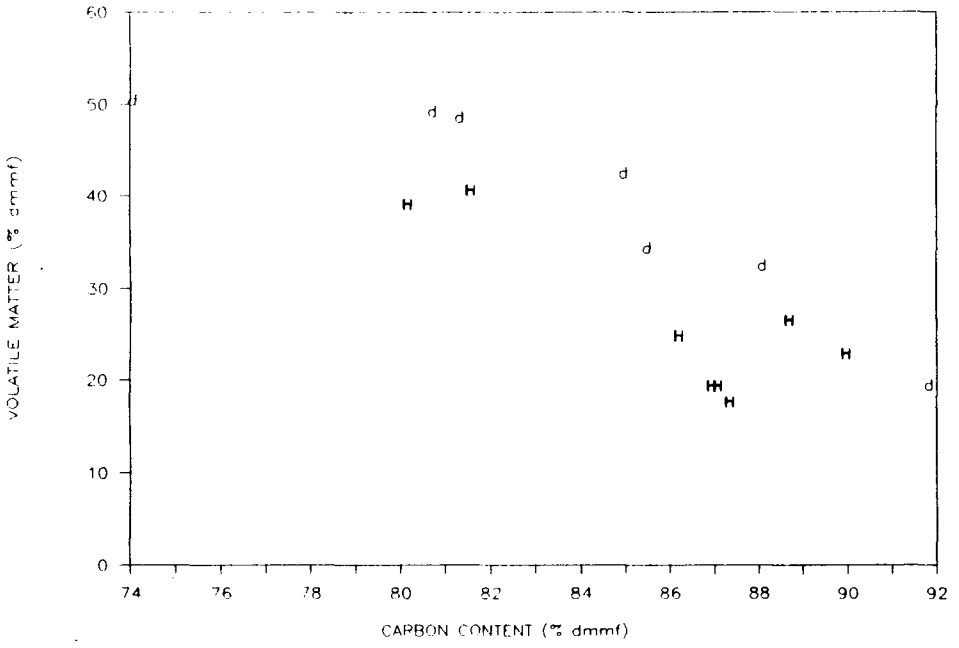

Figure B.1 The Relationship Between Volatile Matter Yield and Carbon Content for Hartshorne Seam, (H), Argonne, (d), and SIU, (S), Coals.

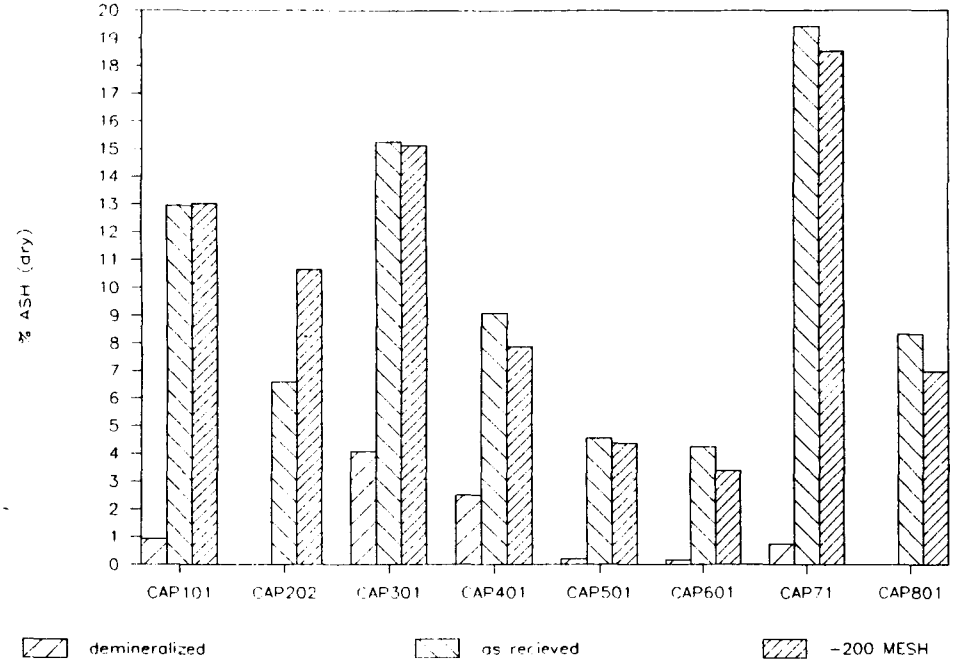

Figure B.2 TGA Ash Yields of Argonne Premium Coal Samples Demonstrating the Effect of Demineralization. Yields Are in Good Agreement With Published ASTM Data.

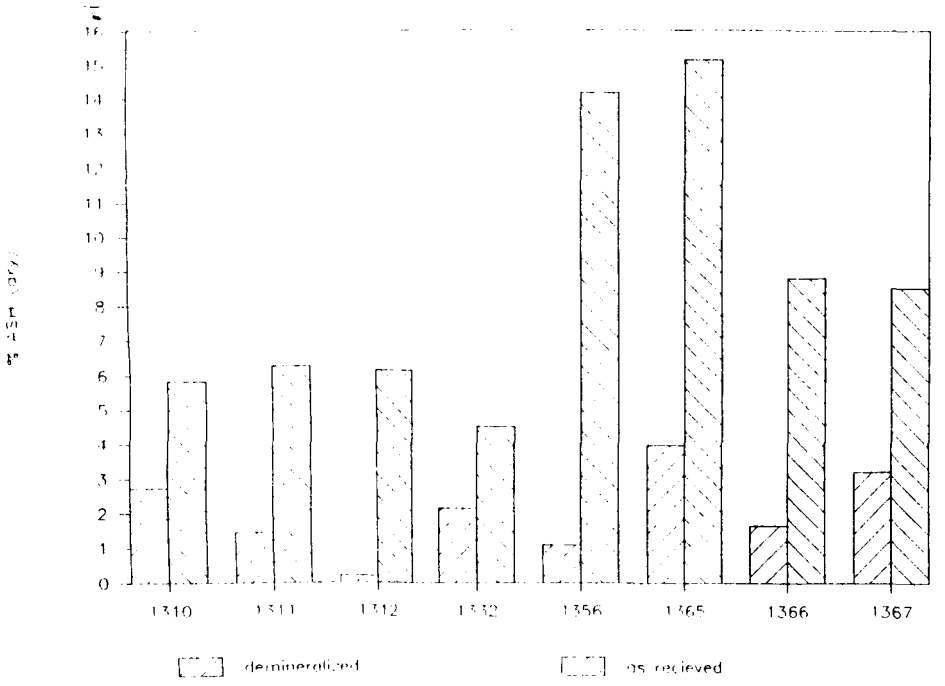

Figure B.3 TGA Ash Yields of the Hartshorne Coals Demonstrating the Effect of Demineralization.

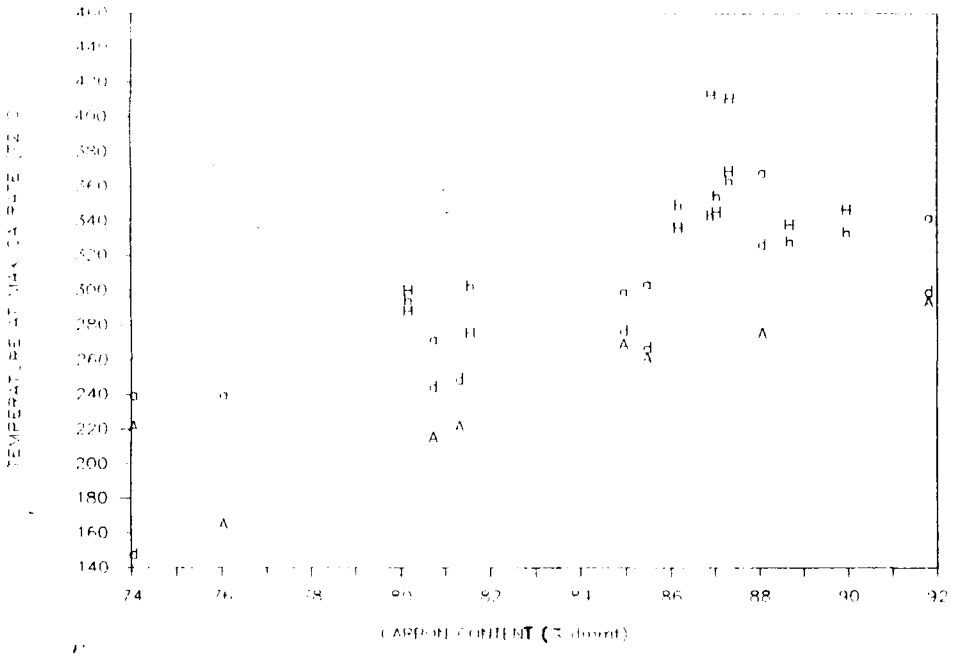

Figure B.4 The Effect of Carbon Content on TGA Combustion Profile Temperature 2 for Hartshorne -200 Mesh Coals, (H), Hartshorne Demineralized Coals, (h), Argonne as Received Coals, (a), Argonne Ground Coals, (A), and Argonne Demineralized Coals, (d).

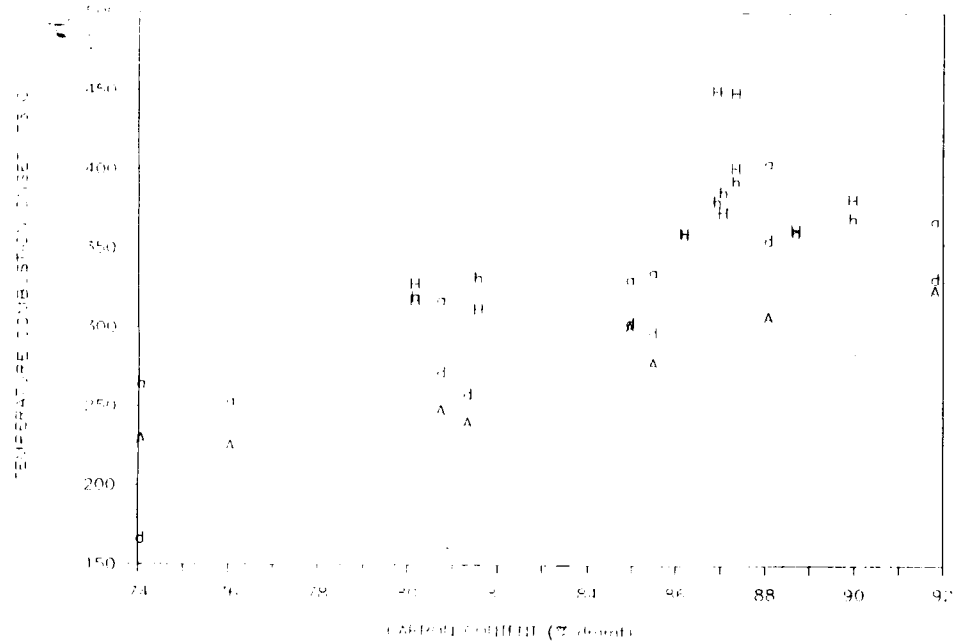

Figure B.5 The Effect of Carbon Content on TGA Combustion Profile Temperature 3 for Hartshorne -200 Mesh Coals, (H), Hartshorne Demineralized Coals, (h), Argonne as Received Coals, (a), Argonne Ground Coals, (A), and Argonne Demineralized Coals, (d).

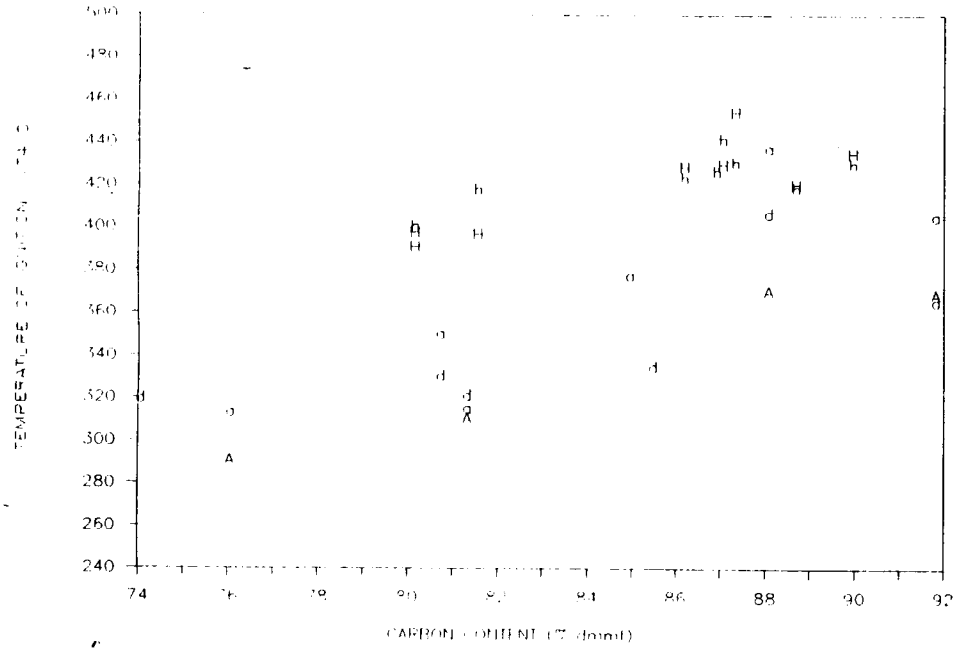

Figure B.6 The Effect of Carbon Content on TGA Combustion Profile Temperature 4 for Hartshorne -200 Mesh Coals, (H), Hartshorne Demineralized Coals, (h), Argonne as Received Coals, (a), Argonne Ground Coals, (A), and Argonne Demineralized Coals, (d).

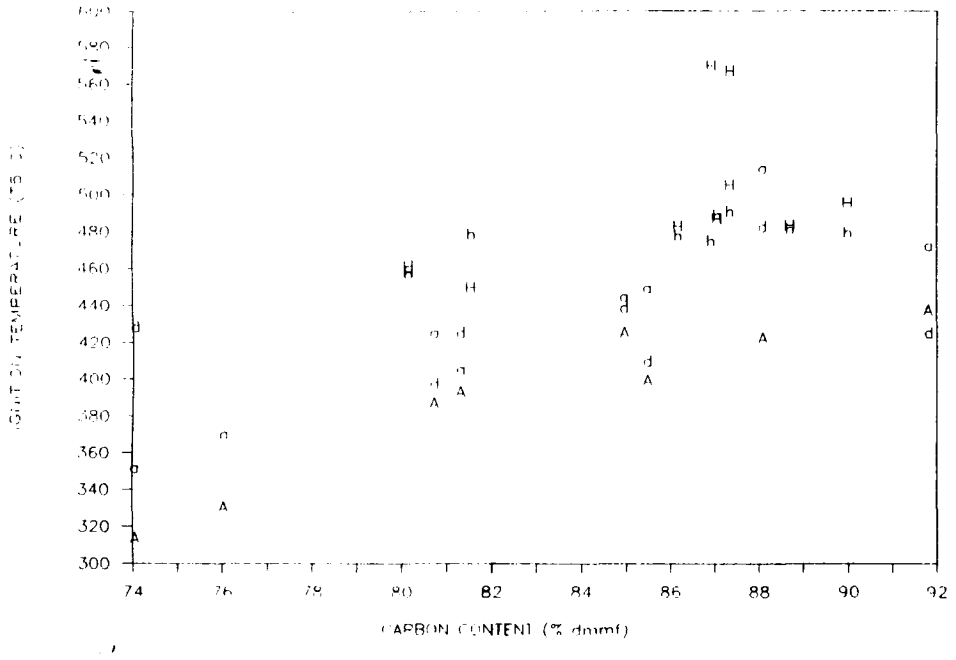

Figure B.7 The Effect of Carbon Content on TGA Combustion Profile Temperature 5 for Hartshorne -200 Mesh Coals, (H), Hartshorne Demineralized Coals, (h), Argonne as Received Coals, (a), Argonne Ground Coals, (A), and Argonne Demineralized Coals, (d).

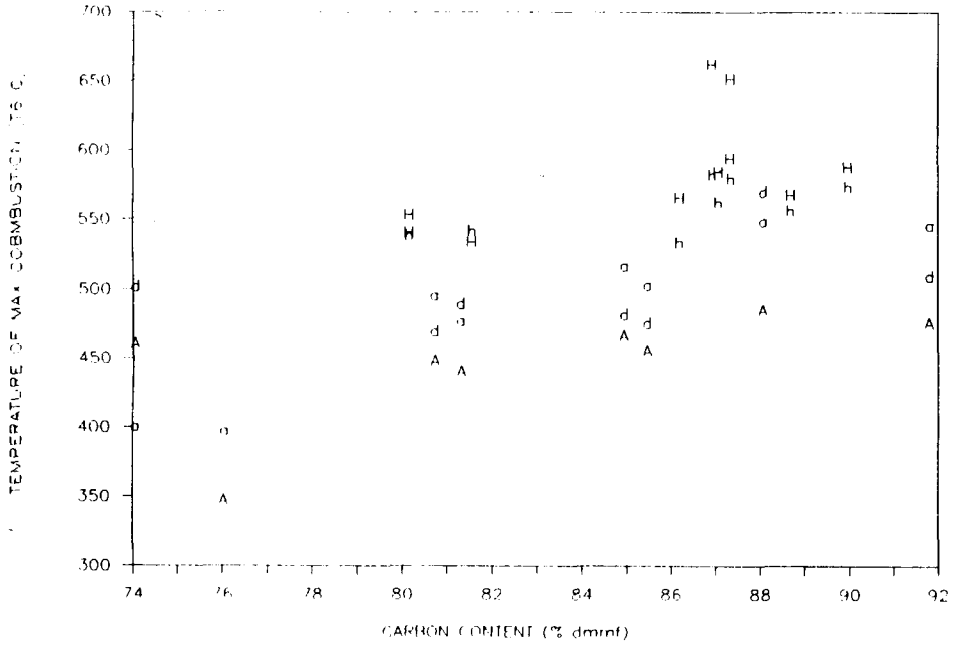

Figure B.8 The Effect of Carbon Content on TGA Combustion Profile Temperature 6 for Hartshorne -200 Mesh Coals, (H), Hartshorne Demineralized Coals, (h), Argonne as Received Coals, (a), Argonne Ground Coals, (A), and Argonne Demineralized Coals, (d).

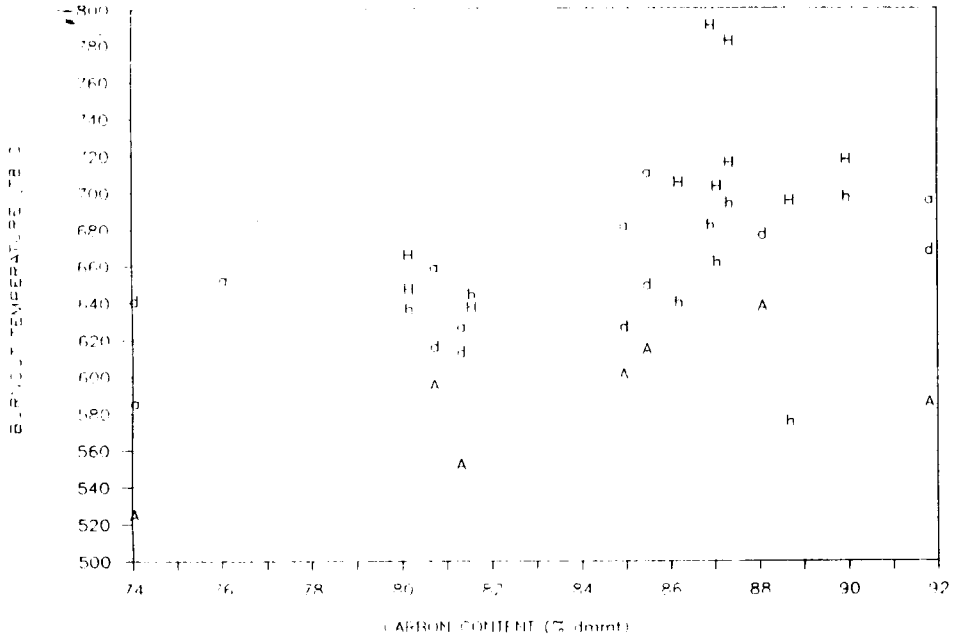

Figure B.9 The Effect of Carbon Content on TGA Combustion Profile Temperature 8 for Hartshorne -200 Mesh Coals, (H), Hartshorne Demineralized Coals, (h), Argonne as Received Coals, (a), Argonne Ground Coals, (A), and Argonne Demineralized Coals, (d).

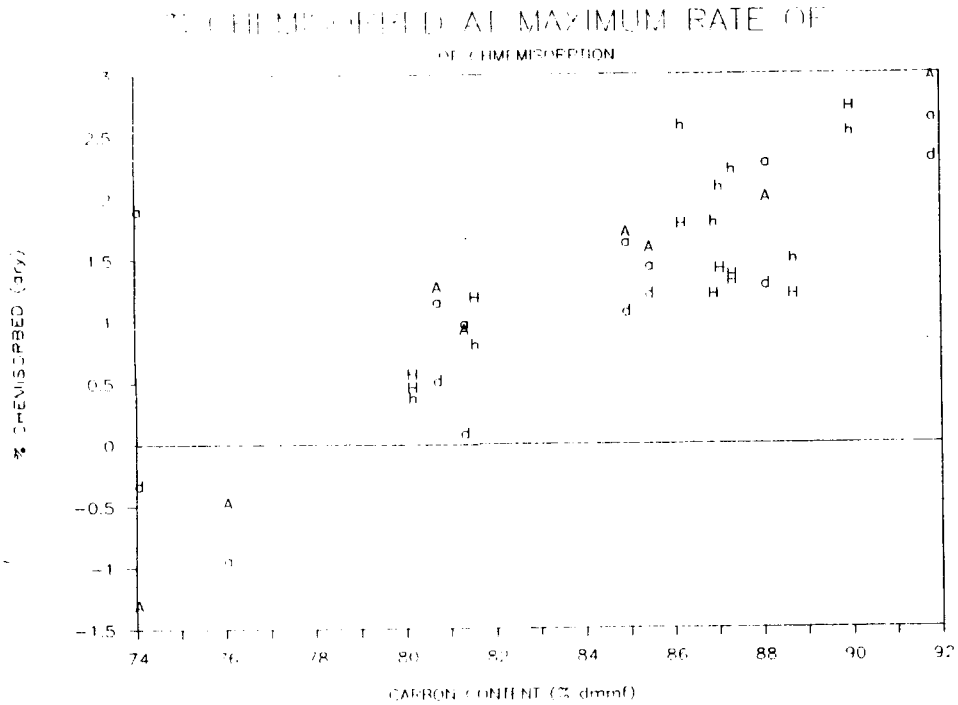

Figure B.10 The Effect of Carbon Content on TGA Combustion Profile Maximum Weight Chemisorbed for Hartshorne -200 Mesh Coals, (H), Hartshorne Demineralized Coals, (h), Argonne as Received Coals, (a), Argonne Ground Coals, (A), and Argonne Demineralized Coals, (d).

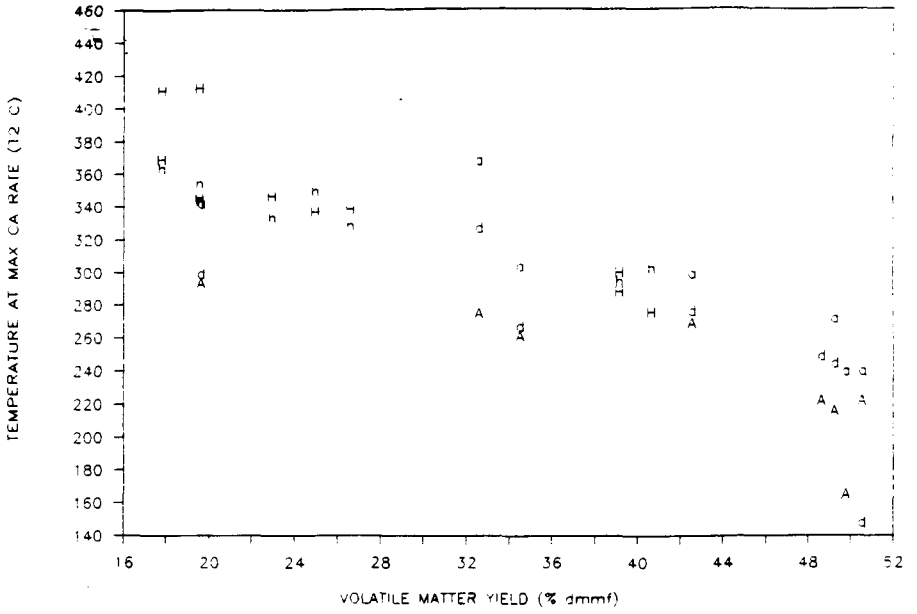

Figure B.11 The Effect of Volatile Matter Yield on TGA Combustion Profile Temperature 2 for Hartshorne -200 Mesh Coals, (H), Hartshorne Demineralized Coals, (h), Argonne as Received Coals, (a), Argonne Ground Coals, (A), and Argonne Demineralized Coals, (d).

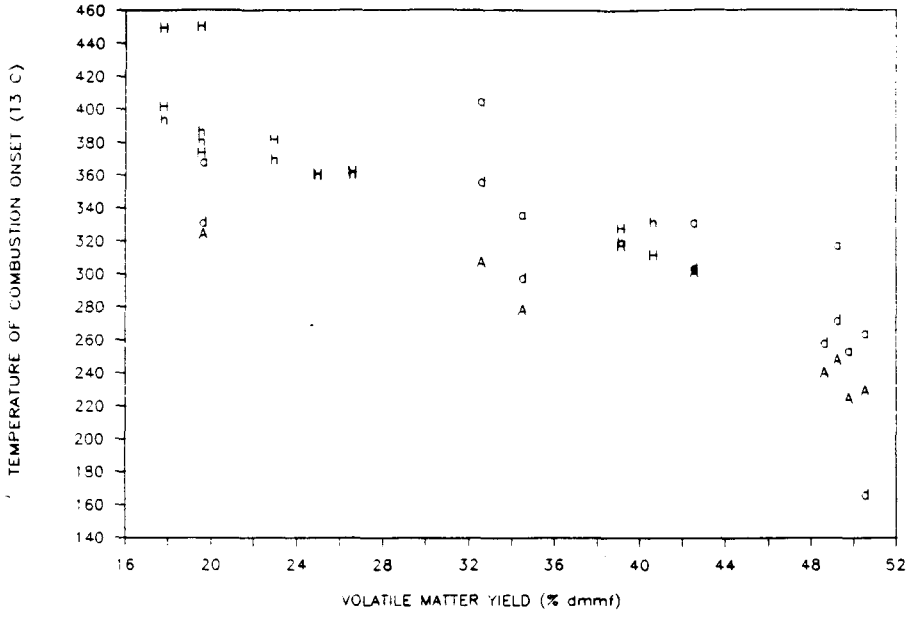

Figure B.12 The Effect of Volatile Matter Yield on TGA Combustion Profile Temperature 3 for Hartshorne -200 Mesh Coals, (H), Hartshorne Demineralized Coals, (h), Argonne as Received Coals, (a), Argonne Ground Coals, (A), and Argonne Demineralized Coals, (d).

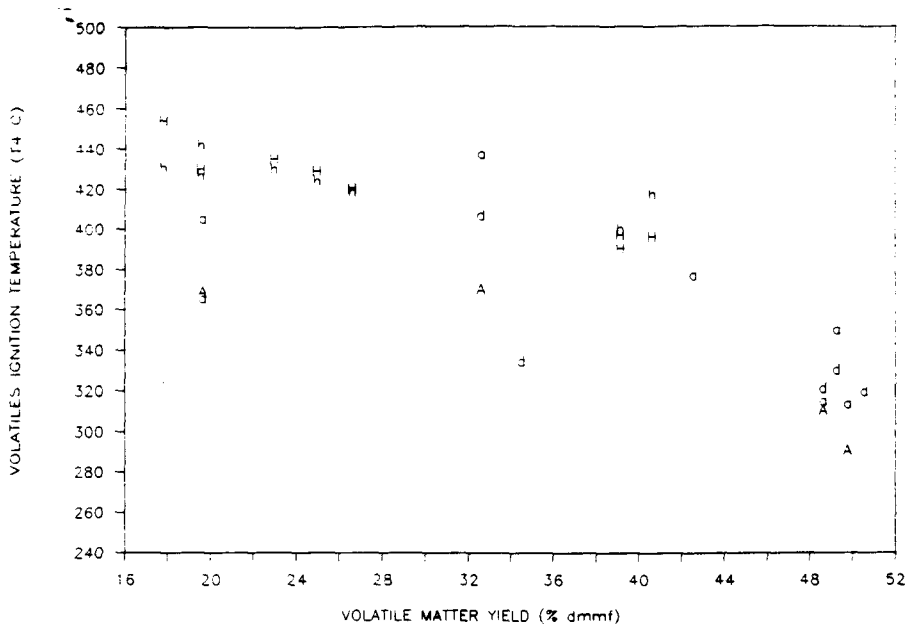

Figure B.13 The Effect of Volatile Matter Yield on TGA Combustion Profile Temperature 4 for Hartshorne -200 Mesh Coals, (H), Hartshorne Demineralized Coals, (h), Argonne as Received Coals, (a), Argonne Ground Coals, (A), and Argonne Demineralized Coals, (d).

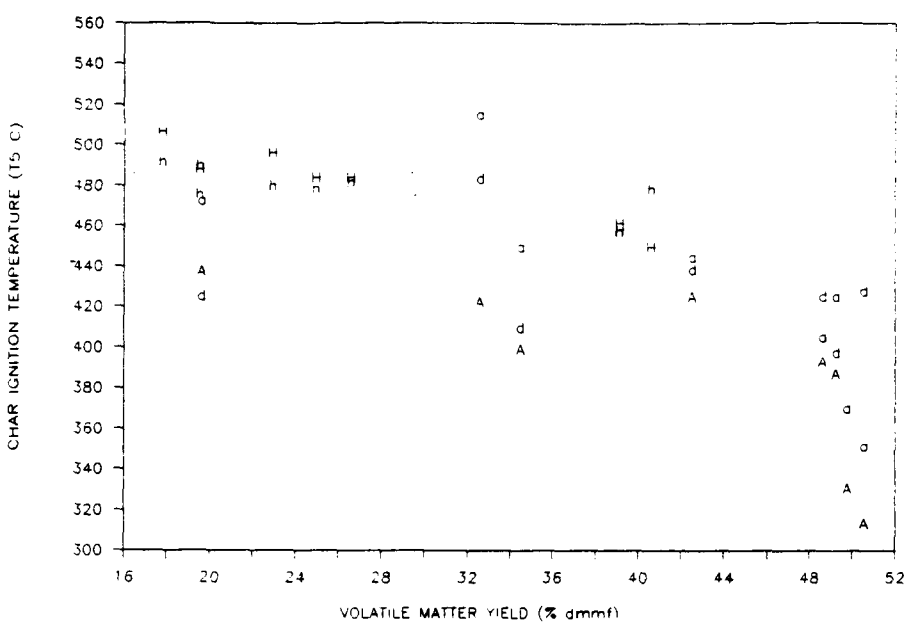

Figure B.14 The Effect of Volatile Matter Yield on TGA Combustion Profile Temperature 5 for Hartshorne -200 Mesh Coals, (H), Hartshorne Demineralized Coals, (h), Argonne as Received Coals, (a), Argonne Ground Coals, (A), and Argonne Demineralized Coals, (d).

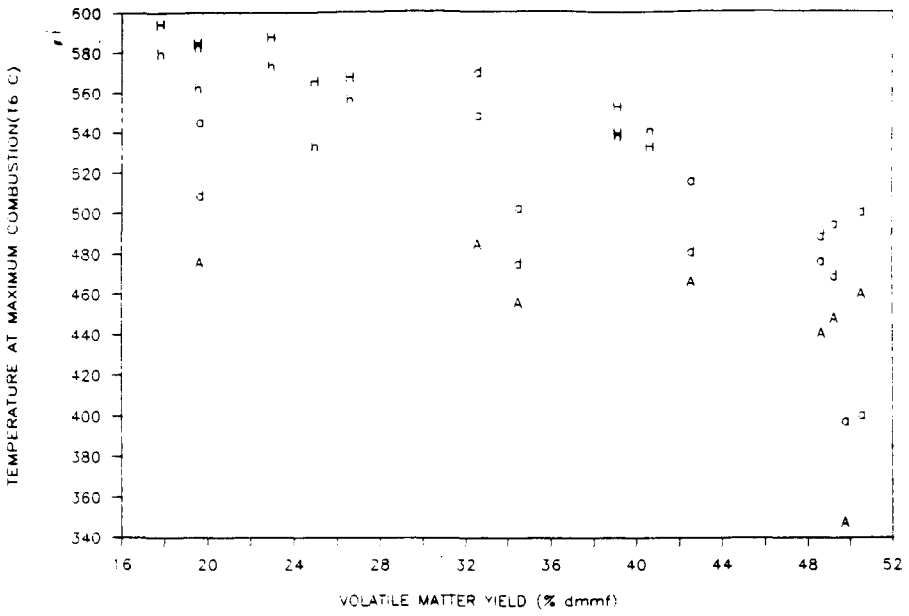

Figure B.15 The Effect of Volatile Matter Yield on TGA Combustion Profile Temperature 6 for Hartshorne -200 Mesh Coals, (H), Hartshorne Demineralized Coals, (h), Argonne as Received Coals, (a), Argonne Ground Coals, (A), and Argonne Demineralized Coals, (d).

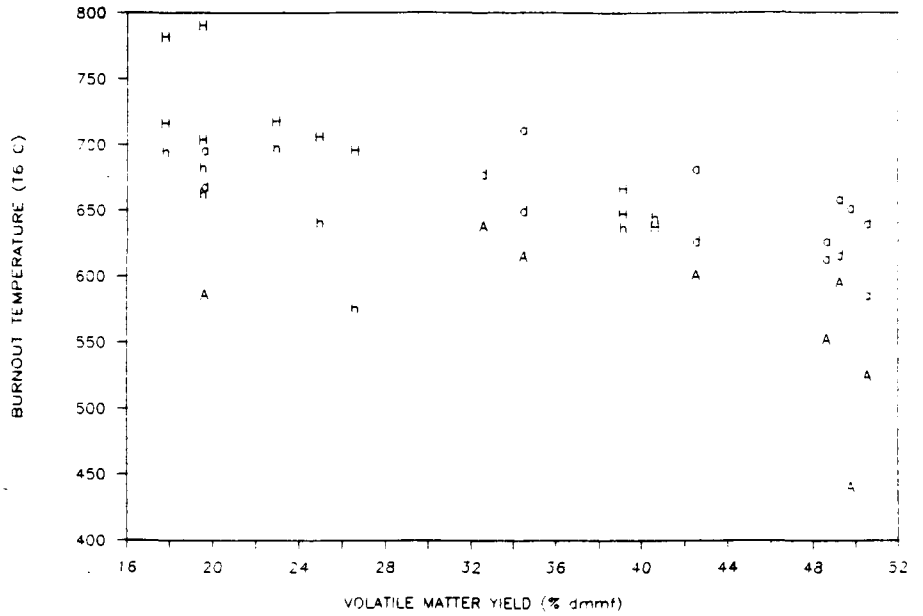

Figure B.16 The Effect of Volatile Matter Yield on TGA Combustion Profile Temperature 8 for Hartshorne -200 Mesh Coals, (H), Hartshorne Demineralized Coals, (h), Argonne as Received Coals, (a), Argonne Ground Coals, (A), and Argonne Demineralized Coals, (d).

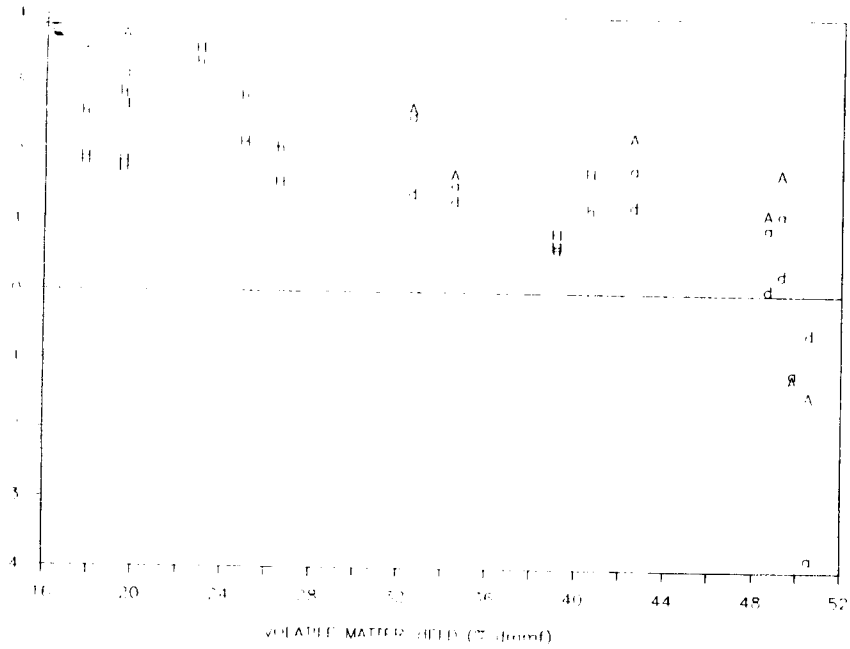

Figure B.17 The Effect of Volatile Matter Yield on TGA Combustion Profile Maximum Weight Chemisorbed for Hartshorne -200 Mesh Coals, (H), Hartshorne Demineralized Coals, (h), Argonne as Received Coals, (a), Argonne Ground Coals, (A), and Argonne Demineralized Coals, (d).

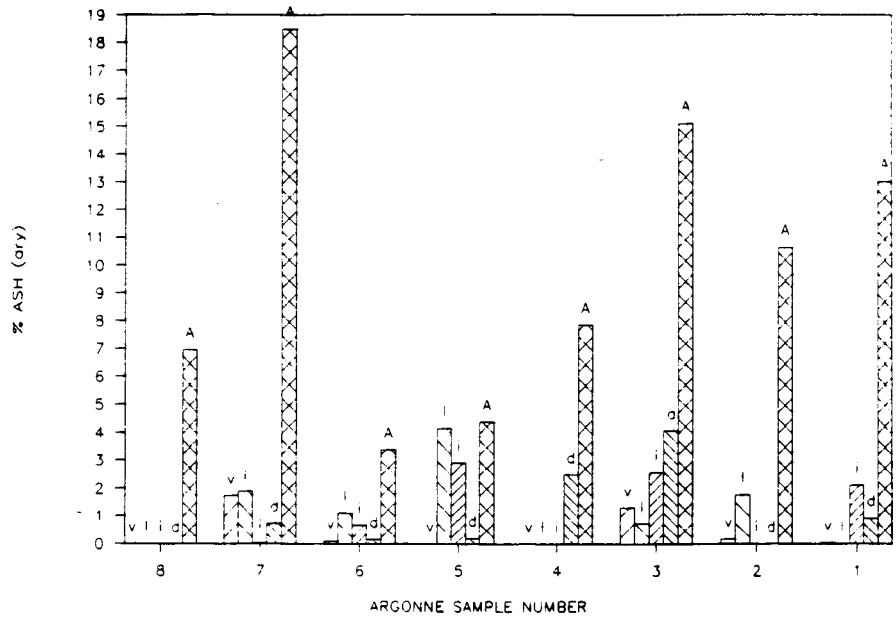

Figure B.18 TGA Ash Yields of Argonne Premium Coal Samples and Macerals Derived from Them. Data Demonstrates the Effect of Demineralization. Note That Not All Macerals Are Demineralized to the Same Extent.

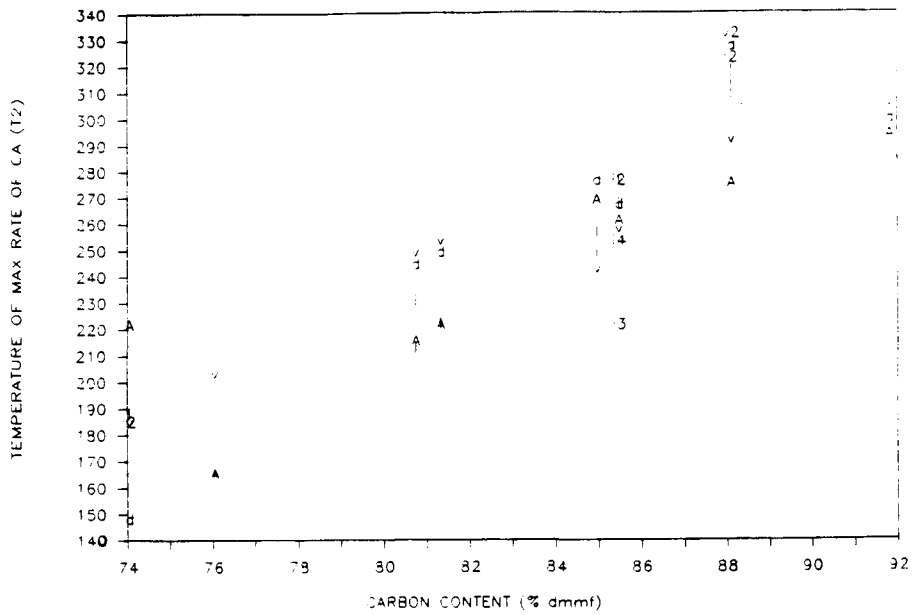

Figure B.19 The Effect of Carbon Content on TGA Combustion Profile Temperature 2 for Argonne Ground Coals, (A), Argonne Demineralized Coals, (d), Liptinites, (l), Vitrinites, (v), and Inertinites, (i).

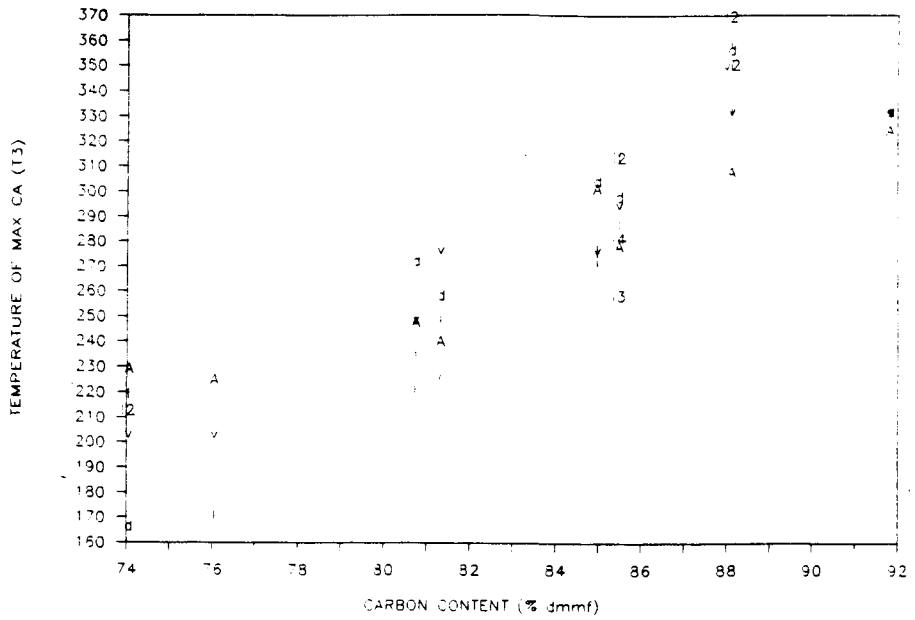

Figure B.20 The Effect of Carbon Content on TGA Combustion Profile Temperature 3 for Argonne Ground Coals, (A), Argonne Demineralized Coals, (d), Liptinites, (l), Vitrinites, (v), and Inertinites, (i).

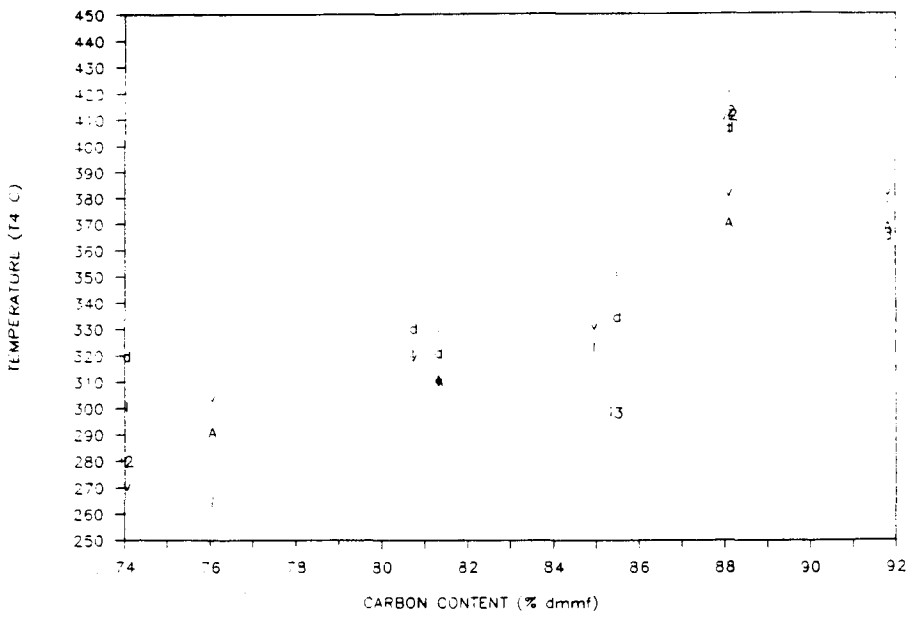

Figure B.21 The Effect of Carbon Content on TGA Combustion Profile Temperature 4 for Argonne Ground Coals, (A), Argonne Demineralized Coals, (d), Liptinites, (l), Vitrinites, (v), and Inertinites, (i).

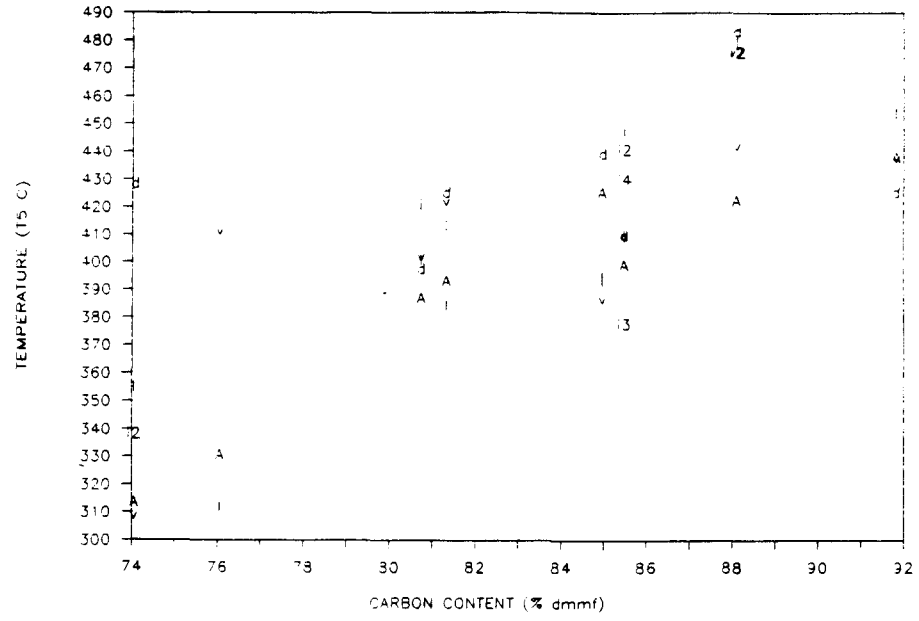

Figure B.22 The Effect of Carbon Content on TGA Combustion Profile Temperature 5 for Argonne Ground Coals, (A), Argonne Demineralized Coals, (d), Liptinites, (l), Vitrinites, (v), and Inertinites, (i).

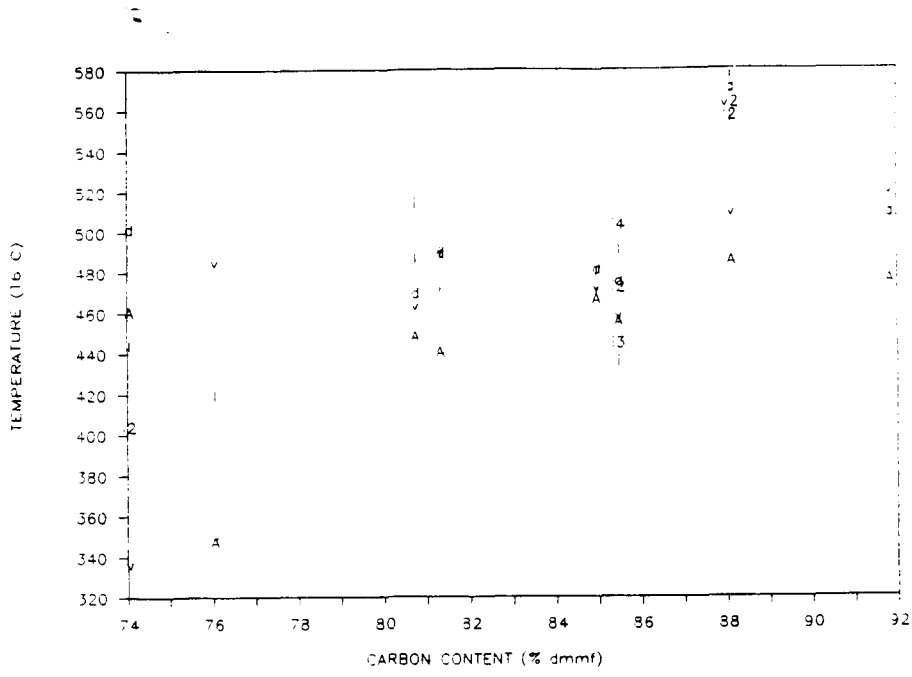

Figure B.23 The Effect of Carbon Content on TGA Combustion Profile Temperature 6 for Argonne Ground Coals, (A), Argonne Demineralized Coals, (d), Liptinites, (l), Vitrinites, (v), and Inertinites, (i).

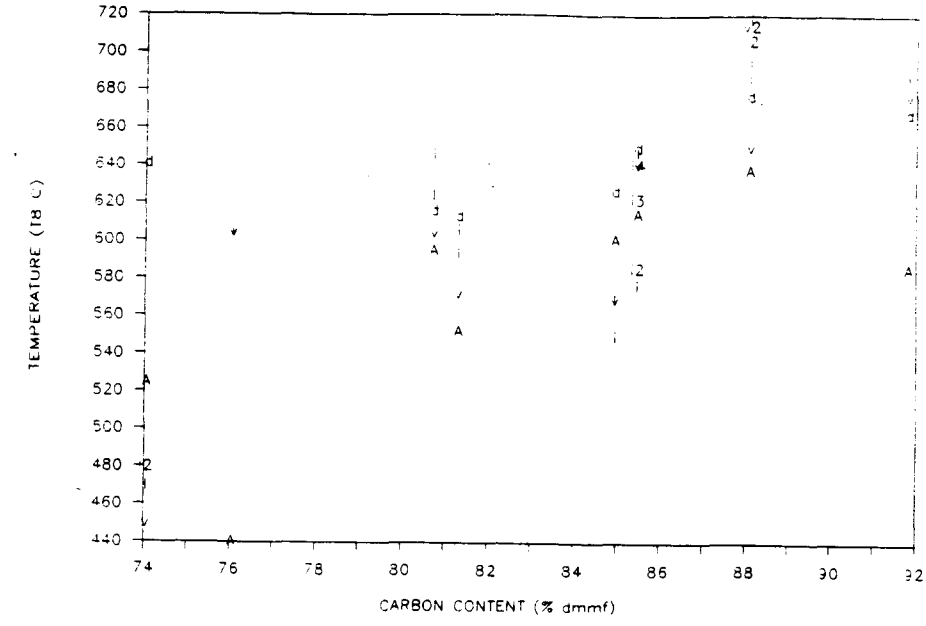

Figure B.24 The Effect of Carbon Content on TGA Combustion Profile Temperature 8 for Argonne Ground Coals, (A), Argonne Demineralized Coals, (d), Liptinites, (l), Vitrinites, (v), and Inertinites, (i).

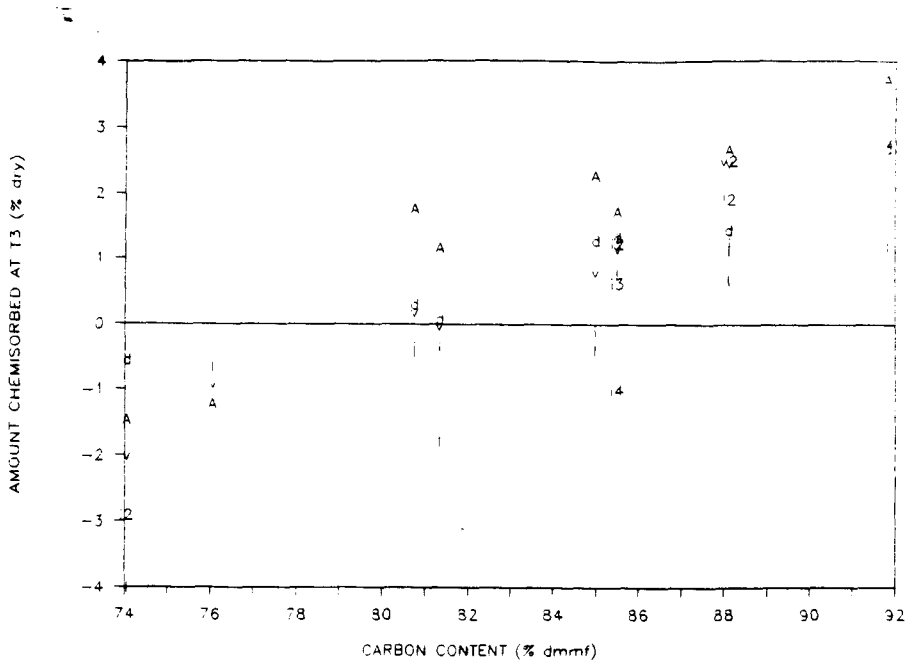

Figure B.25 The Effect of Carbon Content on TGA Combustion Profile Maximum Weight Chemisorbed for Argonne Ground Coals, (A), Argonne Demineralized Coals, (d), Liptinites, (l), Vitrinites, (v), and Inertinites, (i).

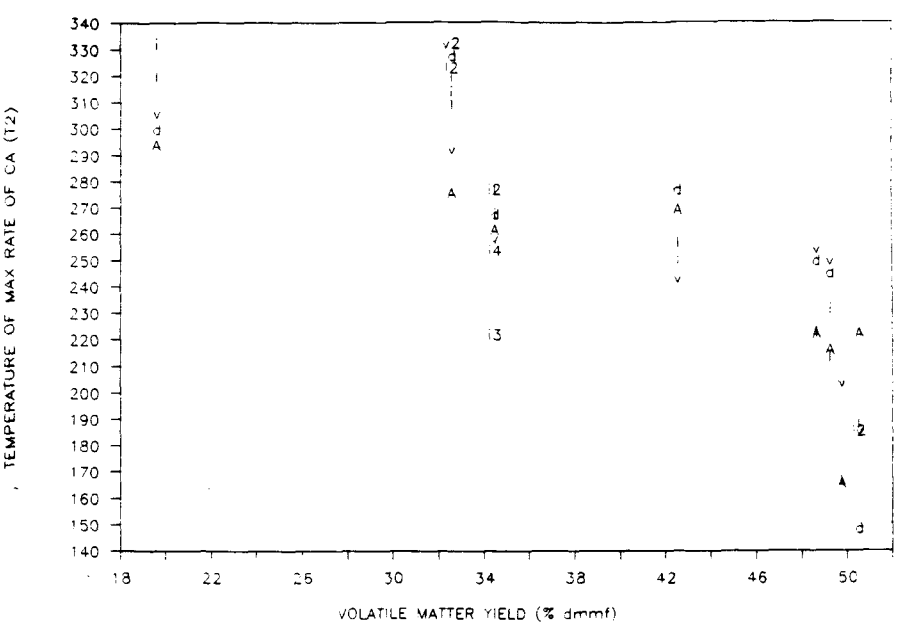

Figure B.26 The Effect of Volatile Matter Yield on TGA Combustion Profile Temperature 2 for Argonne Ground Coals, (A), Argonne Demineralized Coals, (d), Liptinites, (l), Vitrinites, (v), and Inertinites, (i).

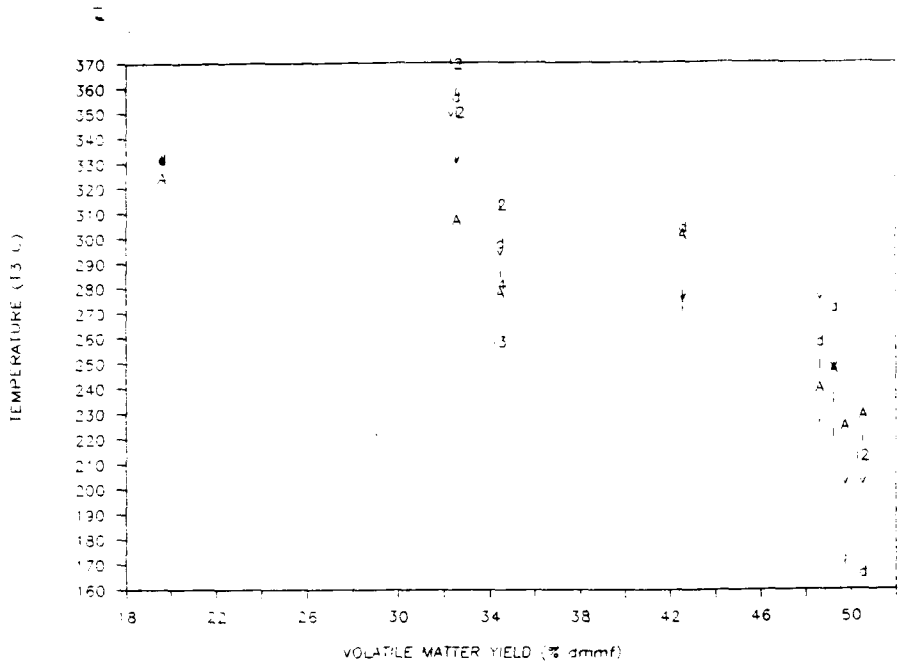

Figure B.27 The Effect of Volatile Matter Yield on TGA Combustion Profile Temperature 3 for Argonne Ground Coals, (A), Argonne Demineralized Coals, (d), Liptinites, (l), Vitrinites, (v), and Inertinites, (i).

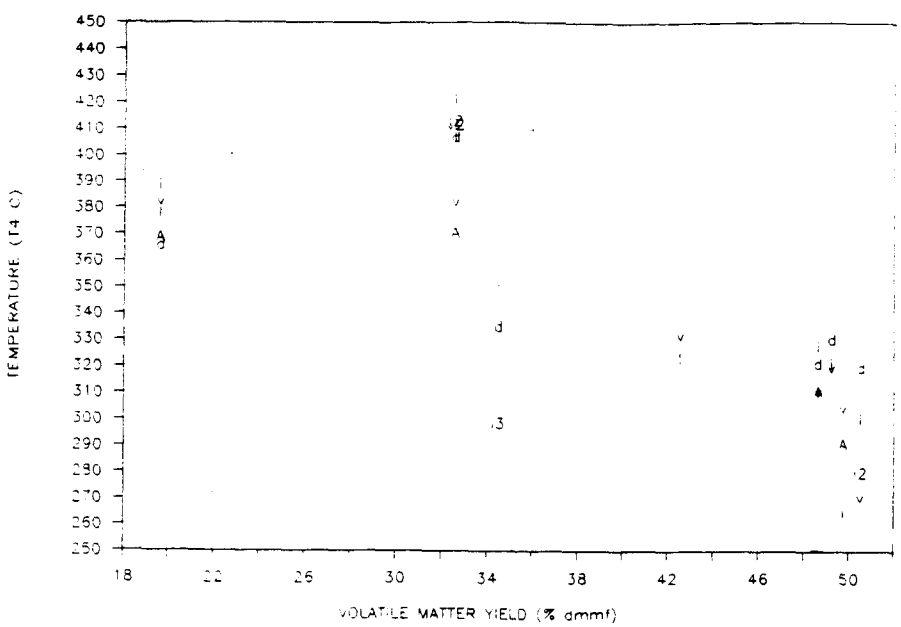

Figure B.28 The Effect of Volatile Matter Yield on TGA Combustion Profile Temperature 4 for Argonne Ground Coals, (A), Argonne Demineralized Coals, (d), Liptinites, (l), Vitrinites, (v), and Inertinites, (i).

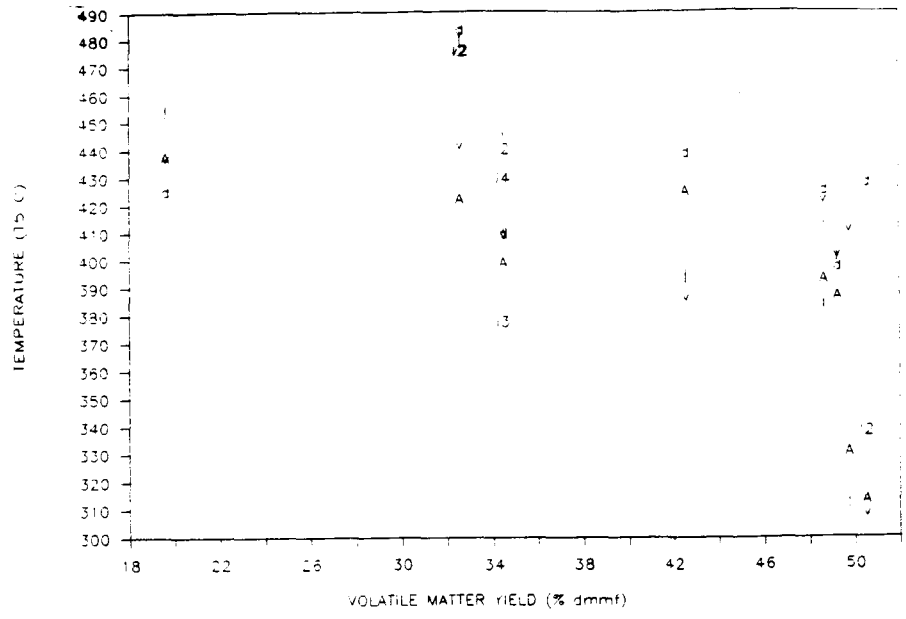

Figure B.29 The Effect of Volatile Matter Yield on TGA Combustion Profile Temperature 5 for Argonne Ground Coals, (A), Argonne Demineralized Coals, (d), Liptinites, (l), Vitrinites, (v), and Inertinites, (i).

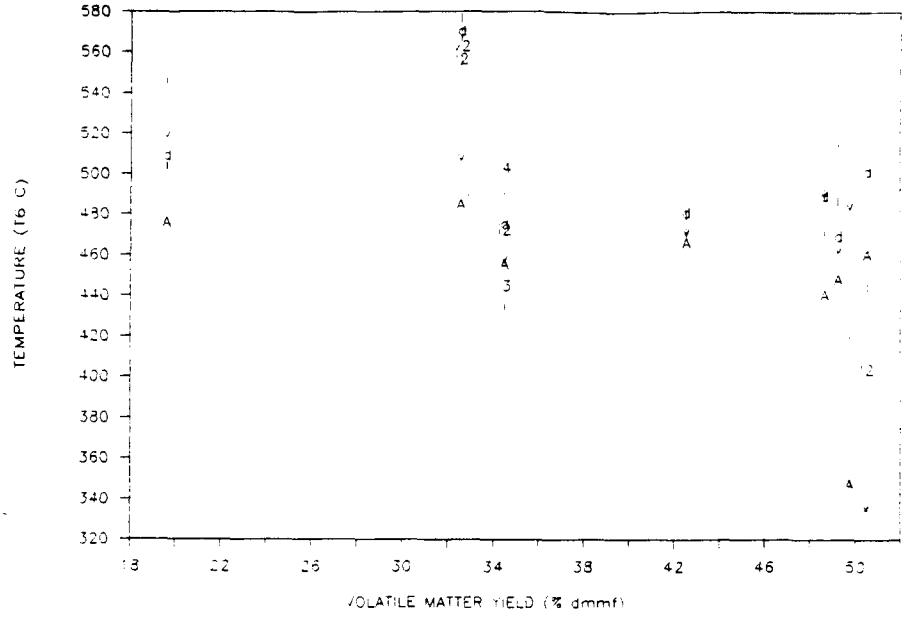

Figure B.30 The Effect of Volatile Matter Yield on TGA Combustion Profile Temperature 6 for Argonne Ground Coals, (A), Argonne Demineralized Coals, (d), Liptinites, (l), Vitrinites, (v), and Inertinites, (i).

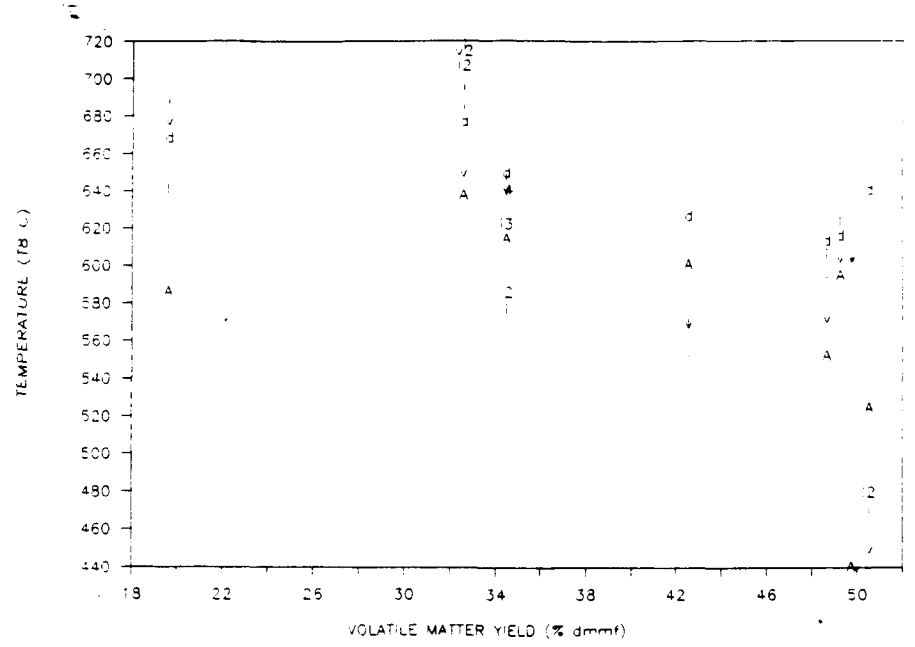

Figure B.31 The Effect of Volatile Matter Yield on TGA Combustion Profile Temperature 8 for Argonne Ground Coals, (A), Argonne Demineralized Coals, (d), Liptinites, (l), Vitrinites, (v), and Inertinites, (i).

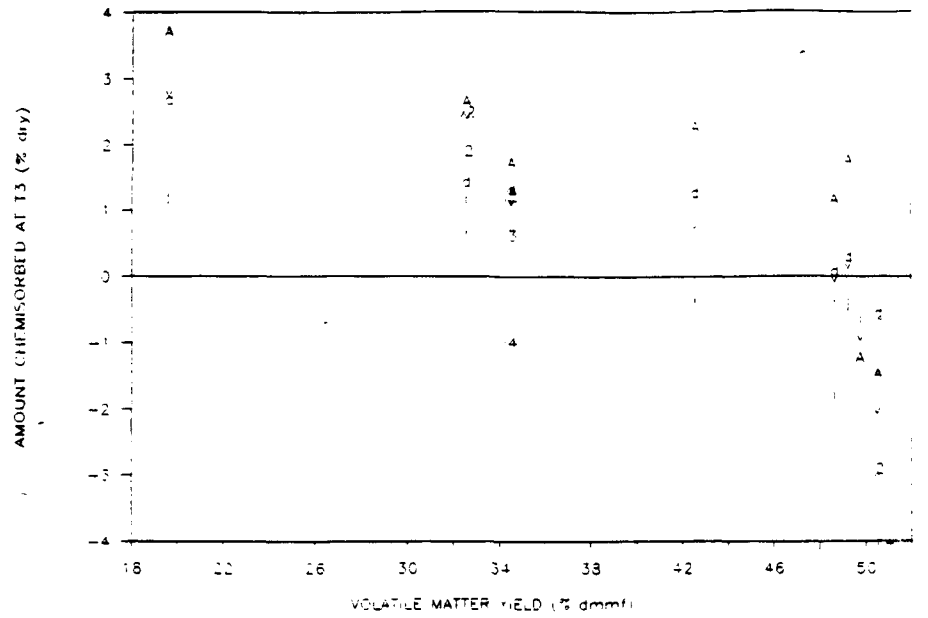

Figure B.32 The Effect of Volatile Matter Yield on TGA Combustion Profile Maximum Weight Chemisorbed for Argonne Ground Coals, (A), Argonne Demineralized Coals, (d), Liptinites, (l), Vitrinites, (v), and Inertinites, (i).

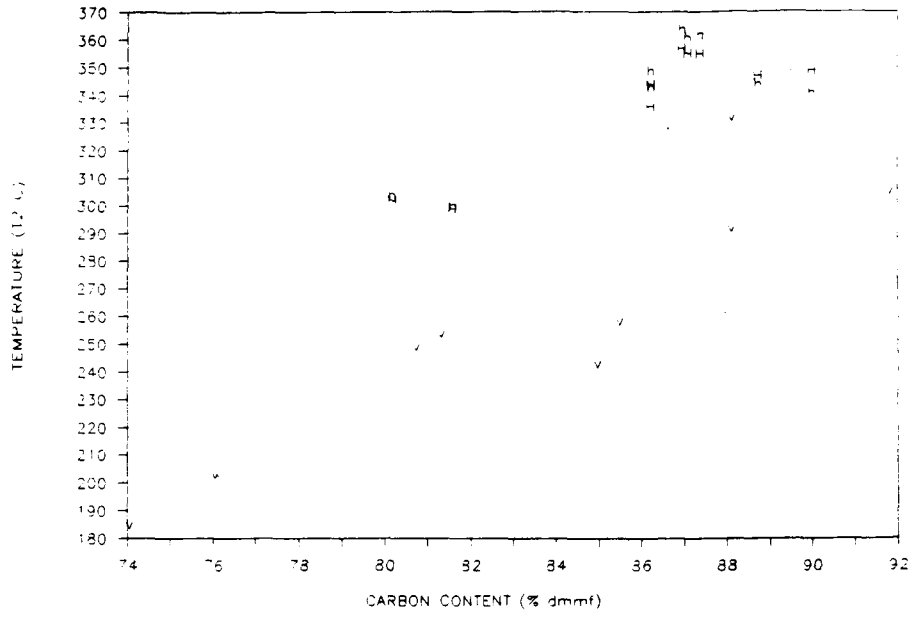

Figure B.33 The Effect of Carbon Content on TGA Combustion Profile Temperature 2 for Argonne Demineralized Vitrinites, (v), Hartshorne Raw Vitrinites, (H), and Hartshorne Demineralized Vitrinites, (h).

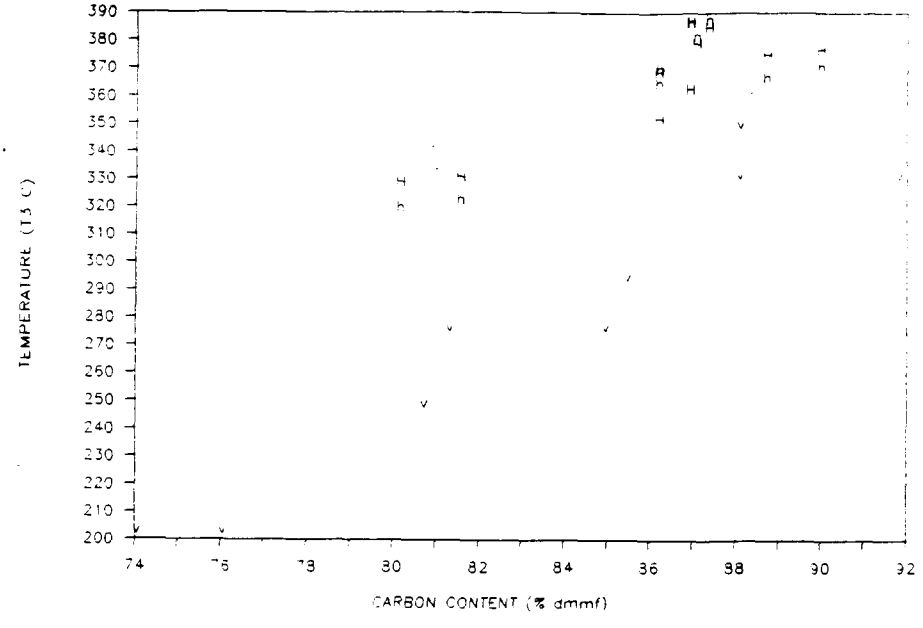

Figure B.34 The Effect of Carbon Content on TGA Combustion Profile Temperature 3 for Argonne Demineralized Vitrinites, (v), Hartshorne Raw Vitrinites, (H), and Hartshorne Demineralized Vitrinites, (h).

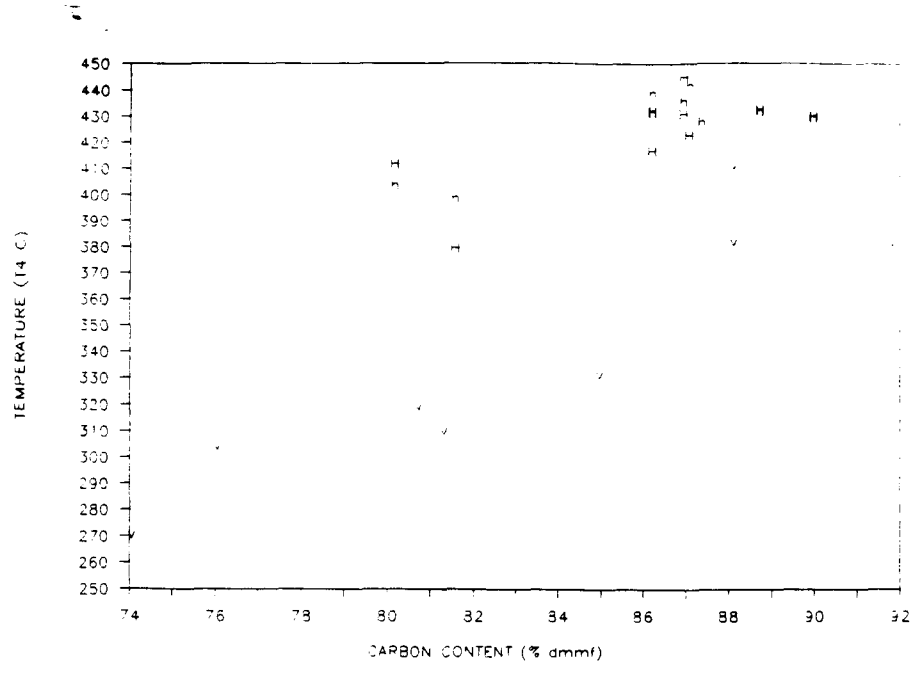

Figure B.35 The Effect of Carbon Content on TGA Combustion Profile Temperature 4 for Argonne Demineralized Vitrinites, (v), Hartshorne Raw Vitrinites, (H), and Hartshorne Demineralized Vitrinites, (h).

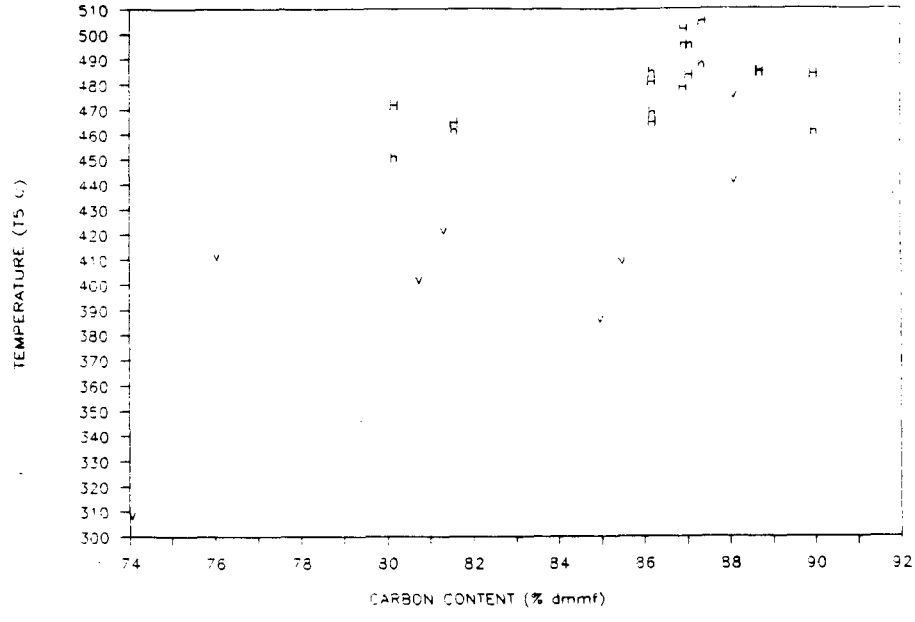

Figure B.36 The Effect of Carbon Content on TGA Combustion Profile Temperature 5 for Argonne Demineralized Vitrinites, (v), Hartshorne Raw Vitrinites, (H), and Hartshorne Demineralized Vitrinites, (h).

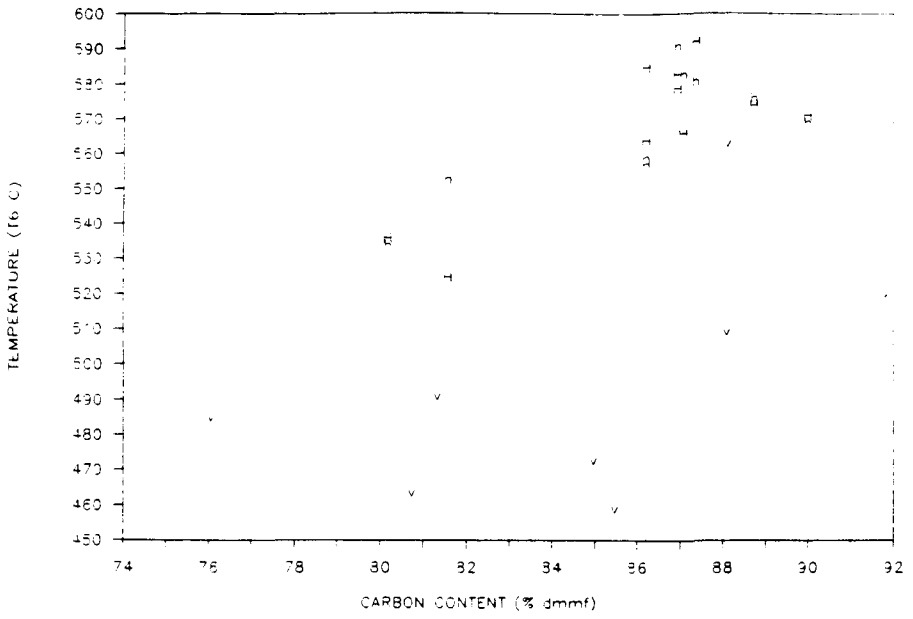

Figure B.37 The Effect of Carbon Content on TGA Combustion Profile Temperature 6 for Argonne Demineralized Vitrinites, (v), Hartshorne Raw Vitrinites, (H), and Hartshorne Demineralized Vitrinites, (h).

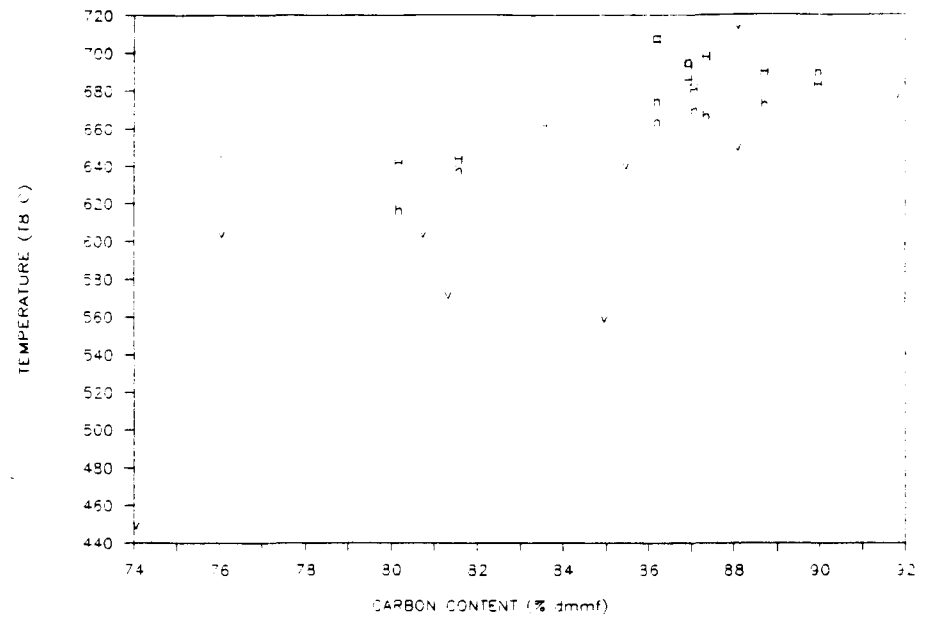

Figure B.38 The Effect of Carbon Content on TGA Combustion Profile Temperature 8 for Argonne Demineralized Vitrinites, (v), Hartshorne Raw Vitrinites, (H), and Hartshorne Demineralized Vitrinites, (h).

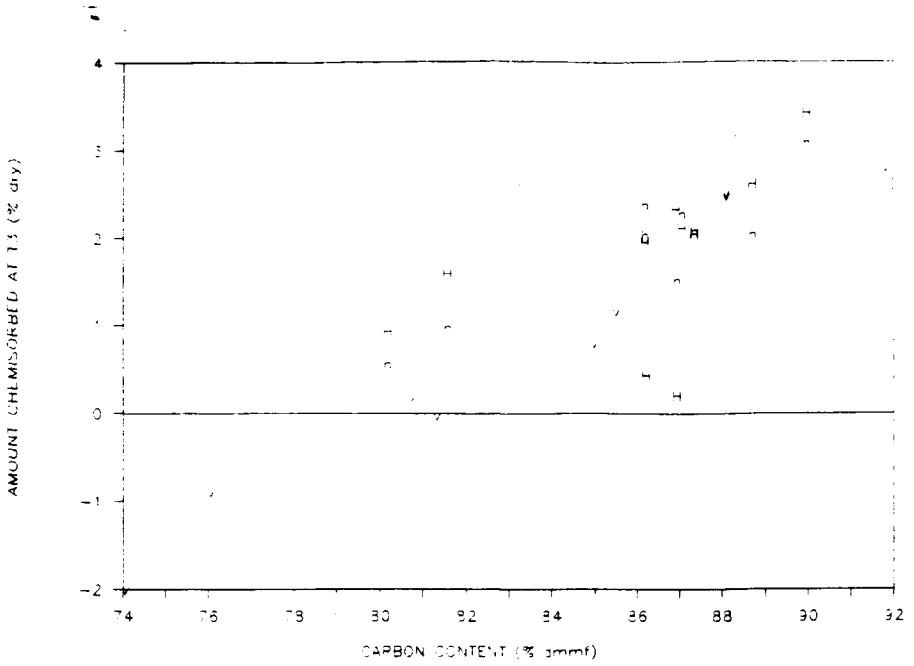

Figure B.39 The Effect of Carbon Content on TGA Combustion Profile Maximum Weight Chemisorbed for Argonne Demineralized Vitrinites, (v), Hartshorne Raw Vitrinites, (H), and Hartshorne Demineralized Vitrinites, (h).

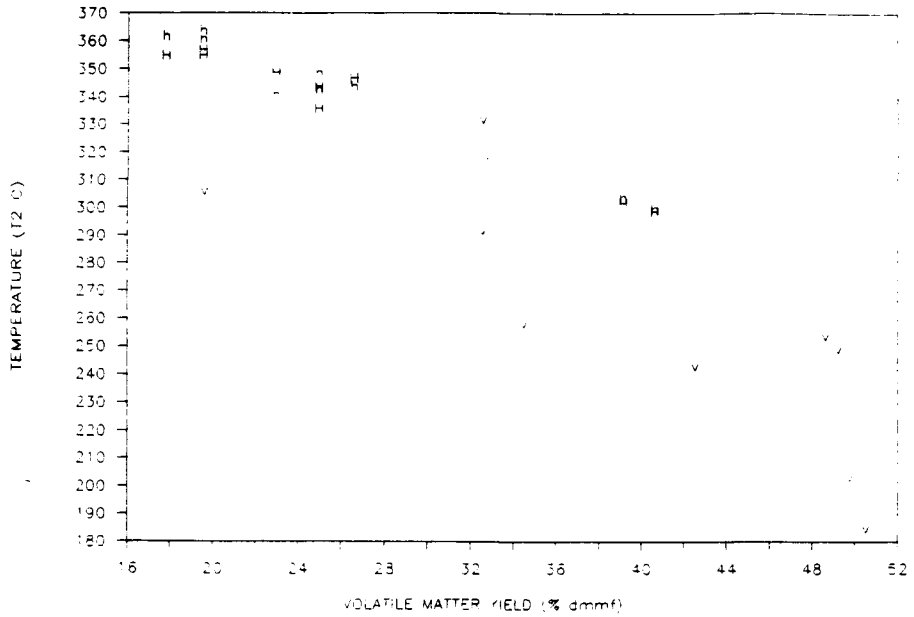

Figure B.40 The Effect of Volatile Matter Yield on TGA Combustion Profile Temperature 2 for Argonne Demineralized Vitrinites, (v), Hartshorne Raw Vitrinites, (H), and Hartshorne Demineralized Vitrinites, (h).

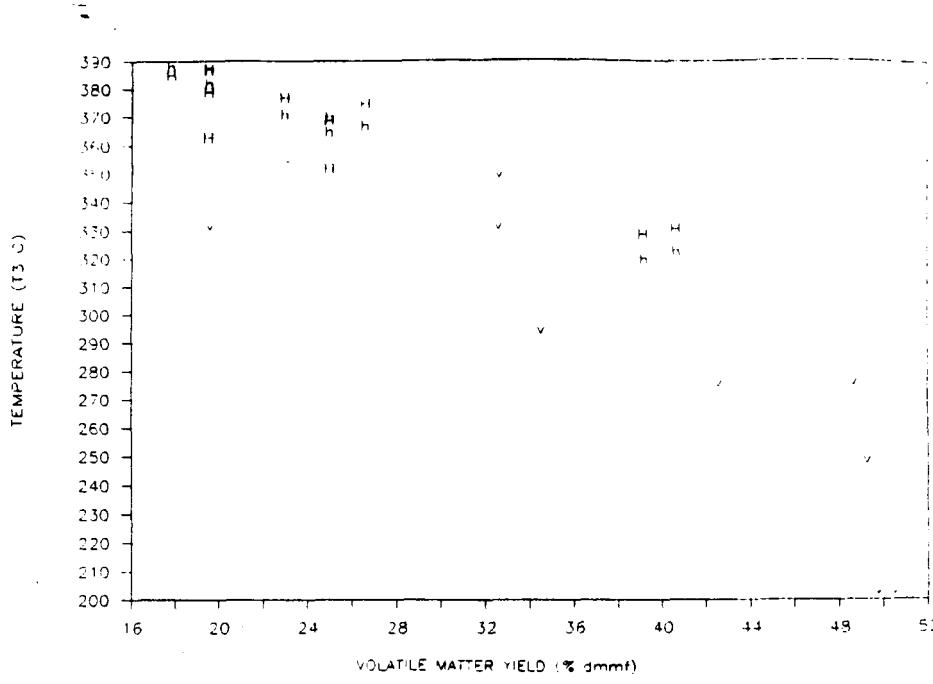

Figure B.41 The Effect of Volatile Matter Yield on TGA Combustion Profile Temperature 3 for Argonne Demineralized Vitrinites, (v), Hartshorne Raw Vitrinites, (H), and Hartshorne Demineralized Vitrinites, (h).

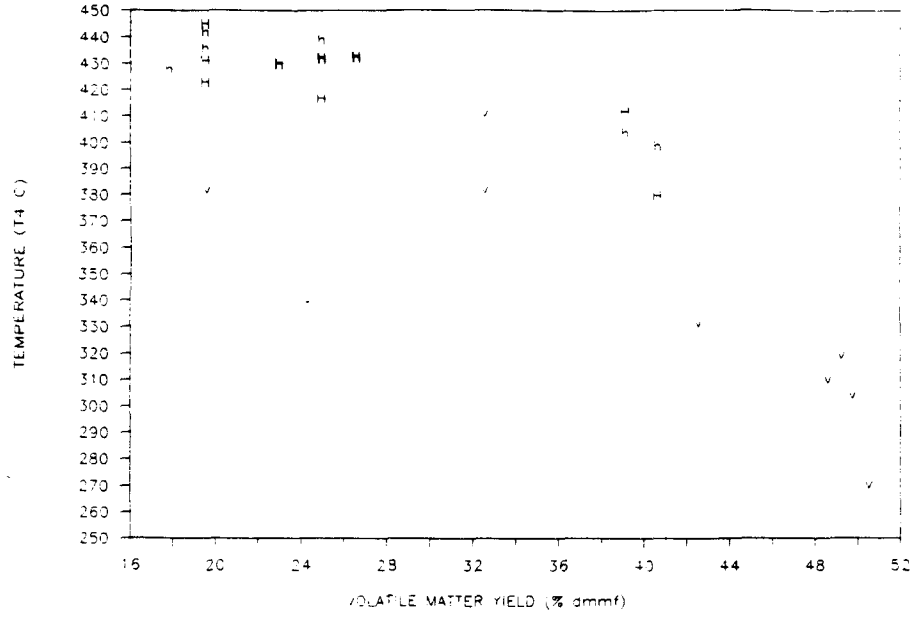

Figure B.42 The Effect of Volatile Matter Yield on TGA Combustion Profile Temperature 4 for Argonne Demineralized Vitrinites, (v), Hartshorne Raw Vitrinites, (H), and Hartshorne Demineralized Vitrinites, (h).

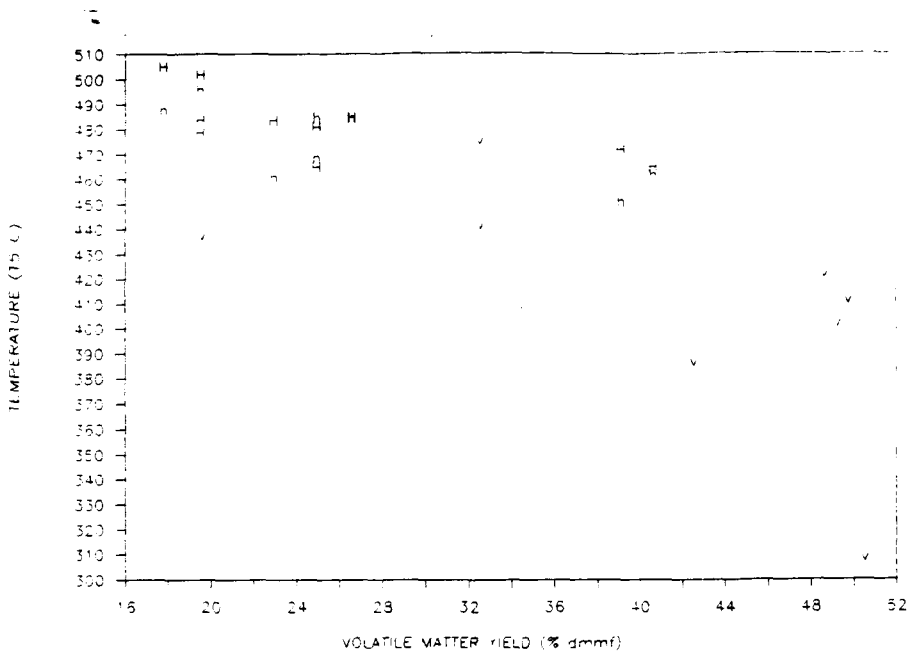

Figure B.43 The Effect of Volatile Matter Yield on TGA Combustion Profile Temperature 5 for Argonne Demineralized Vitrinites, (v), Hartshorne Raw Vitrinites, (H), and Hartshorne Demineralized Vitrinites, (h).

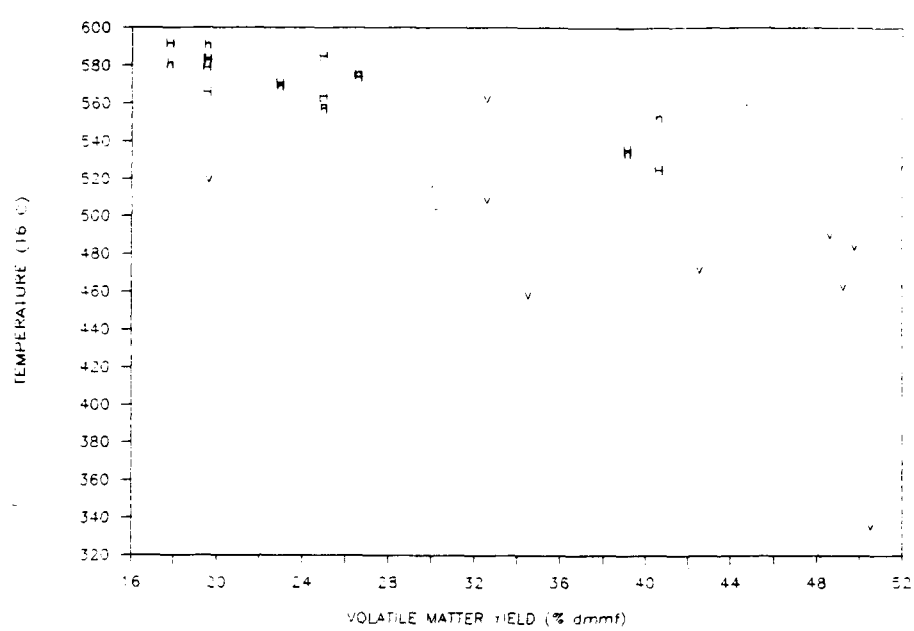

Figure B.44 The Effect of Volatile Matter Yield on TGA Combustion Profile Temperature 6 for Argonne Demineralized Vitrinites, (v), Hartshorne Raw Vitrinites, (H), and Hartshorne Demineralized Vitrinites, (h).

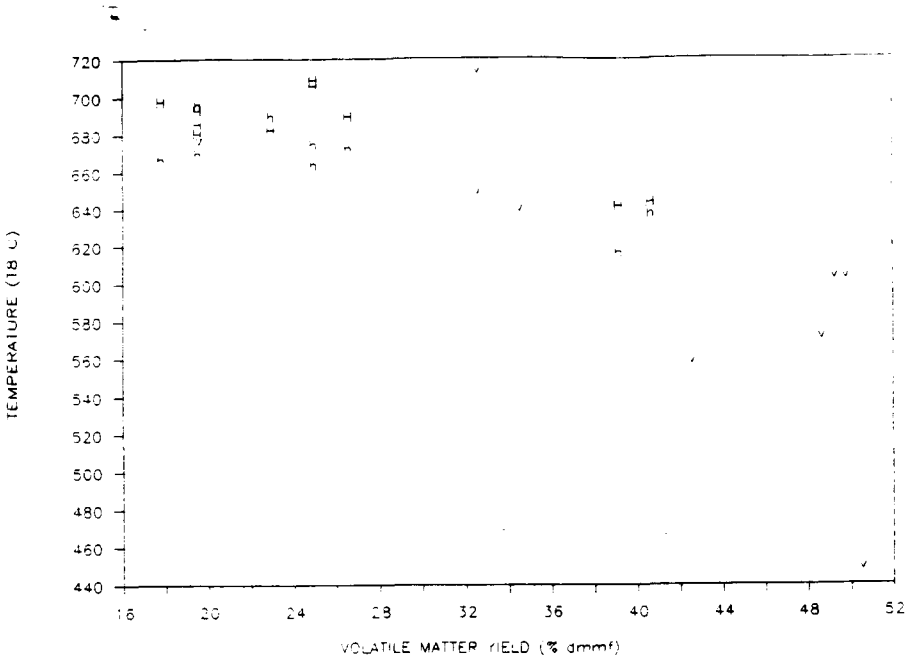

Figure B.45 The Effect of Volatile Matter Yield on TGA Combustion Profile Temperature 8 for Argonne Demineralized Vitrinites, (v), Hartshorne Raw Vitrinites, (H), and Hartshorne Demineralized Vitrinites, (h).

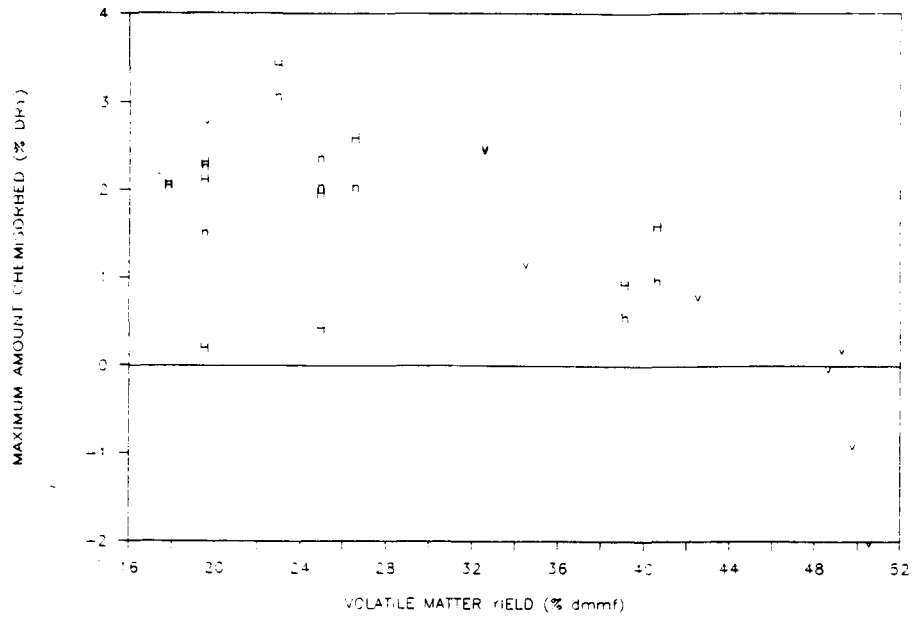

Figure B.46 The Effect of Volatile Matter Yield on TGA Combustion Profile Maximum Weight Chemisorbed for Argonne Ground Coals, (A), Argonne Demineralized Coals, (d), Liptinites, (l), Vitrinites, (v), and Inertinites, (i).

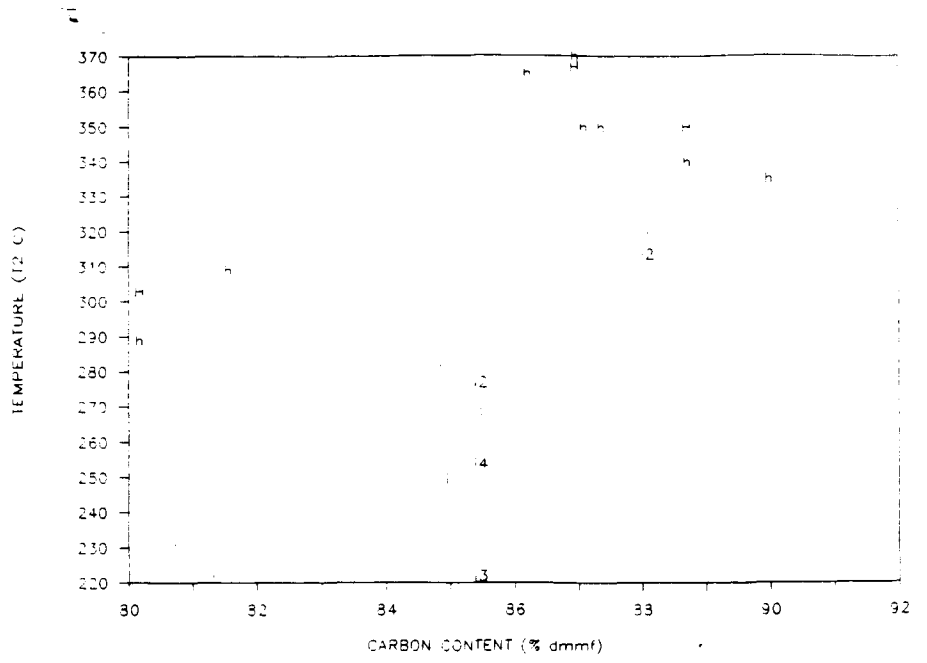

Figure B.47 The Effect of Carbon Content on TGA Combustion Profile Temperature 2 for Argonne Demineralized Inertinites, (i), Hartshorne Raw Inertinites, (H), and Hartshorne Demineralized Inertinites, (h).

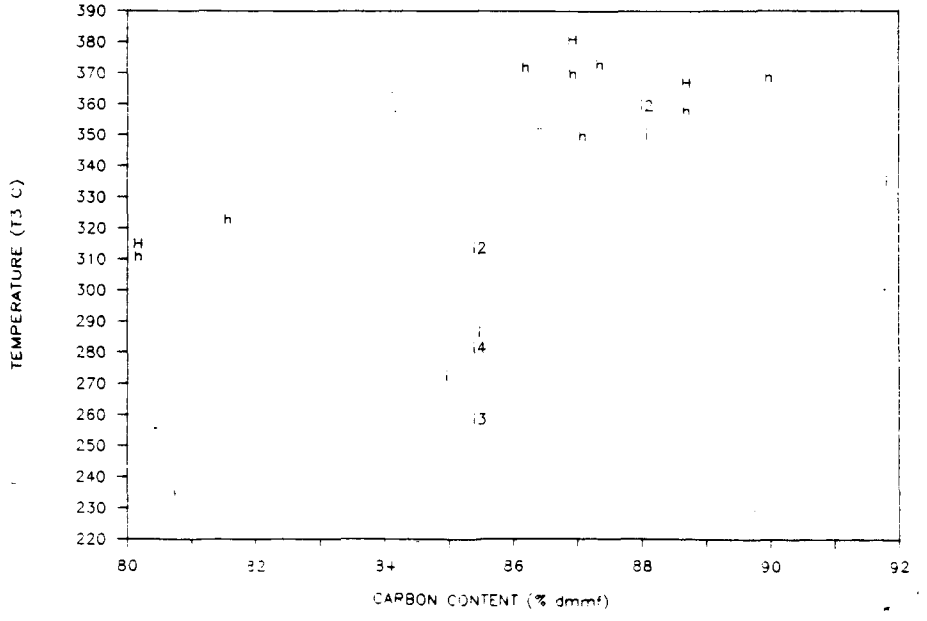

Figure B.48 The Effect of Carbon Content on TGA Combustion Profile Temperature 3 for Argonne Demineralized Inertinites, (i), Hartshorne Raw Inertinites, (H), and Hartshorne Demineralized Inertinites, (h).

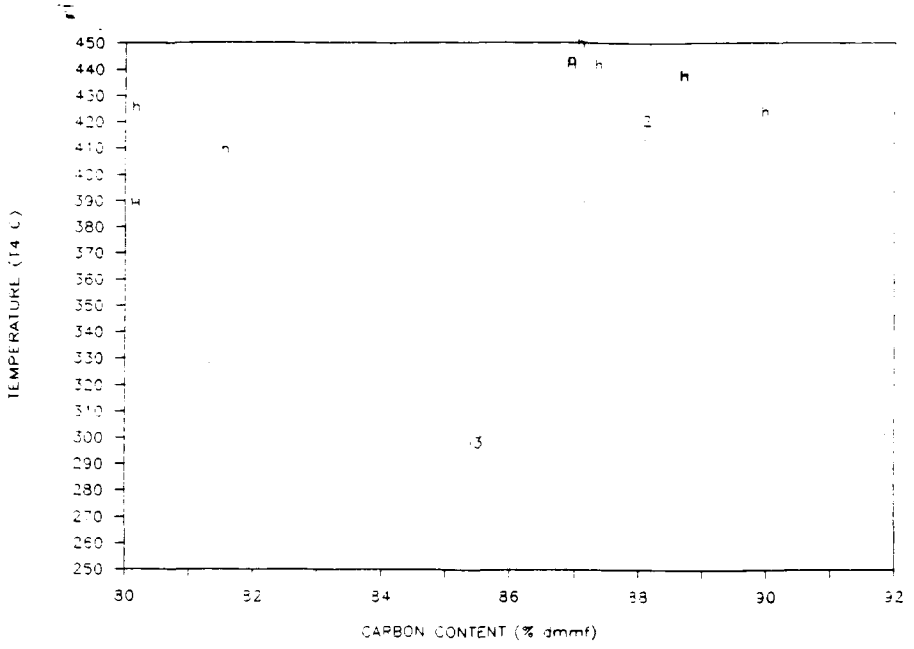

Figure B.49 The Effect of Carbon Content on TGA Combustion Profile Temperature 4 for Argonne Demineralized Inertinites, (i), Hartshorne Raw Inertinites, (H), and Hartshorne Demineralized Inertinites, (h).

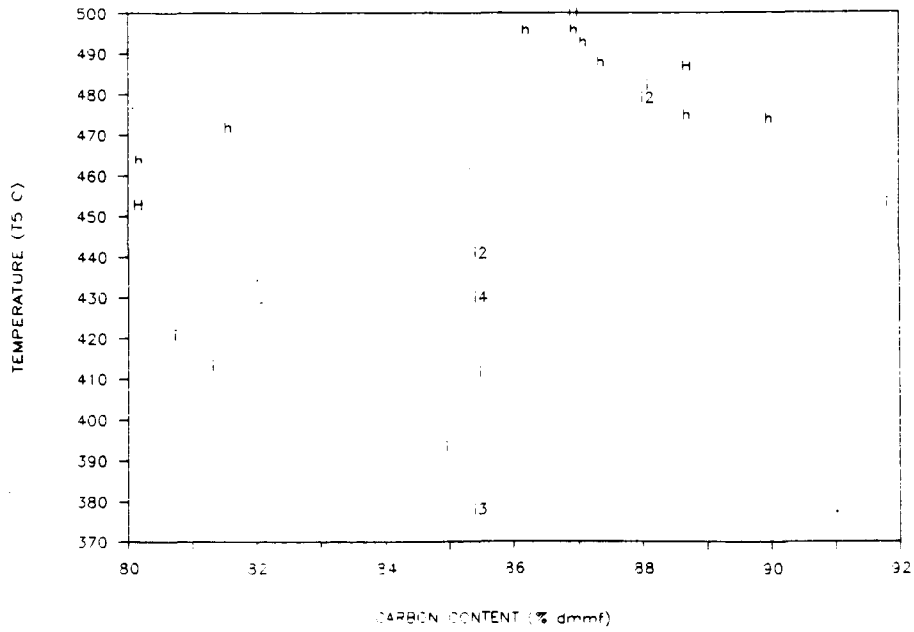

Figure B.50 The Effect of Carbon Content on TGA Combustion Profile Temperature 5 for Argonne Demineralized Inertinites, (i), Hartshorne Raw Inertinites, (H), and Hartshorne Demineralized Inertinites, (h).

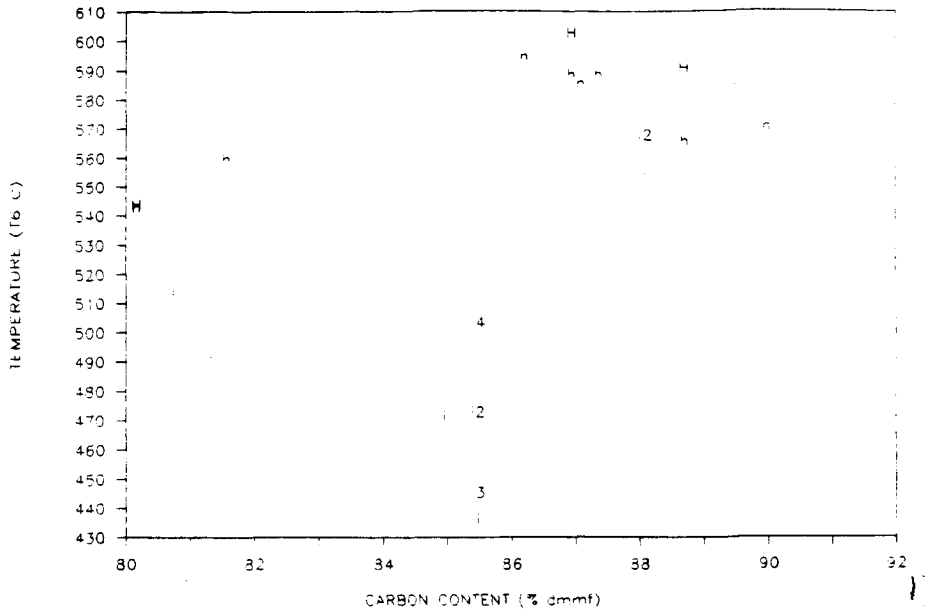

Figure B.51 The Effect of Carbon Content on TGA Combustion Profile Temperature 6 for Argonne Demineralized Inertinites, (i), Hartshorne Raw Inertinites, (H), and Hartshorne Demineralized Inertinites, (h).

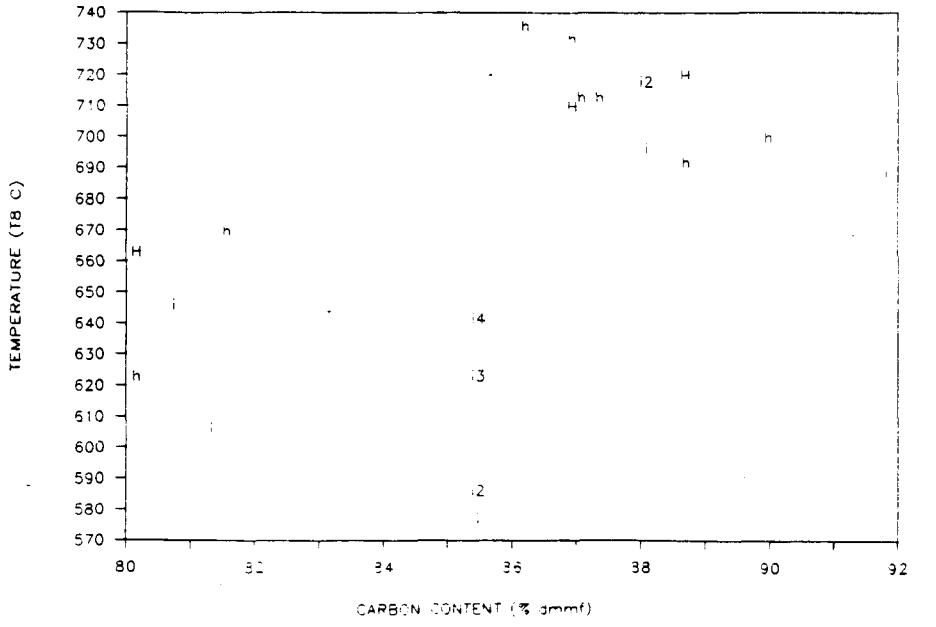

Figure B.52 The Effect of Carbon Content on TGA Combustion Profile Temperature 8 for Argonne Demineralized Inertinites, (i), Hartshorne Raw Inertinites, (H), and Hartshorne Demineralized Inertinites, (h).

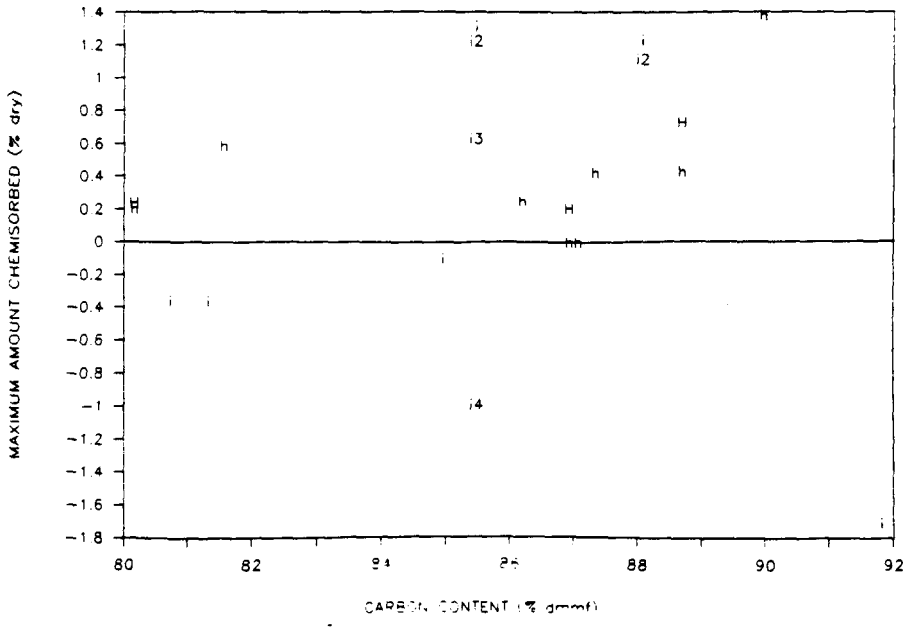

Figure B.53 The Effect of Carbon Content on TGA Combustion Profile Maximum Weight Chemisorbed for Argonne Demineralized Inertinites, (i), Hartshorne Raw Inertinites, (H), and Hartshorne Demineralized Inertinites, (h).

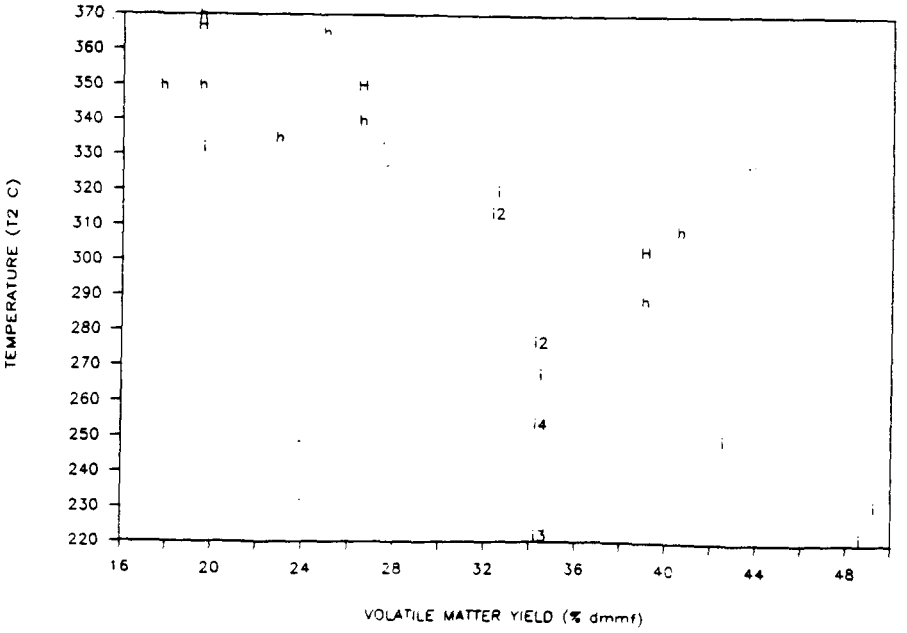

Figure B.54 The Effect of Volatile Matter Yield on TGA Combustion Profile Temperature 2 for Argonne Demineralized Inertinites, (i), Hartshorne Raw Inertinites, (H), and Hartshorne Demineralized Inertinites, (h).

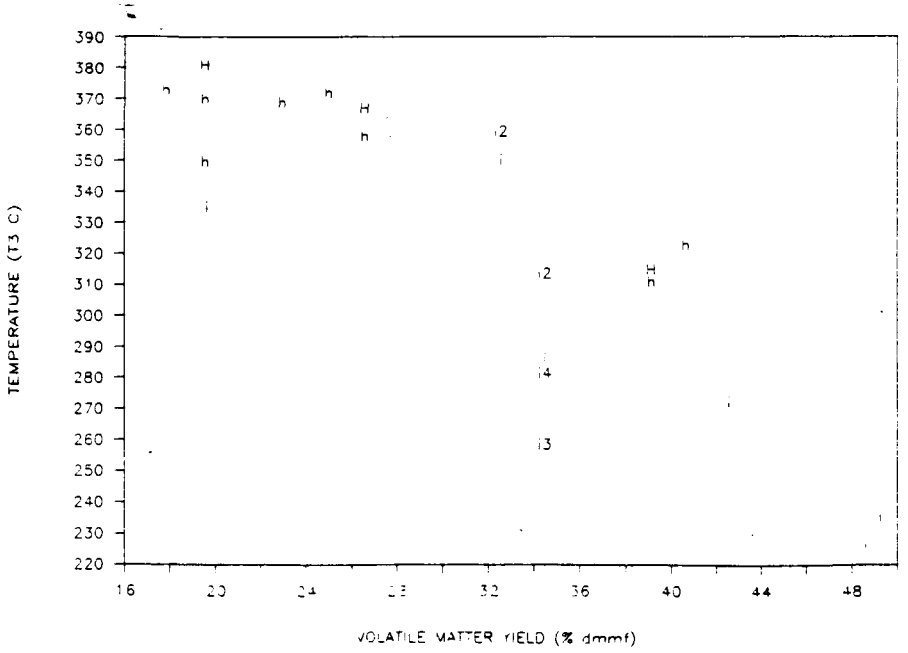

Figure B.55 The Effect of Volatile Matter Yield on TGA Combustion Profile Temperature 3 for Argonne Demineralized Inertinites, (i), Hartshorne Raw Inertinites, (H), and Hartshorne Demineralized Inertinites, (h).

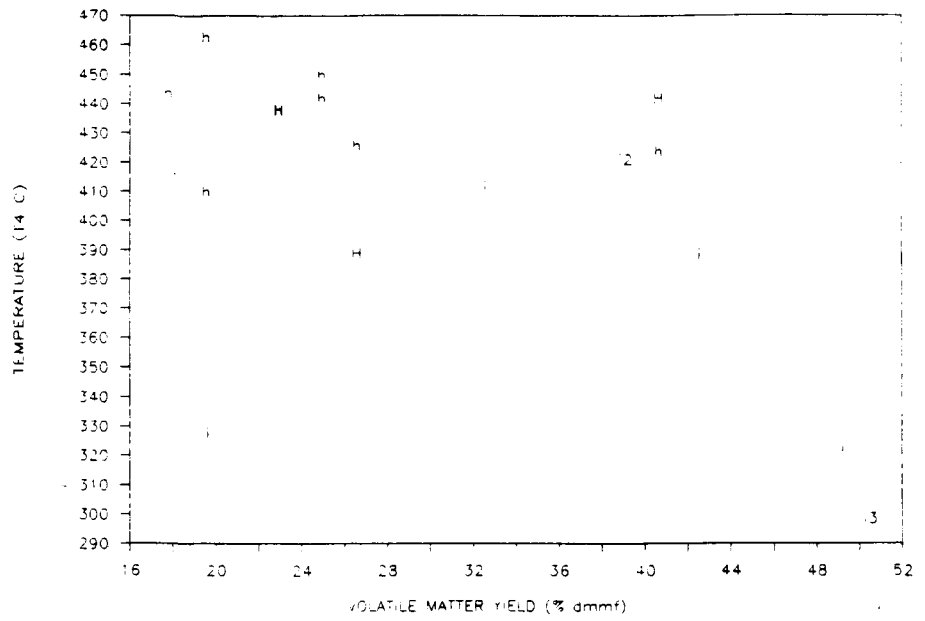

Figure B.56 The Effect of Volatile Matter Yield on TGA Combustion Profile Temperature 4 for Argonne Demineralized Inertinites, (i), Hartshorne Raw Inertinites, (H), and Hartshorne Demineralized Inertinites, (h).

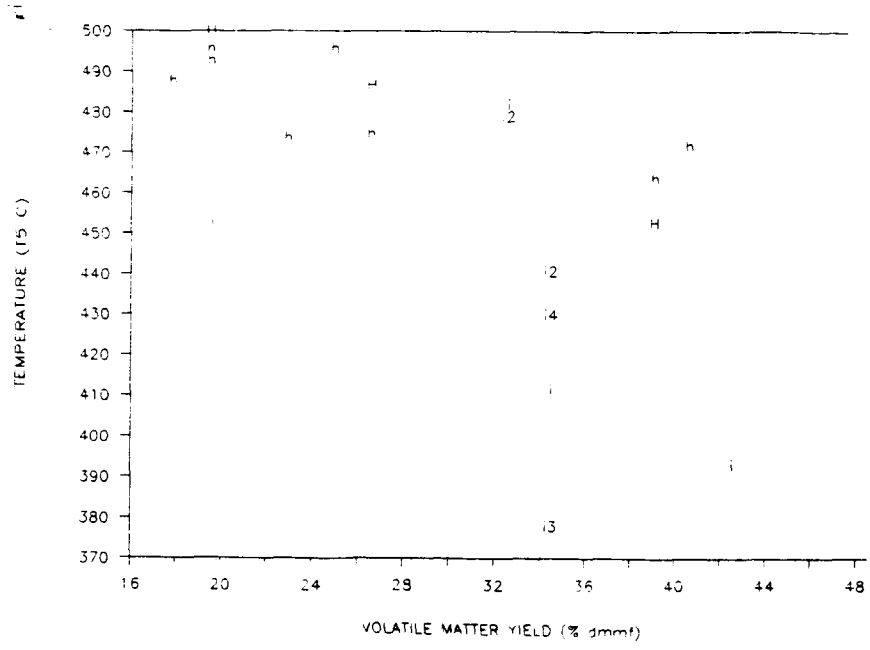

Figure B.57 The Effect of Volatile Matter Yield on TGA Combustion Profile Temperature 5 for Argonne Demineralized Inertinites, (i), Hartshorne Raw Inertinites, (H), and Hartshorne Demineralized Inertinites, (h).

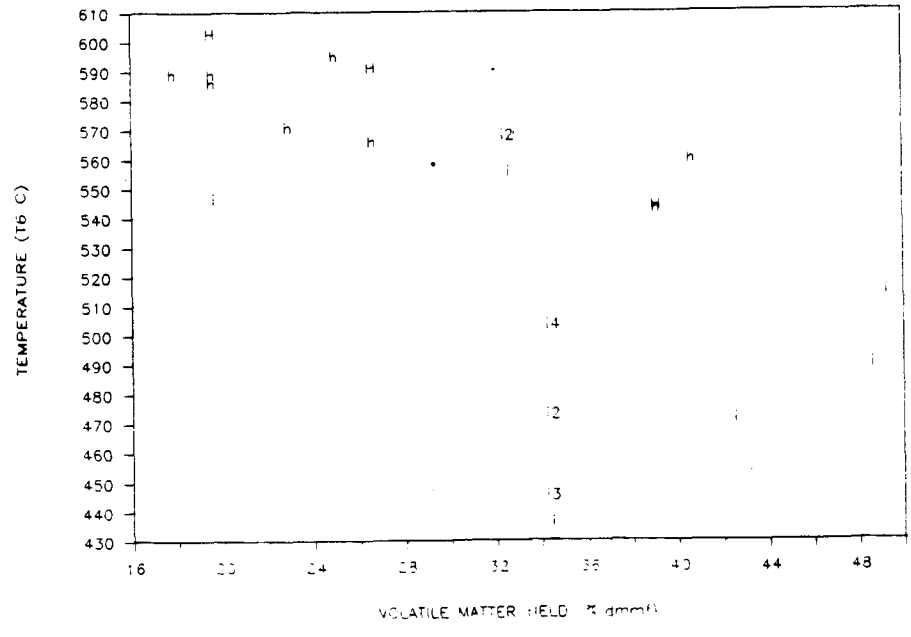

Figure B.58 The Effect of Volatile Matter Yield on TGA Combustion Profile Temperature 6 for Argonne Demineralized Inertinites, (i), Hartshorne Raw Inertinites, (H), and Hartshorne Demineralized Inertinites, (h).

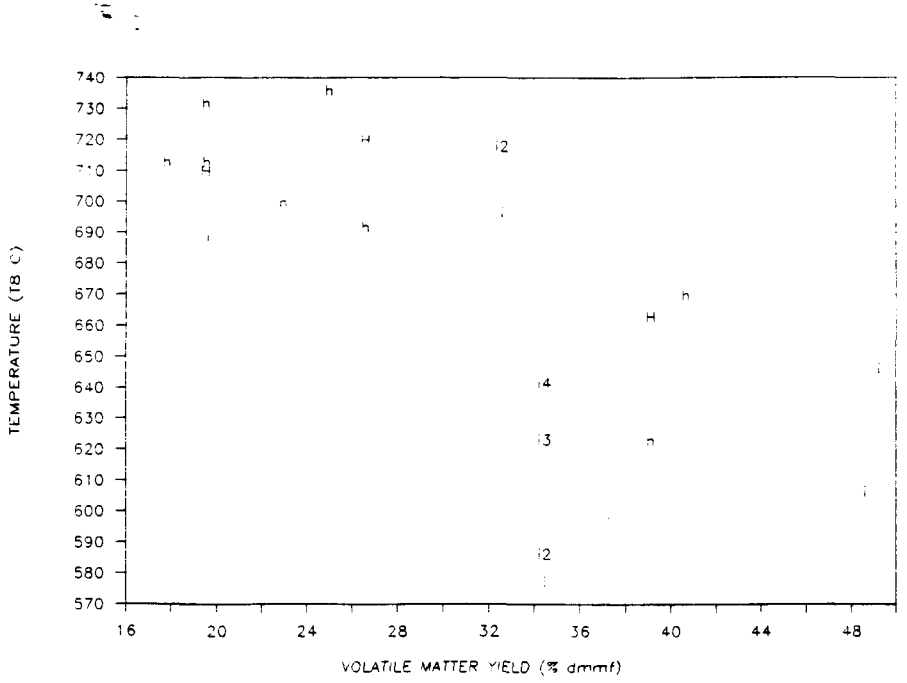

Figure B.59 The Effect of Volatile Matter Yield on TGA Combustion Profile Temperature 8 for Argonne Demineralized Inertinites, (i), Hartshorne Raw Inertinites, (H), and Hartshorne Demineralized Inertinites, (h).

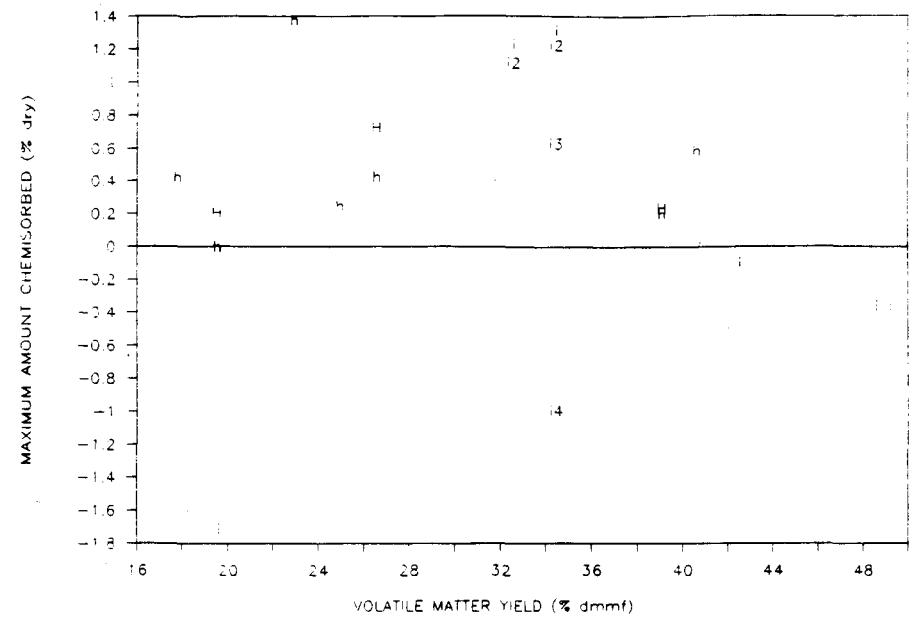

Figure B.60 The Effect of Volatile Matter Yield on TGA Combustion Profile Maximum Weight Chemisorbed for Argonne Demineralized Inertinites, (i), Hartshorne Raw Inertinites, (H), and Hartshorne Demineralized Inertinites, (h).

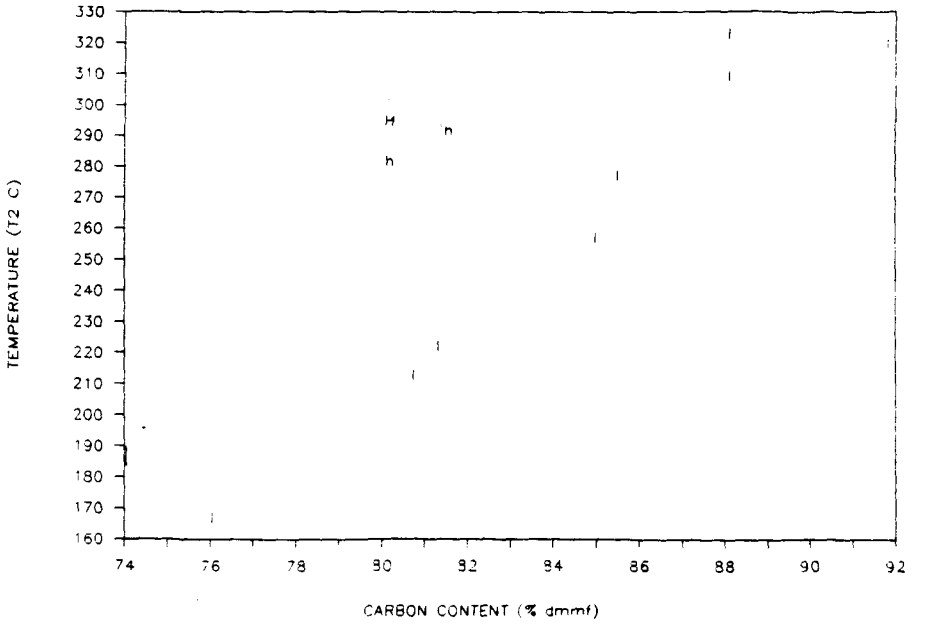

Figure B.61 The Effect of Carbon Content on TGA Combustion Profile Temperature 2 for Argonne Demineralized Liptinites, (l), Hartshorne Raw Liptinites, (H), and Hartshorne Demineralized Liptinites, (h).

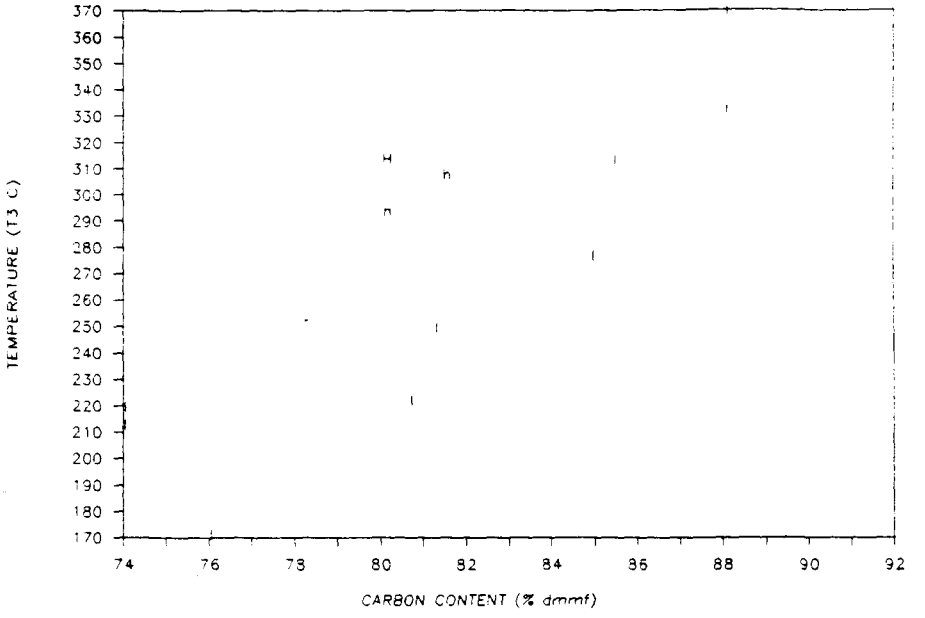

Figure B.62 The Effect of Carbon Content on TGA Combustion Profile Temperature 3 for Argonne Demineralized Liptinites, (l), Hartshorne Raw Liptinites, (H), and Hartshorne Demineralized Liptinites, (h).

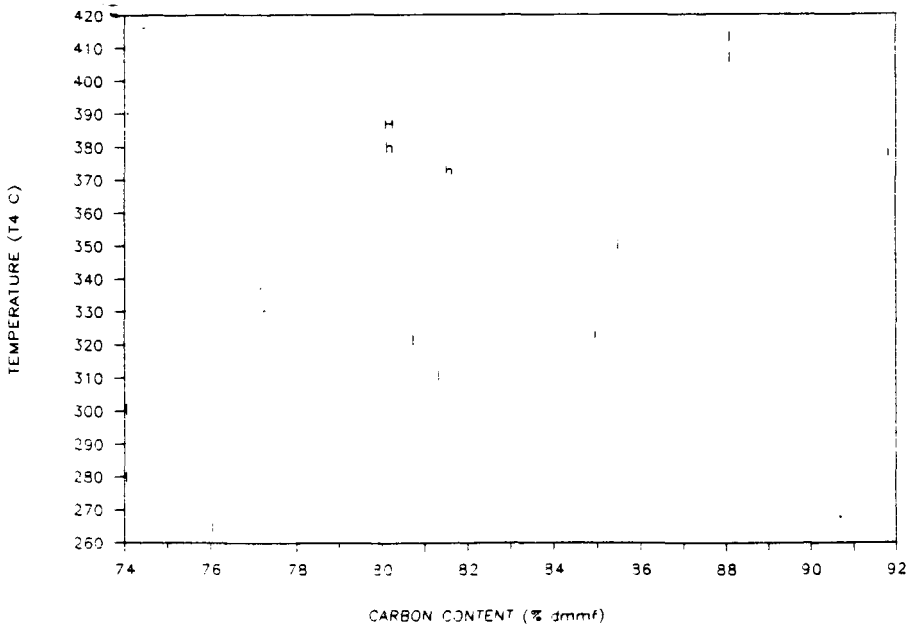

Figure B.63 The Effect of Carbon Content on TGA Combustion Profile Temperature 4 for Argonne Demineralized Liptinites, (l), Hartshorne Raw Liptinites, (H), and Hartshorne Demineralized Liptinites, (h).

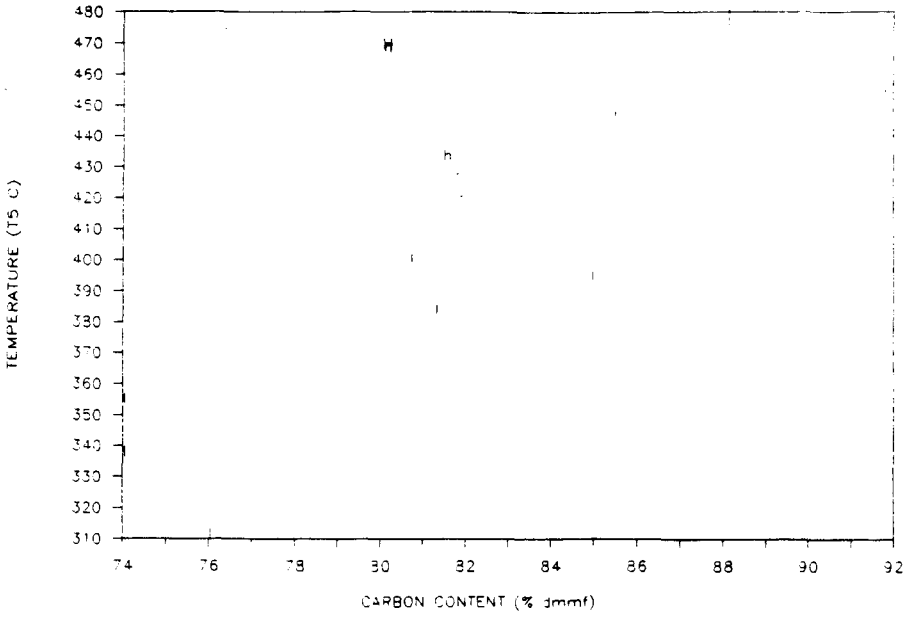

Figure B.64 The Effect of Carbon Content on TGA Combustion Profile Temperature 5 for Argonne Demineralized Liptinites, (l), Hartshorne Raw Liptinites, (H), and Hartshorne Demineralized Liptinites, (h).

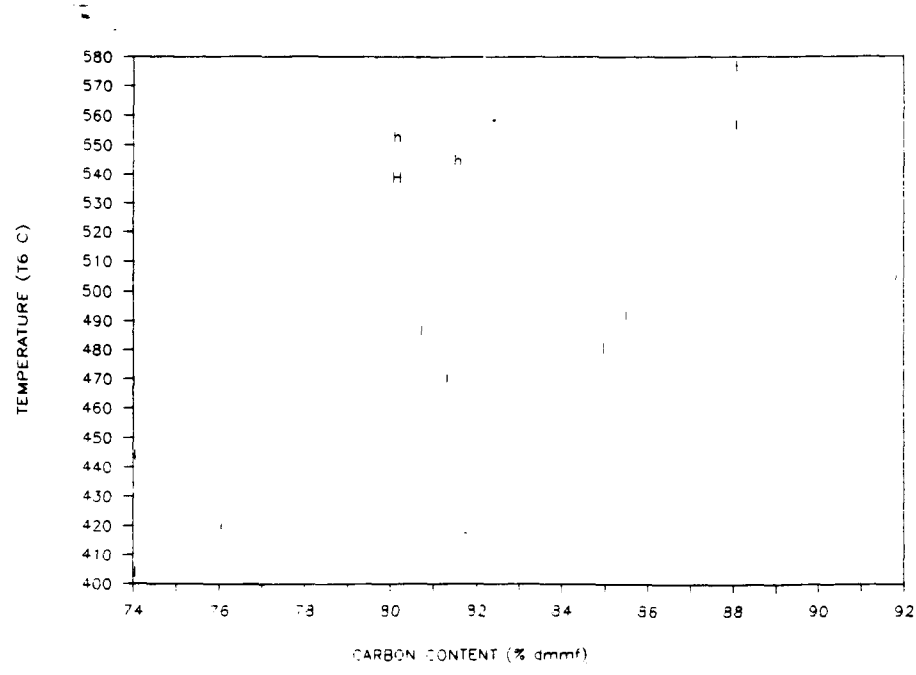

Figure B.65 The Effect of Carbon Content on TGA Combustion Profile Temperature 6 for Argonne Demineralized Liptinites, (l), Hartshorne Raw Liptinites, (H), and Hartshorne Demineralized Liptinites, (h).

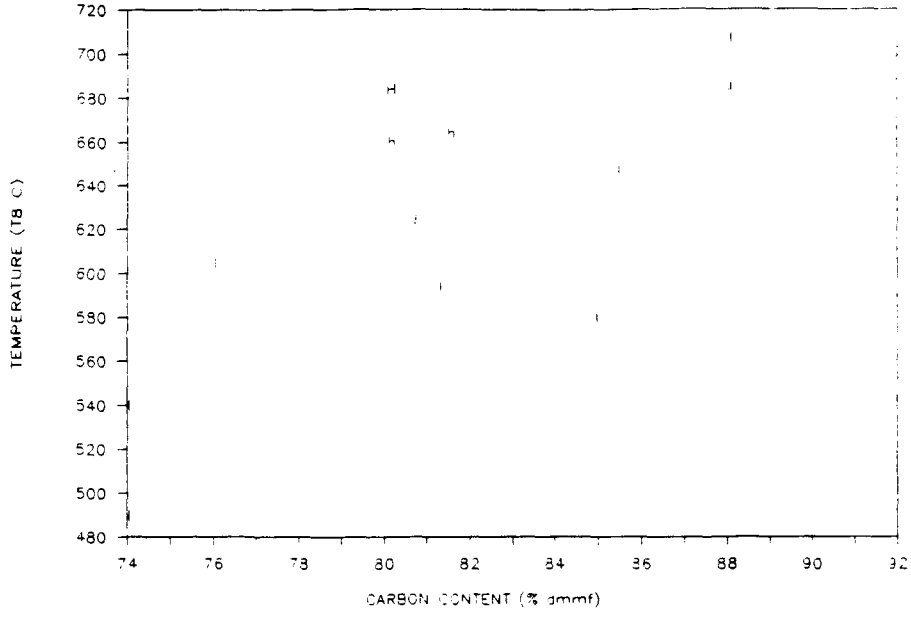

Figure B.66 The Effect of Carbon Content on TGA Combustion Profile Temperature 8 for Argonne Demineralized Liptinites, (l), Hartshorne Raw Liptinites, (H), and Hartshorne Demineralized Liptinites, (h).

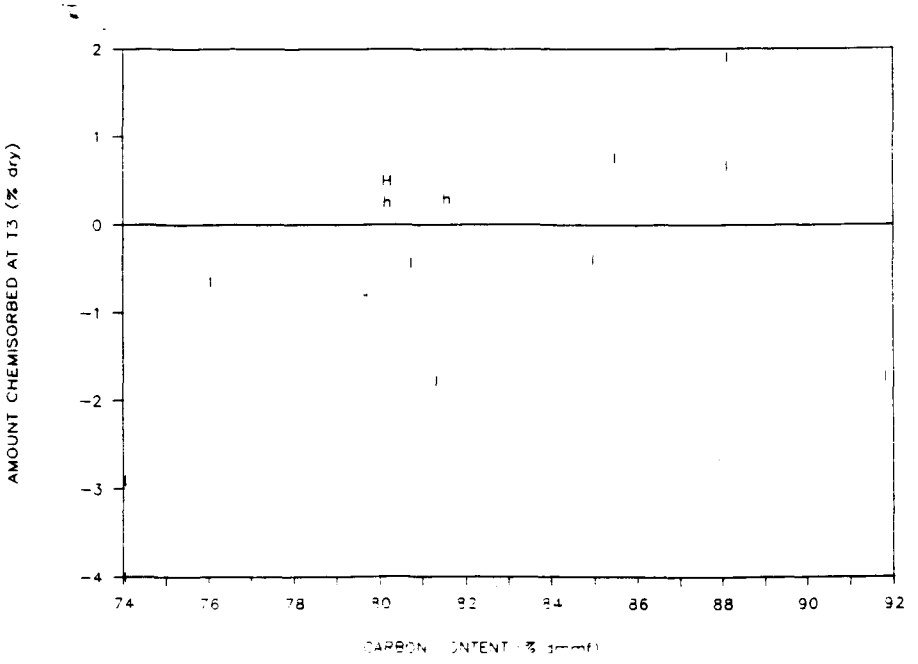

Figure B.67 The Effect of Carbon Content on TGA Combustion Profile Maximum Weight Chemisorbed for Argonne Demineralized Liptinites, (I), Hartshorne Raw Liptinites, (H), and Hartshorne Demineralized Liptinites, (h).

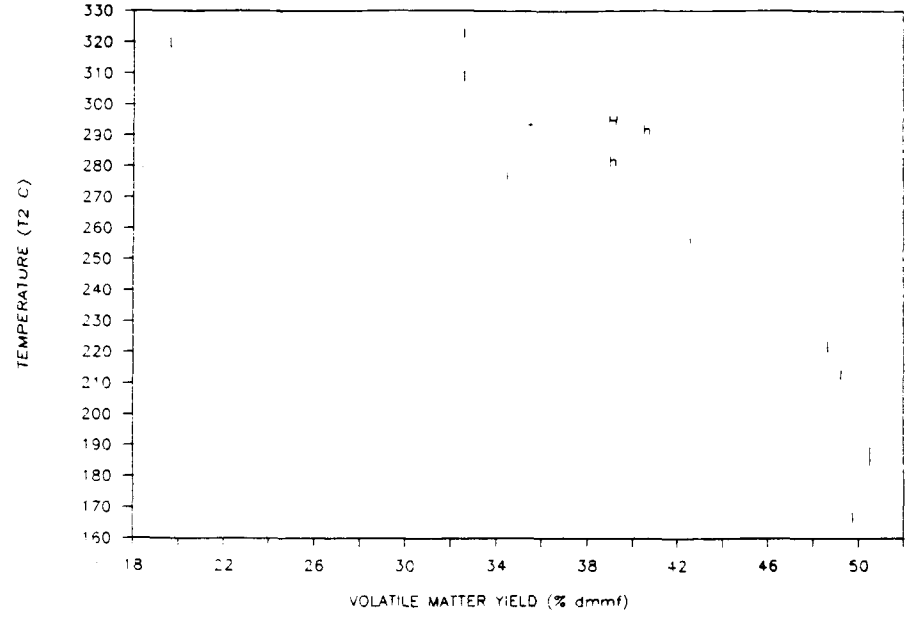

Figure B.68 The Effect of Volatile Matter Yield on TGA Combustion Profile Temperature 2 for Argonne Demineralized Liptinites, (I), Hartshorne Raw Liptinites, (H), and Hartshorne Demineralized Liptinites, (h).

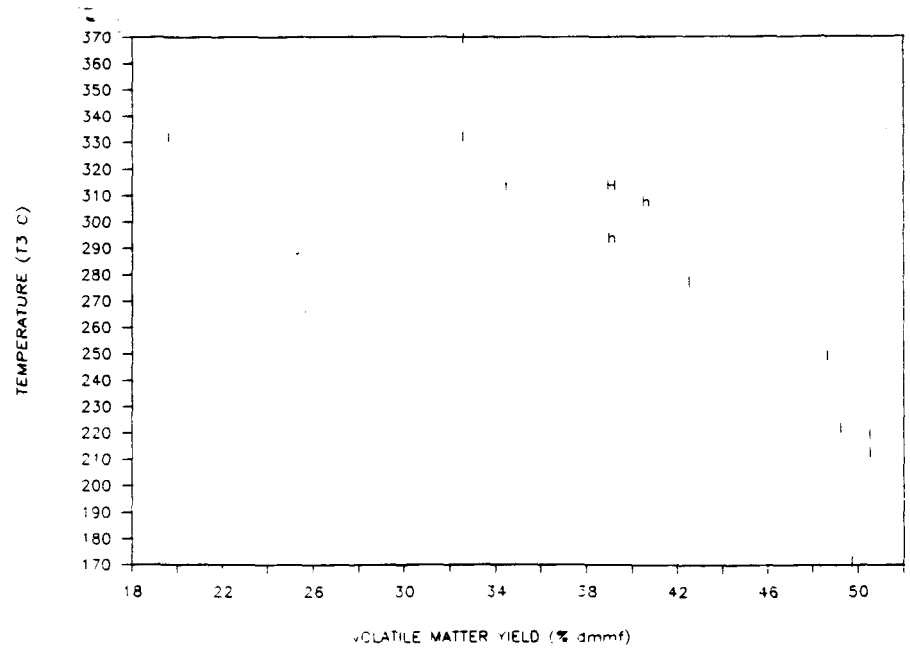

Figure B.69 The Effect of Volatile Matter Yield on TGA Combustion Profile Temperature 3 for Argonne Demineralized Liptinites, (l), Hartshorne Raw Liptinites, (H), and Hartshorne Demineralized Liptinites, (h).

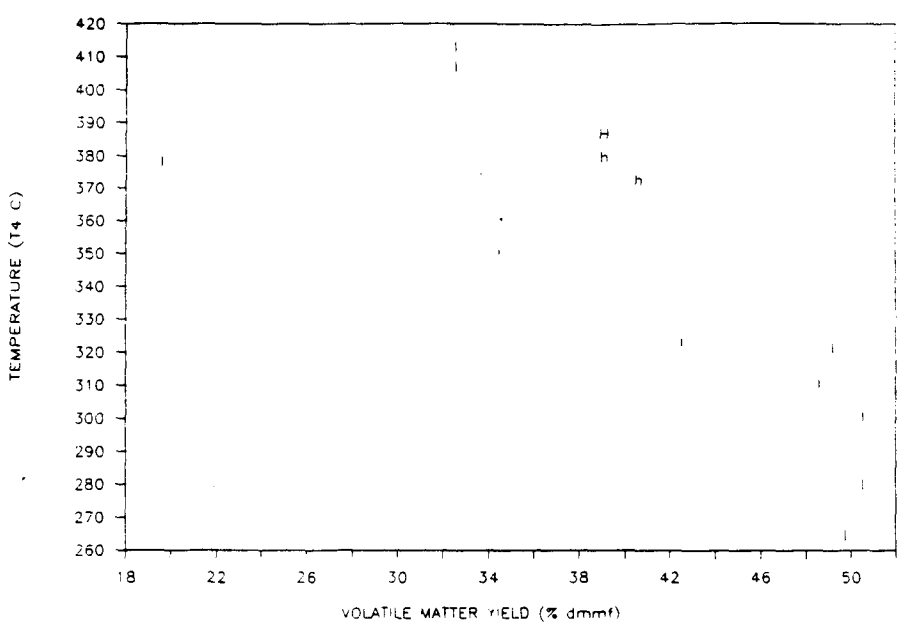

Figure B.70 The Effect of Volatile Matter Yield on TGA Combustion Profile Temperature 4 for Argonne Demineralized Liptinites, (l), Hartshorne Raw Liptinites, (H), and Hartshorne Demineralized Liptinites, (h).

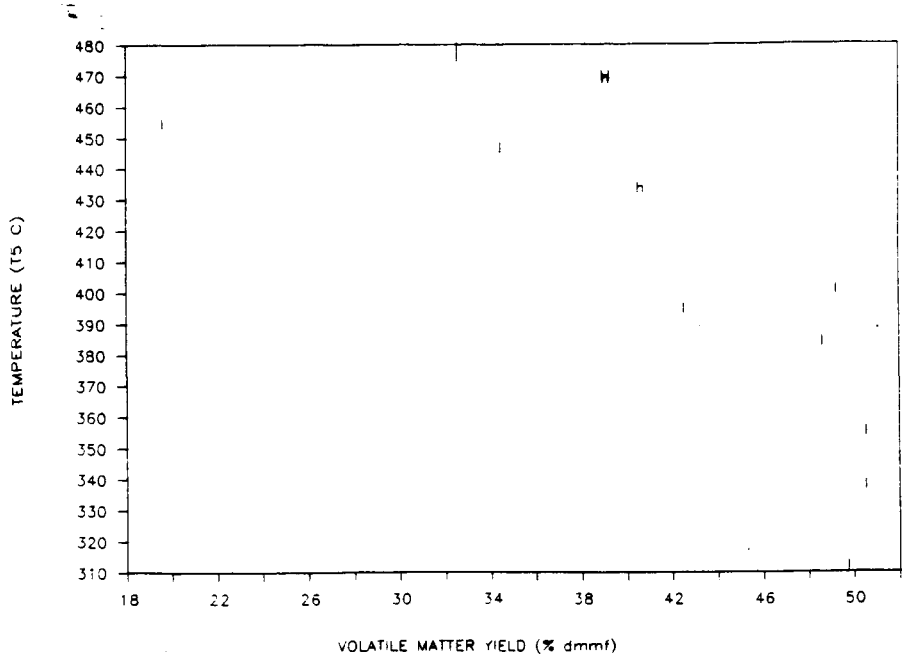

Figure B.71 The Effect of Volatile Matter Yield on TGA Combustion Profile Temperature 5 for Argonne Demineralized Liptinites, (l), Hartshorne Raw Liptinites, (H), and Hartshorne Demineralized Liptinites, (h).

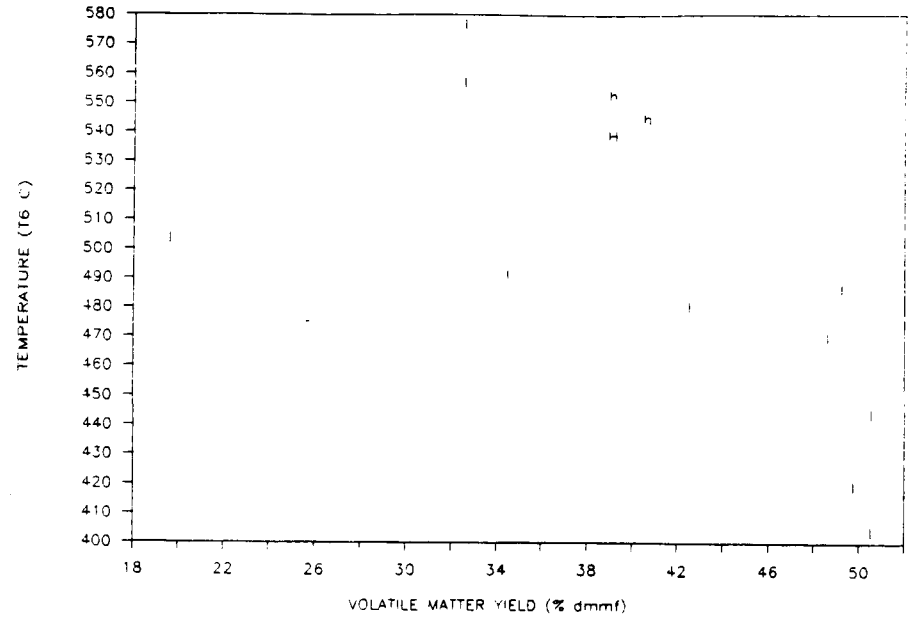

Figure B.72 The Effect of Volatile Matter Yield on TGA Combustion Profile Temperature 6 for Argonne Demineralized Liptinites, (l), Hartshorne Raw Liptinites, (H), and Hartshorne Demineralized Liptinites, (h).

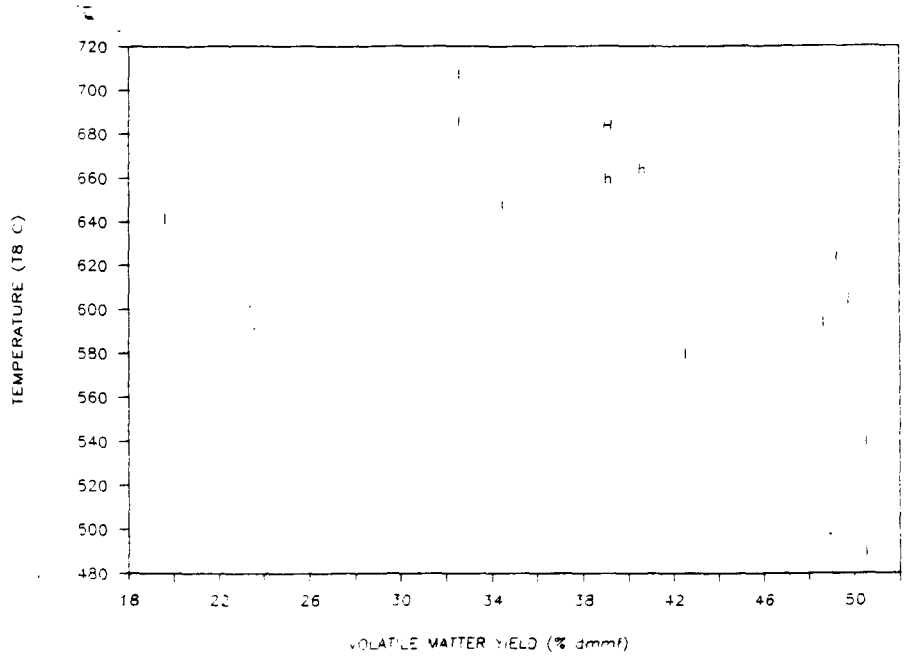

Figure B.73 The Effect of Volatile Matter Yield on TGA Combustion Profile Temperature 8 for Argonne Demineralized Liptinites, (l), Hartshorne Raw Liptinites, (H), and Hartshorne Demineralized Liptinites, (h).

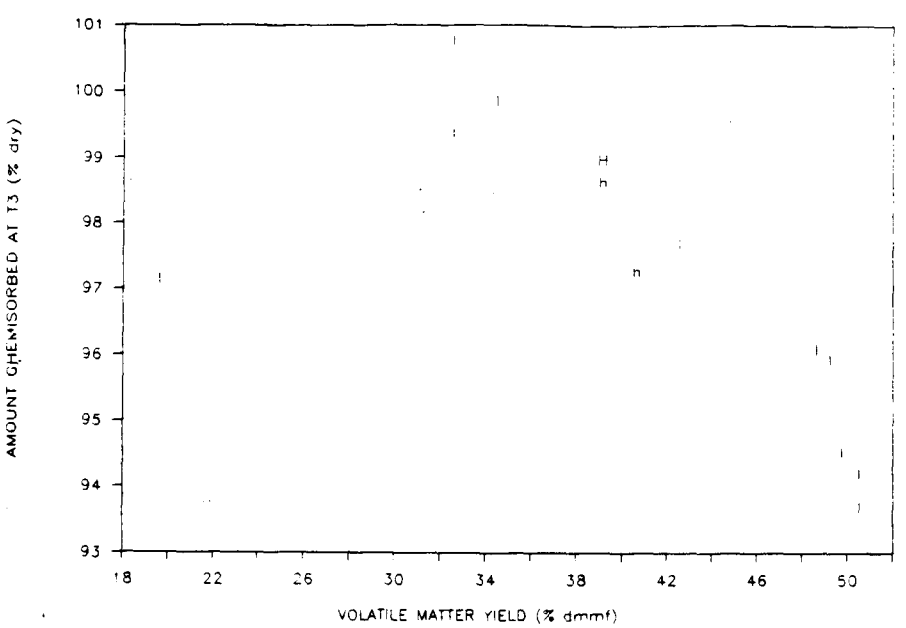

Figure B.74 The Effect of Volatile Matter Yield on TGA Combustion Profile Maximum Weight Chemisorbed for Argonne Demineralized Liptinites, (l), Hartshorne Raw Liptinites, (H), and Hartshorne Demineralized Liptinites, (h).

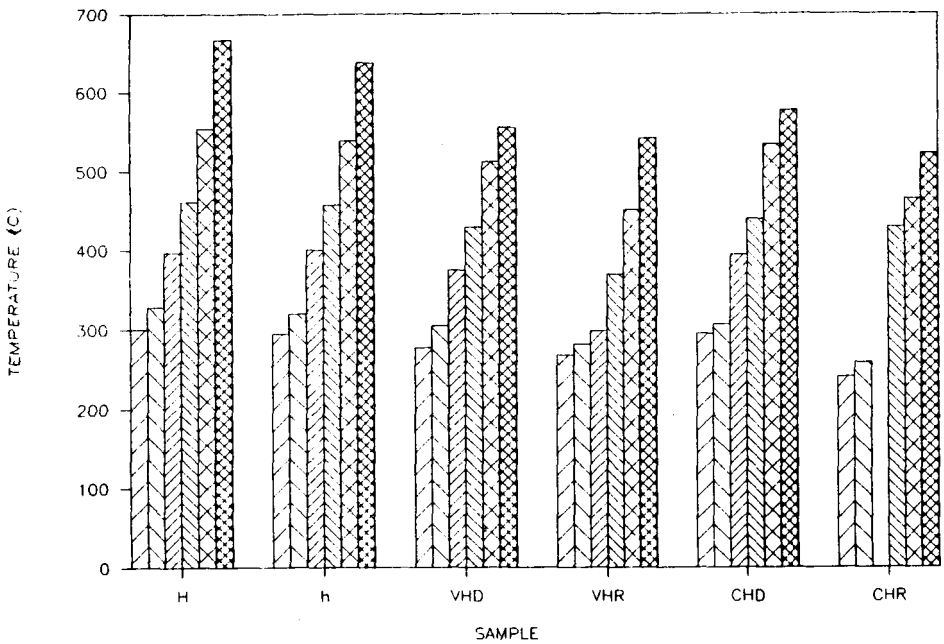

Figure B.75 Combustion Profile Temperatures for Hartshorne SIU 1310 Coal, (H), Demineralized 1310 Coal, (h), Elkhorn #3 Vitrain, (VHR), The Demineralized Vitrain, (VHD), Elkhorn #3 Clarain, (CHR), and The Demineralized Clarain, (CHD).

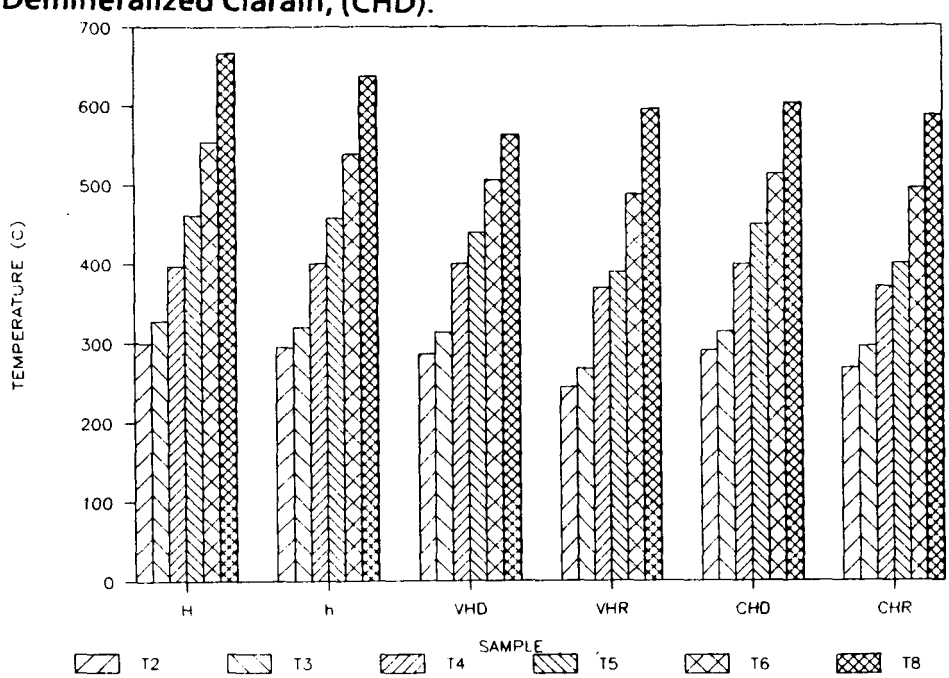

Figure B.76 Combustion Profile Temperatures for Hartshorne SIU 1310 Coal, (H), Demineralized 1310 Coal, (h), Pittsburgh #8 Vitrain, (VHR), The Demineralized Vitrain, (VHD), Pittsburgh #8 Clarain, (CHR), and The Demineralized Clarain, (CHD).

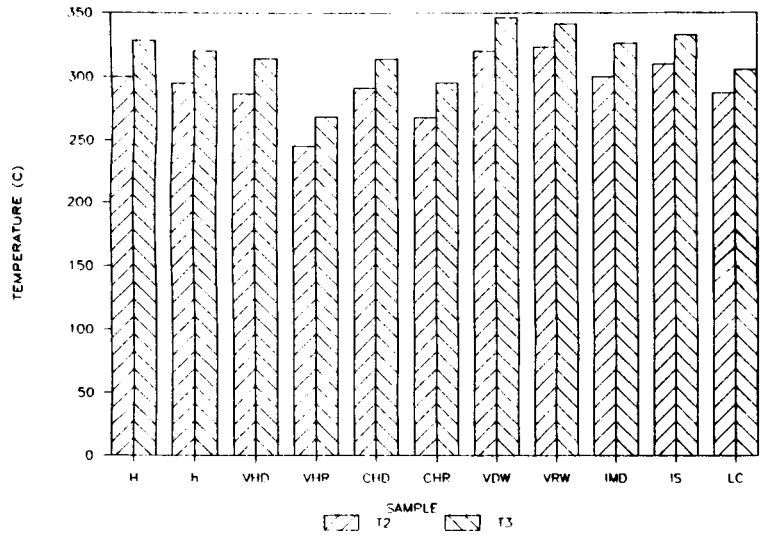

Figure B.77 Combustion Profile Temperatures T2 and T3 for Hartshorne SIU 1310 Coal, (H), Demineralized 1310 Coal, (h), Elkhorn #3 Vitrain, (VHR), The Demineralized Vitrain, (VHD), Elkhorn #3 Clarain, (CHR), The Demineralized Clarain, (CHD) A Vitrinite Maceral Obtained from the Vitrain, (VDW), A Vitrinite Maceral Obtained from the Clarain, (VRW), An Inertinite Maceral Fraction Obtained from the clarain, (IMD), a 1.5 Sink Fraction, (IS), and a Liptinite Maceral Obtained from the Vitrain.

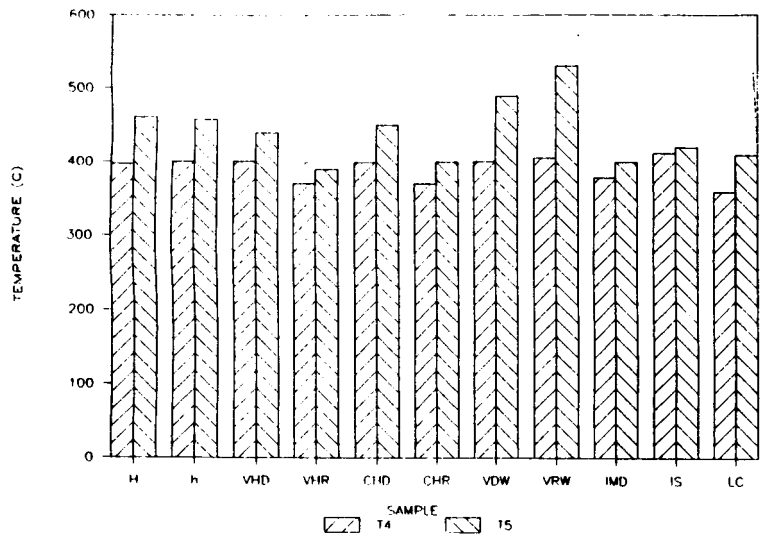

Figure B.78 Combustion Profile Temperatures T4 and T5 for Hartshorne SIU 1310 Coal, (H), Demineralized 1310 Coal, (h), Elkhorn #3 Vitrain, (VHR), The Demineralized Vitrain, (VHD), Elkhorn #3 Clarain, (CHR), The Demineralized Clarain, (CHD), A Vitrinite Maceral Obtained from the Vitrain, (VDW), A Vitrinite Maceral Obtained from the Clarain, (VRW), An Inertinite Maceral Fraction Obtained from the Clarain, (IMD), a 1.5 Sink Fraction, (IS), and a Liptinite Maceral Obtained from the Vitrain.

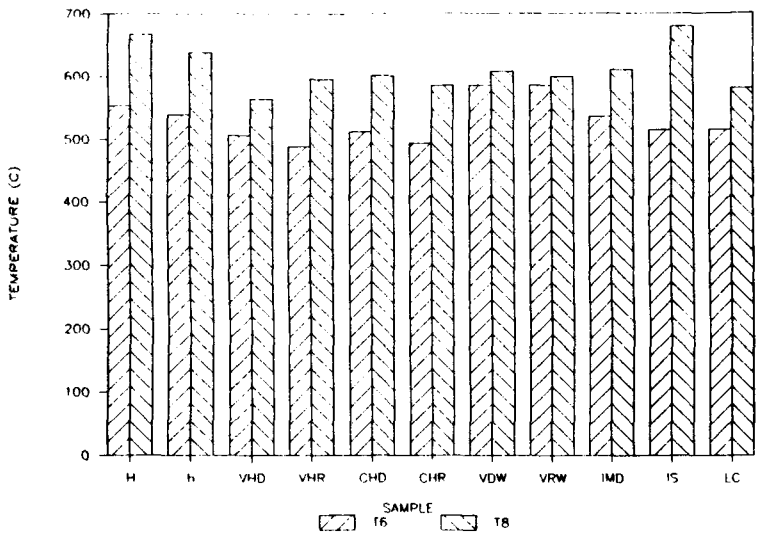

Figure B.79 Combustion Profile Temperatures T6 and T8 for Hartshorne SIU 1310 Coal, (H), Demineralized 1310 Coal, (h), Elkhorn #3 Vitrain, (VHR), The Demineralized Vitrain, (VHD), Elkhorn #3 Clarain, (CHR), The Demineralized Clarain, (CHD) A Vitrinite Maceral Obtained from the Vitrain, (VDW), A Vitrinite Maceral Obtained from the Clarain, (VRW), An Inertinite Maceral Fraction Obtained from the Clarain, (IMD), a 1.5 Sink Fraction, (IS), and a Liptinite Maceral Obtained from the Vitrain.

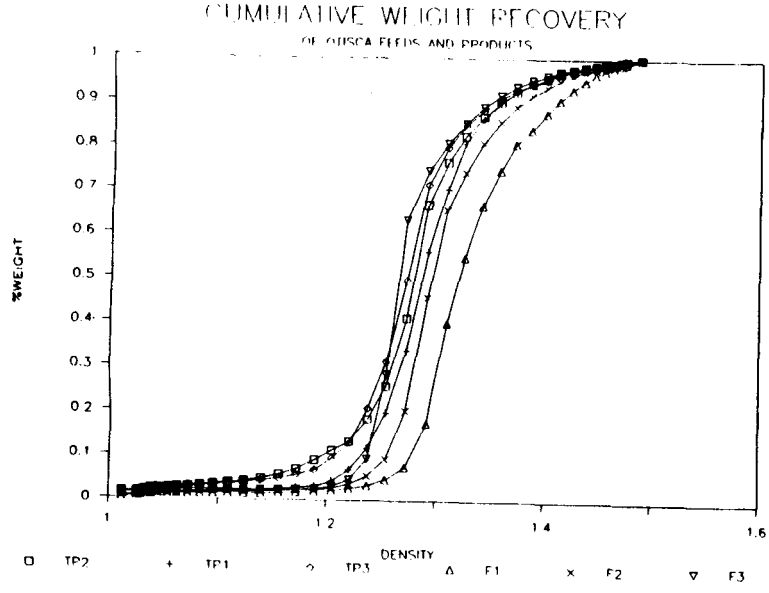

Figure B.80 DGC Cumulative Weight Recovery Curves for OTISCA Coals and Products.

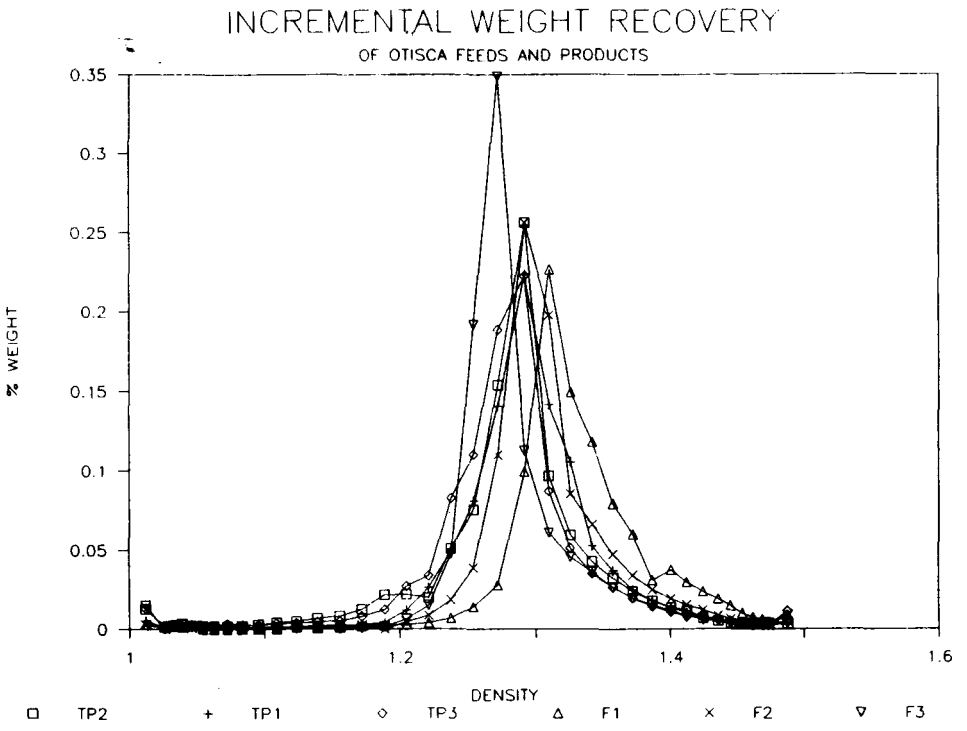

Figure B.81 Incremental Weight Recovery Curves for OTISCA Coals and Products.

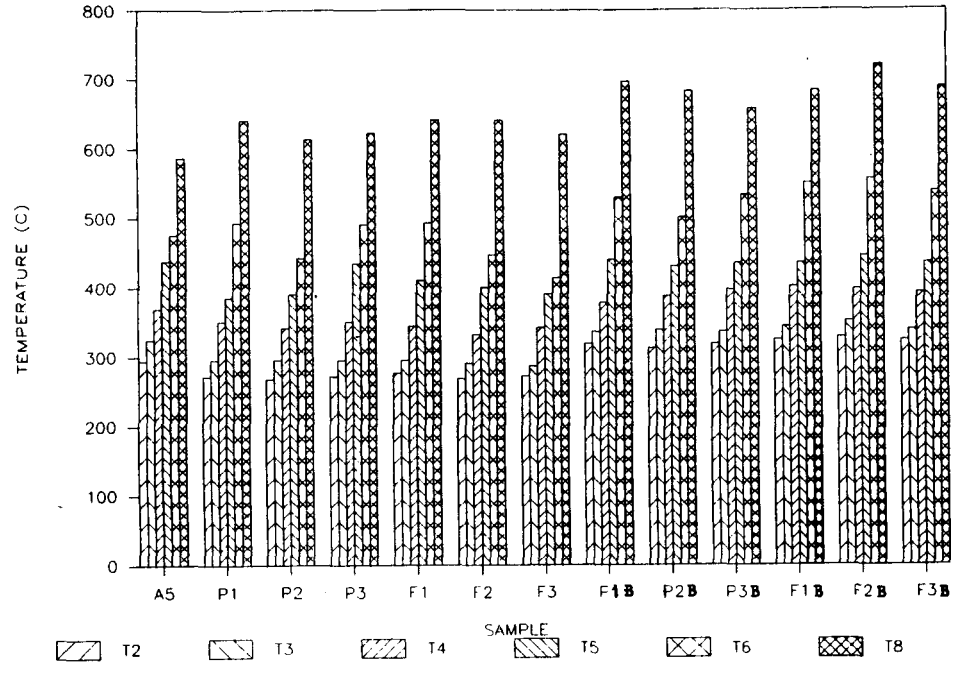

Figure B.82 Combustion Profile Temperatures for OTISCA Coals and Products.

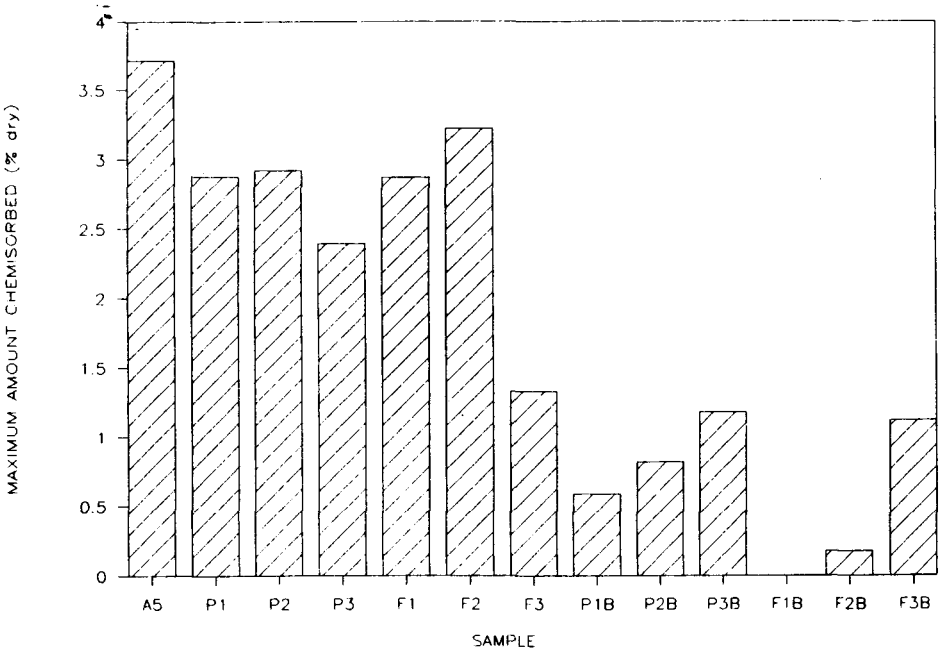

Figure B.83 Weight Chemisorbed During Combustion Profile Test for OTISCA Coals and Products.

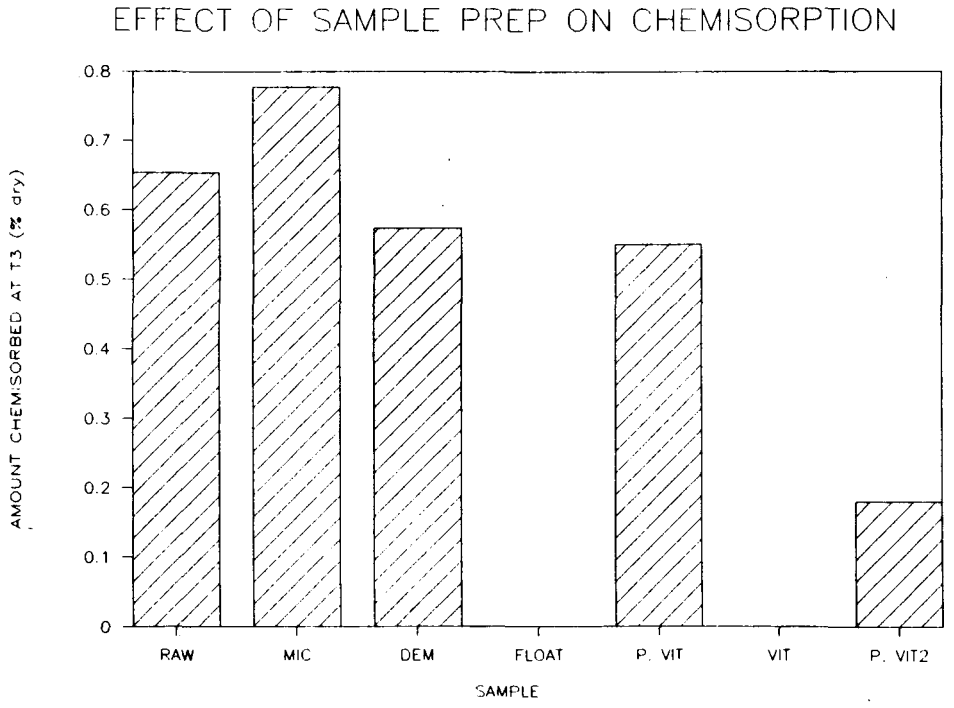

Figure B.84 Weight Chemisorbed During Combustion Profile Test for Coal Samples Used In the SCE Study.

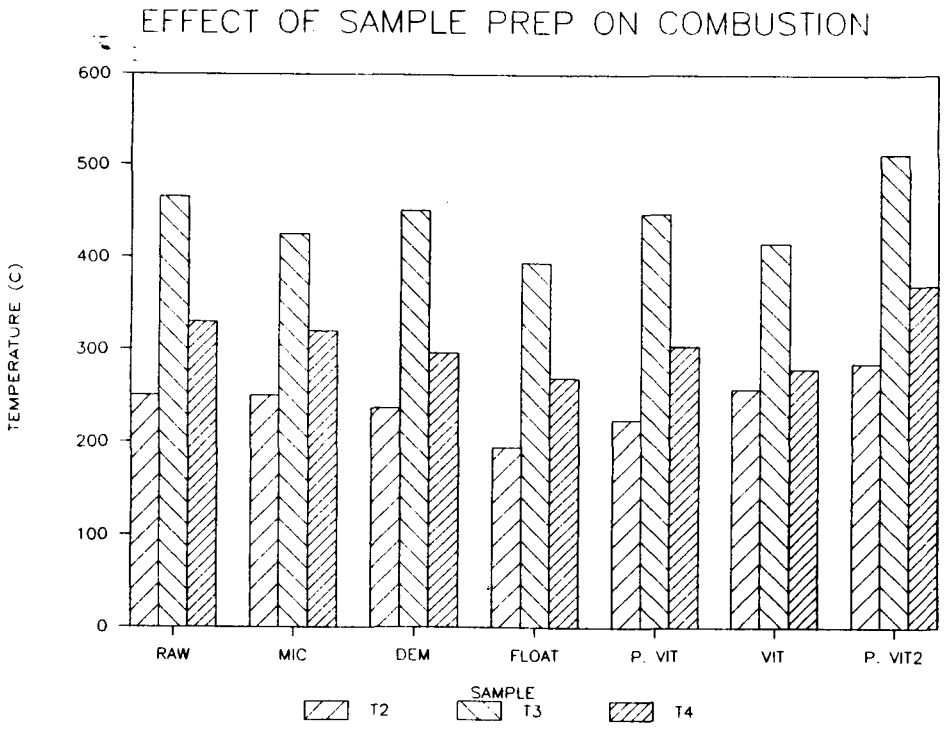

Figure B.85 Combustion Profile Temperatures T2, T3, and T4 of Coal Samples Used In the SCE Study.

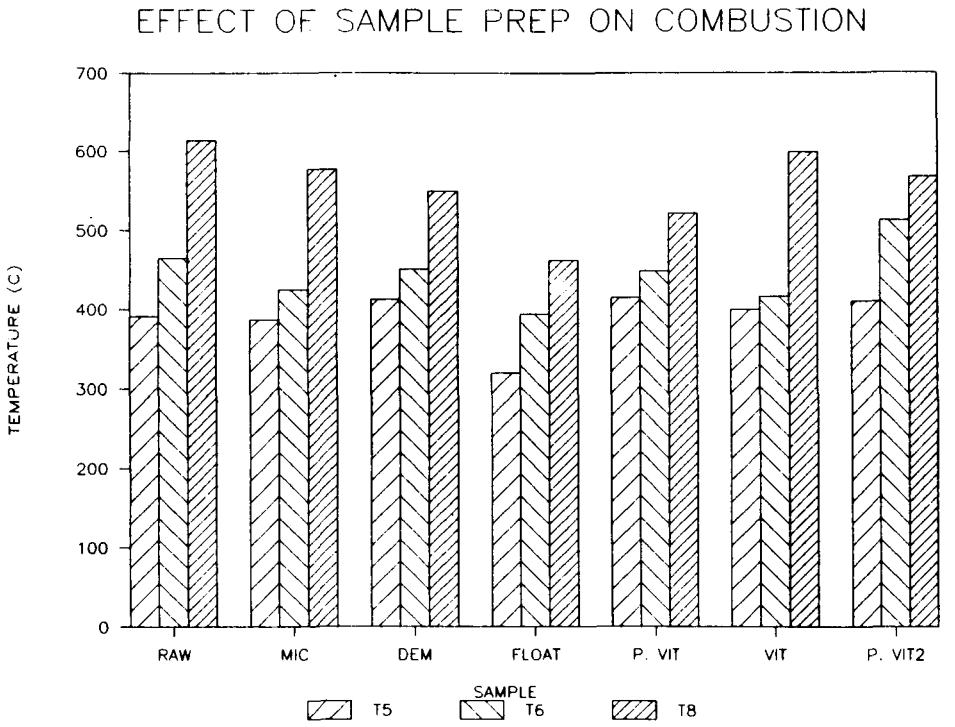

Figure B.86 Combustion Profile Temperatures T5, T6, and T8 of Coal Samples Used In the SCE Study.

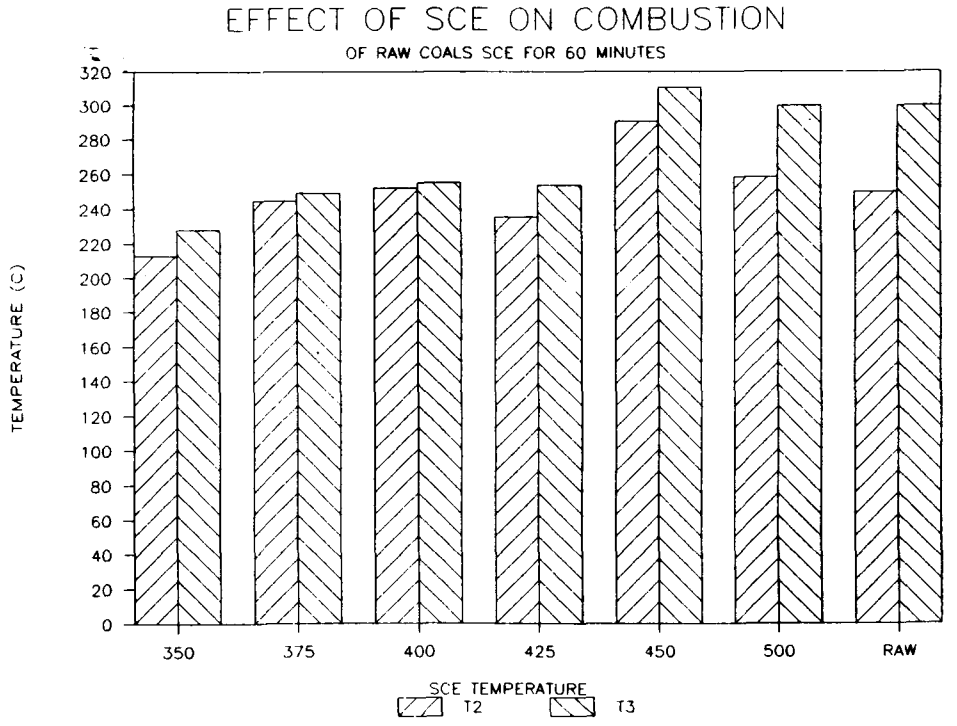

Figure B.87 Combustion Profile Temperatures T2, and T3, of Coal SCE Products Obtained from Raw Coal SIU 647.

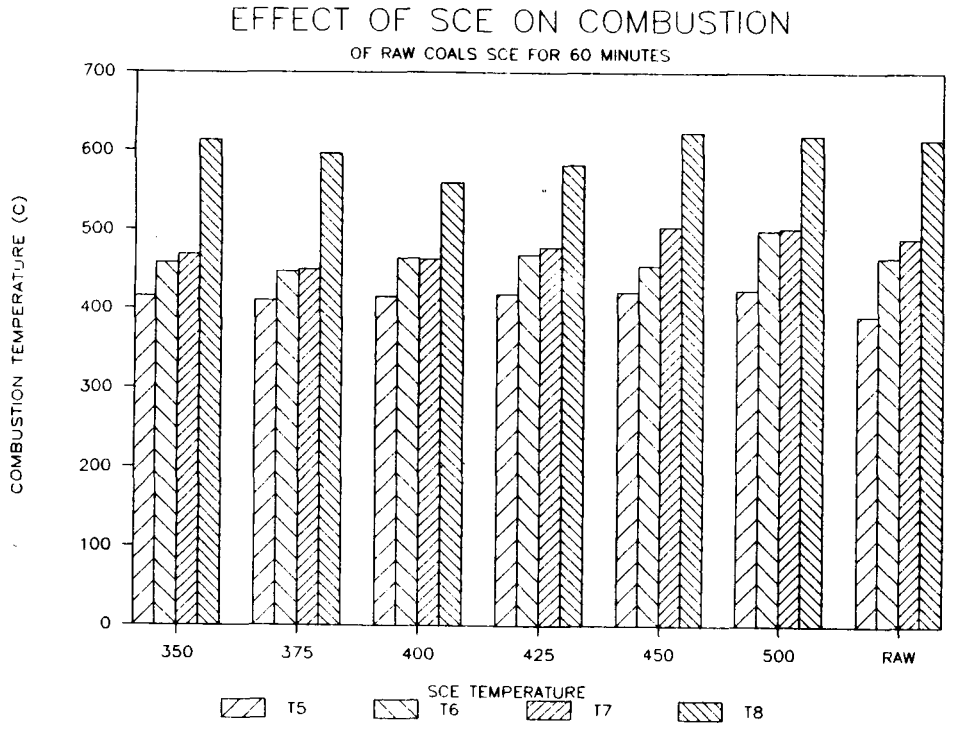

Figure B.88 Combustion Profile Temperatures T5, T6, T7, and T8 of SCE Products Obtained from Raw Coal SIU 647.

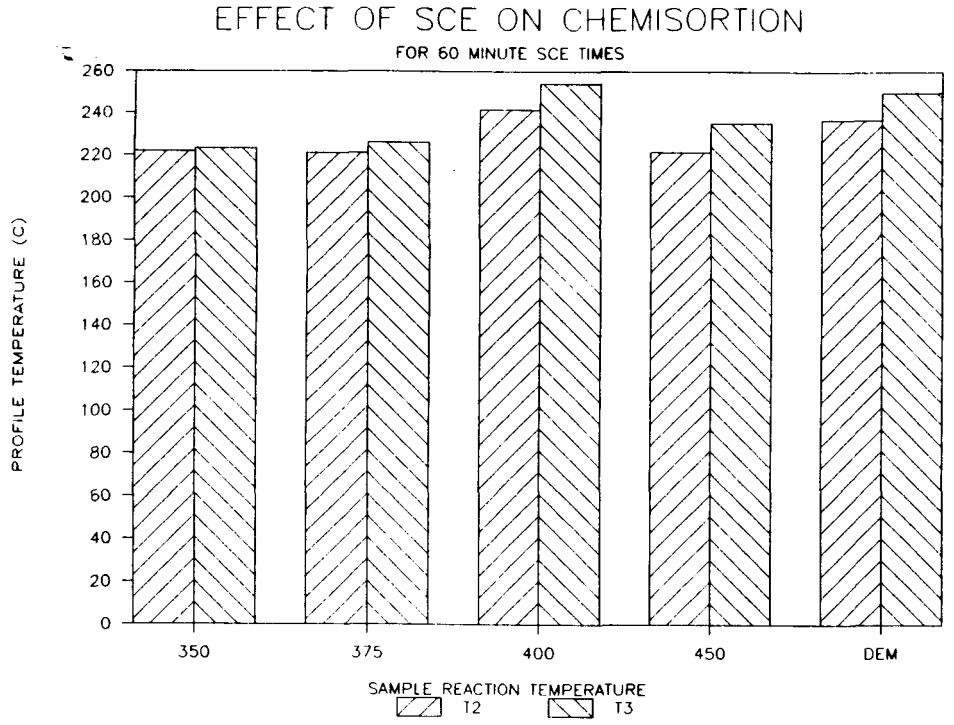

Figure B.89 Combustion Profile Temperatures T2, and T3, of Coal SCE Products Obtained from Demineralized Coal SIU 647.

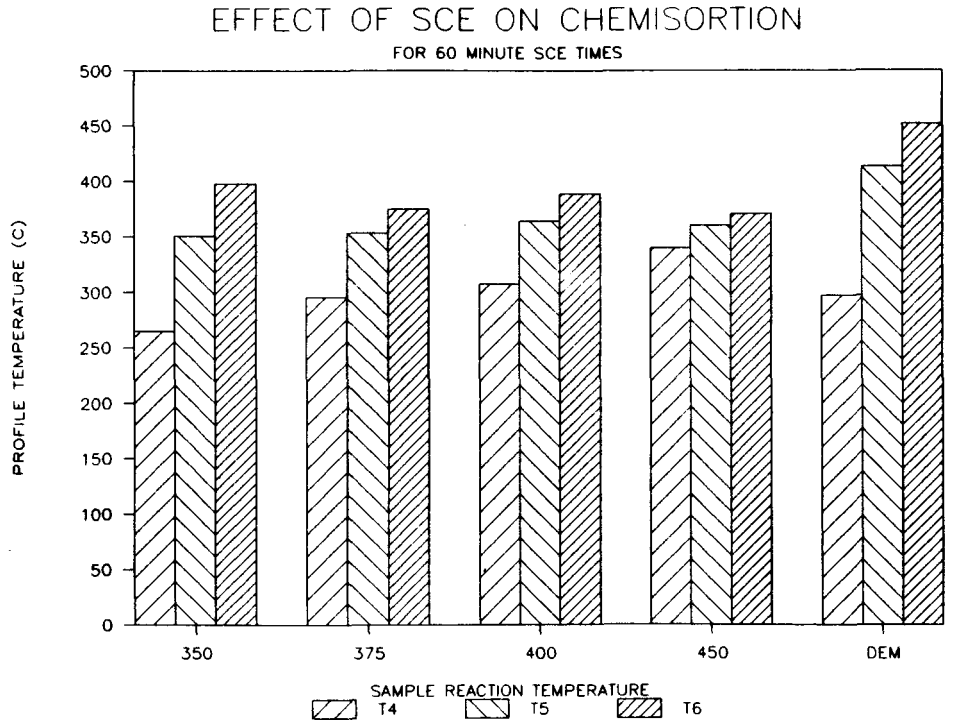

Figure B.90 Combustion Profile Temperatures T4, T5, and T6, of SCE Products Obtained from Demineralized Coal SIU 647.

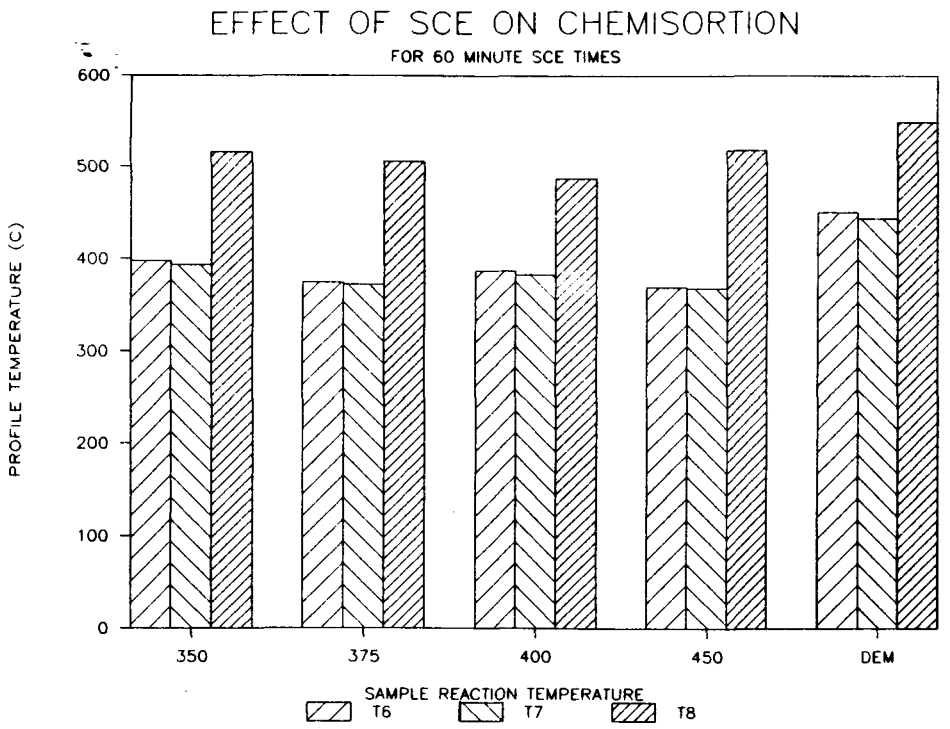

Figure B.91 Combustion Profile Temperatures T6, T7, and T8 of SCE Products Obtained from Demineralized Coal SIU 647.

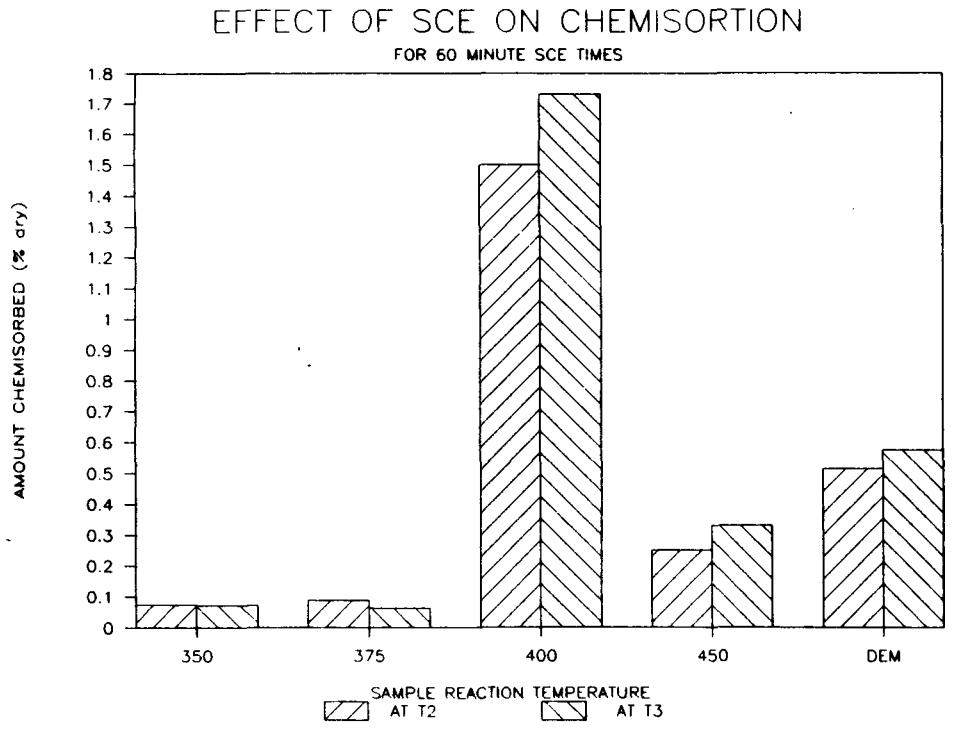

Figure B.92 Weight Chemisorbed During Combustion Profile Test of SCE Products Obtained from Demineralized Coal SIU 647.

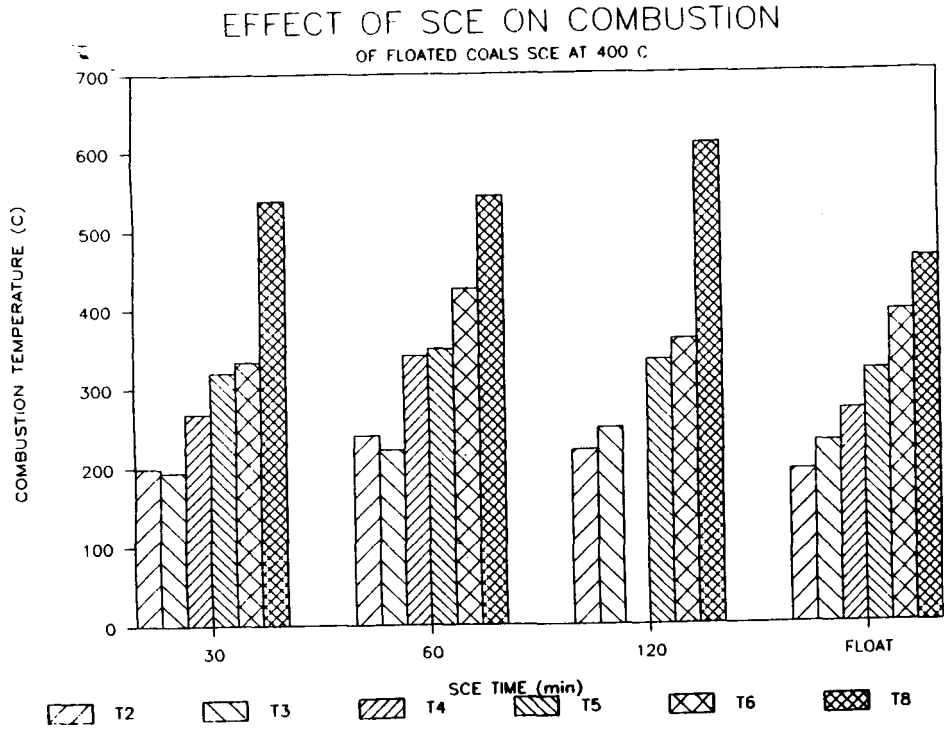

Figure B.93 Combustion Profile Temperatures of SCE Products Obtained from Floated Coal SIU 647.

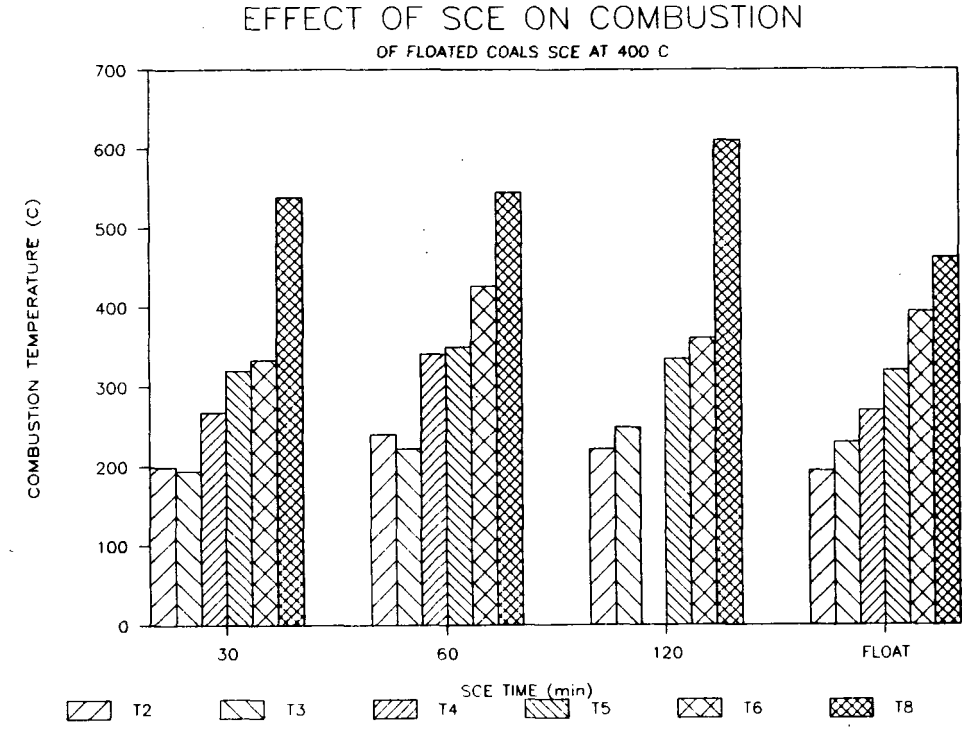

Figure B.94 Combustion Profile Temperatures T6, T7, and T8 of SCE Products Obtained from Demineralized Coal SIU 647 at Various reaction Times and 400°C.

APPENDIX C

DETAILS OF COMBUSTION PROFILE MODEL

Activation Energies

For the purpose of analysis and for aid in distinguishing between various coals on the figures that follow, each coal was given a single character file code. These codes are listed in Table C1. The data labels used on the various figures that follow refer back to the coals described in this table.

Coal combustion in a TGA behaves according to first order kinetics. In the TGA, samples used are small and thinly spread. Since there is an excess air supply, the oxygen concentration remains constant as combustion proceeds. Coal, therefore, behaves according to the first order process described in equation 1:

$$-(dW/dt) = kW \text{ or } k = (-dW/dt)/W \qquad (1)$$

where k = the specific reaction rate,

dW/dt = instantaneous rate of weight loss, and

W = weight of unburned combustible.

The Arrhenius Equation (Equation 2) relates the specific reaction rate to temperature:

$$k = A \exp(-E/RT) \text{ or } \log k = \log A - E/(2.303RT) \qquad (2)$$

where A = the frequency factor,

E = activation energy,

R = universal gas constant, and

T = absolute temperature (°K).

So k is obtained at various temperatures by Equation 1, and the activation energy is derived from Equation 2. The slope of the line k vs. 1/T is the activation energy.

These are apparent activation energies. Activation energies, when used in this study, always refer to apparent activation energies.

Table C2 shows the value used to determine the Arrhenius values from which the activation energies were determined for demineralized vitrinite from coal 1356 (the file code is "5"). At 25°C temperature intervals, values from the weight loss curve and corresponding first derivative curve are listed and are found by multiplying the rate of weight loss values from the derivative curve by the heating rate and dividing by the original weight. Time, converted from minute to second units will give the k values listed. Temperature values are found by converting to Kelvin scale, taking the reciprocal and multiplying by 1000. By plotting log k vs. (1/T * 1000), Arrhenius plots are obtained from which activation energies are calculated. Figure C1 shows the Arrhenius plot for demineralized vitrinite of coal 1356. Activation energies are found for regions of linearity. Here, as in most bituminous coals, three regions of linearity are seen. From slopes of these three regions, three activation energies are determined in the appropriate units. E1 was determined to be 225.85 kJ/mole. E2 was found to be 57.42 kJ/mole. E3 was found to be 241.64 kJ/mole. Values of activation energies determined for each coal are listed in Table C3. Values are listed with matching file codes which were defined earlier. For some coals, especially the high ranked ones, only two activation energies exist. This agrees with data for anthracitic coals. The values described in this table do not show much consistency within each rank series. Smith et al. (1981) had noted four activation energy regions for each bituminous coal. One of these activation energies which he noted was a small transition region which was not distinguishable on the coals used in this study. Therefore, three activation energy regions in Table C3 are defined as follows: E1 is the region where light volatiles evolve and are combusted, E2 is the region where higher molecular weight volatiles evolve from pores and are combusted, E3 is the diffusion controlled char combustion region. Since temper-

ature values were taken every 25°C to draw slopes lines, there was a possibility that each region from which the slopes were drawn was not totally representative of the region. The second volatile activation energy (E2) showed the least variation (from 34.69 to 81.35 kJ/mole), and these values showed good reliability. With E1 and E3, higher activation energies are observed, and values vary much more (from 82.03 to 545.49 kJ/mole). These values do not show strict boundary values at the highest and lowest temperatures, so less confidence can be taken in these values. A continuous plot of Arrhenius points might have given better results. For example, the demineralized vitrinite of coal 1312, labeled "3" has an E1 of 539.11 kJ/mole, compared to a range of 84.22 to 225.85 kJ/mole for the other E1 values in that set. This high value occurred because only two points were used to calculate the slope. A 25°C temperature increment may be too large to clearly define the slope. Also, E1 and E2 do not show clear boundary conditions on the outer ends of the Arrhenius plots, adding possible slope calculating errors. The general trends indicate E1 and E3 to be higher than E2. For this reason, it is best to compare the plots as a whole, rather than the individual values seen in Table C3.

Variations in Activation Energies of Raw Whole Coals

Figure C2 shows a comparison of the Arrhenius plots for raw whole coals, 1310 (labeled "g"), 1311 (labeled "h"), and 1366 (labeled "m"). Comparison of E2, the most reliable activation energy values, showed values of 57.52 kJ/mole for coal 1310, 58.7 kJ/mole for coal 1311, and 63.8 kJ/mole for coal 1366. E3 values of 205.76 kJ/mole for coal 1310, 224.9 kJ/mole for coal 1311, and 217.72 kJ/mole for coal 1366 were observed. Although displaced on the reciprocal temperature scale, the slopes are similar. The general observation here is that in the distinctive regions of combustion, the values of the slopes appear relatively constant and do not change markedly with rank. This is significant since earlier work had shown different

activation energies for coals of different ranks. However, previous work was not done on a single seam. Results from the single Hartshorne seam coals appear to indicate that differences in activation energies are a function of composition rather than rank. Coals from the same seam show similar activation energies within the seam regardless of rank. Data points at 25°C intervals did not give as much insight as a continuous plot of Arrhenius points might have provided. Unfortunately, the capacity to do this is not available in the Perkin-Elmer TGA7 software used in this study.

Variations in Activation Energies Between Maceral Fractions

Figure C3 shows the relative differences in Arrhenius plots between the three maceral groups of coal 1310. Variations between macerals can be seen. For this reason, macerals were also analyzed separately. Vitrinites have the most slope in E1 and E3, followed by inertinites, then liptinites. E2 values vary less.

Variations in Activation Energies Within Maceral Groups

Figure C4 shows comparative Arrhenius plots for three demineralized vitrinites: coal 1310 (labeled "1"), coal 1311 (labeled "2"), and coal 1366 (labeled "8"). Figure C5 shows a similar comparison for inertinites: coal 1310 (labeled "A"), coal 1311 (labeled "B"), and coal 1366 (labeled "G"). Liptinites also follow this same trend. Each of these curve sets shows similar curves; and thus, the same activation energies for coals of varying rank for each maceral group. Therefore, results from the macerals were similar to previous analysis of raw whole coals.

Since coals and macerals show consistent Arrhenius relationships, especially within maceral groups, it was possible to normalize curves of each group.

Predictive Modeling on Normalized Curves

The above results comparing activation energies and key burning profiles revealed that within each maceral group, the burnoff regions of the curves have similar shapes, but are displaced from one another by constant temperatures, depending upon the temperature at which burnoff commences. The curves within each rank series of eight whole coals or maceral fraction can be normalized by using a characteristic temperature of each curve. The temperature at 50% burnoff (T50) was chosen as the characteristic temperature in this study and was obtained by plotting T/T50 versus moisture ash free (m.a.f.) weight percent gave a normalized burning profile for each coal tested. The eight burnoff curves for the eight coals were normalized into one normalized band for the eight coals tested. Figure C6 illustrates the normalized curve for the rank series of eight raw whole coals. The numbers on the curve correspond to specific samples as defined in Table C1 (See section on activation energies). Although a significant range of weight variation (<20% during initial combustion and 15% during middle stages of combustion) was seen, only a 5% variation was observed at burnout. Even with this scatter, these curves can be represented by a single curve since they have similar burnoff mechanisms.

Figure C7 is the same type of graph, but is for demineralized whole coals. The demineralized coals are more chemically pure and give a tighter band of values than did the raw whole coals. There is, however, still a 15% range of weight variation for the initial combustion portion of the band.

Figure C8 shows the same plot as above, but for demineralized vitrinites. By using macerals, the most recognizably homogeneous quantities in coal, a much tighter band of normalized curves is observed. The weight percent variation of less than 10% during the initial combustion stages and less than 5% weight variation

during middle stages of combustion is observed. Figures C9 and C10 show similar normalized curves for the inertinite and liptinite maceral groups, respectively. The weight percent variation is comparable to that seen for the vitrinites.

Since demineralized macerals gave the best normalized curves of the burnoff region, curve modeling was performed on demineralized whole coals and demineralized maceral groups. The data used for the initial curve fits were from the center most curves of Figures C7, C8, and C9. For a first approximation for curve fitting, the following curves were chosen: (1) for demineralized whole coals, the values from coal 1365 (labeled "d") were chosen; (2) for demineralized vitrinites, the vitrinites of coal 1356 (labeled "5") were chosen; (3) for demineralized inertinites, the inertinites of coal 1312 were chosen; and (4) for demineralized liptinites, the liptinites of coal 1310 were chosen. The center most curve was considered representative of the general shape of the curve.

Curves were modeled using various polynomial regression forms. Given the values of x from the curves above (consisting of 15 data points for each curve), an equation of y as a function of x can be determined. The three polynomial regression forms tried are listed in Table C4, along with the appropriate correlation coefficients. The correlation coefficients are percentage values as to what percentage of the given values exactly match the regression equation. A $r^2 = 1.0$ (100%) is a perfect fit. The best fit of the data is seen with the third type of polynomial which has a 99.995296% correlation with the data. This particular equation has 10 constants; B(0) - B(9). Fitting a data set of 15 values while a 10 constant equation might be seen as unnecessary and give very little degrees of freedom in the equation. However, in this case it was desirable to find the best fit available so equation form 2 with constants B(0) - B(9) was chosen.

Once the curve form was chosen, data was fitted for the demineralized whole coal and the demineralized maceral fractions. Table C5 shows the comparison of

correlation for each data set. The correlation of the macerals are higher than the whole coals. For this reason, a model for each maceral group was done and then used to generate a whole coal curve using the weight percentages present in the original samples. Equation 3 is used to determine the composite modeled burnoff curve:

$$C = (WPL)(L) + (WPI)(I) + (WPV)(V) \quad (3)$$

where C = composite model predicting whole coal burnoff,
WPL = weight percent of liptinite in original sample,
WPI = weight percent of inertinite in original sample,
WPV = weight percent of vitrinite in original sample,
L = value of modeled liptinite burnoff curve,
I = value of modeled inertinite burnoff curve, and
V = value of modeled vitrinite burnoff curve.

Constants used for modeling equations are listed in Table C6. These constants are used in the third linear regression equation of Table C4 to be able to determine y values given x. X corresponds to T/T50 values and y corresponds to the m.a.f. weight percent. X values are determined by using the known value of T50 for each maceral and incrementing T values to provide x values for the model. Thus, if given T50 for each maceral and the weight percent of each maceral present in the original sample, this method can determine the m.a.f. weight percent and hence, the burn-off curve of the whole coal. If maceral interactions are limited or nonexistent, the above equation should predict burnoff behavior similar to that seen for the whole coal. Figures C11, C12, and C13 compare the values predicted from the above modeling equation to that obtained by experiment for coals 1310, 1311, and 1366, respectively.

Figure C11 shows that with high volatile bituminous coal (#1310), there is good agreement for the middle and final stages of combustion, but less agreement in the initial stages of burning. This is mainly due to the fact that the values for the demineralized vitrinite curve modeling were higher than for coal 1310. If 1310 vitrinite were used as a base for the vitrinite model, the correlation might have been better in the initial stages of combustion. This may suggest the need to add a weighting factor in the initial stages of combustion for lower ranked coals.

Figure C12 shows that with medium volatile bituminous coal (#1311), a good agreement is seen between formula and experiment in the initial and final stages of combustion, but there is some disagreement in the middle or maximum reactivity region of combustion. This discrepancy cannot be traced back to the base curve selection as was the case with coal #1310.

Figure 13 illustrates a low volatile bituminous coal (#1366) and follows the same trend as with coal #1311. Once again, the middle stage of combustion is where the least amount of agreement is seen. This disagreement may be the result of maceral interactions between vitrinites and inertinites since no lipid portion is included in maceral samples of coals 1311 and 1366.

The close proximity of the modeled curves with experimental data revealed that modeling of curves from maceral data was a viable practice and that from maceral fractions, it is possible to predict the burnoff behavior of whole coals. The discrepancy observed between experimental data and data from the formula may have been the result of maceral interaction, improper model selection, experimental error, or the effect of maceral separation. The correlation between experimental and modeled data suggest that limited maceral interactions occur during combustion in air. Thus, maceral data can be used to predict the burnoff behavior of whole coals.

To obtain a more accurate model the generalized equations used to fit the center lines were used to fit all of the macerals. A predictive burnoff curve was generated for each raw and demineralized coal by applying Equation 4 with the specific coefficient found in Table C7 for the maceral derived from that specific coal. The results of this effort can be seen in Figures C.14 to C.22. The model accurately predicts the 30 to 60% weight remaining region for coal 1310 and is slightly off in the 0 to 30% wt. remaining region. The model fails to a larger extent in the 60 to 95% wt. remaining region. The model fails to predict the behavior of the 1311 coal over the entire weight loss region. Model predicts the behavior of the 1312 coal very well to the 90% wt. remaining level and the diverges dramatically. The model under-predicts weight loss for 1332 and over predicts wt. loss in 1356 over the entire range. The other coals behave similarly. These results clearly show that the macerals do interact. The lack of consistency, over and under prediction, and the inconsistency in ranges that are predicted well, point to several different types of interactions which seem to be coal dependent. We thus conclude that there are several types of maceral interactions that occur. Additional detail did not increase the accuracy of the prediction and in some cases made it worse.

TABLE C1

FILE CODES FOR ACTIVATION ENERGY DETERMINATION

AND PREDICTIVE MODEL DETERMINATION

SIU No.	Coal Description	File Code
1310	- 200 mesh demineralized vitrinite	1
1311	- 200 mesh demineralized vitrinite	2
1312	- 200 mesh demineralized vitrinite	3
1332	- 200 mesh demineralized vitrinite	4
1356	- 200 mesh demineralized vitrinite	5
1365a[a]	- 200 mesh demineralized vitrinite	6
1365b[a]	- 200 mesh demineralized vitrinite	
1366	- 200 mesh demineralized vitrinite	8
1367	- 200 mesh demineralized vitrinite	9
1310	- 200 mesh demineralized inertinite	A
1311	- 200 mesh demineralized inertinite	B
1312	- 200 mesh demineralized inertinite	C
1332	- 200 mesh demineralized inertinite	D
1356	- 200 mesh demineralized inertinite	E
1365	- 200 mesh demineralized inertinite	F
1366	- 200 mesh demineralized inertinite	G
1367	- 200 mesh demineralized inertinite	H
1310	- 200 mesh demineralized liptinite	I
1332	- 200 mesh demineralized liptinite	J
1310	- 200 mesh raw liptinite	K

TABLE C1 (contd.)

FILE CODES FOR ACTIVATION ENERGY DETERMINATION AND PREDICTIVE MODEL DETERMINATION

SIU No.	Coal Description	File Code
1310	- 200 mesh raw inertinite	L
1311	- 200 mesh raw inertinite	M
1366	- 200 mesh raw inertinite	N
1310	- 200 mesh raw vitrinite	O
1311	- 200 mesh raw vitrinite	P
1312	- 200 mesh raw vitrinite	Q
1332	- 200 mesh raw vitrinite	R
1356	- 200 mesh raw vitrinite	S
1365a[b]	- 200 mesh raw vitrinite	T
1365b[b]	- 200 mesh raw vitrinite	U
1366a[c]	- 200 mesh raw vitrinite	V
1366b[c]	- 200 mesh raw vitrinite	W
1367	- 200 mesh raw vitrinite	X
1310	- 200 mesh demineralized whole coal	Y
1311	- 200 mesh demineralized whole coal	Z
1312	- 200 mesh demineralized whole coal	a
1332	- 200 mesh demineralized whole coal	b
1356	- 200 mesh demineralized whole coal	c
1365	- 200 mesh demineralized whole coal	d
1366	- 200 mesh demineralized whole coal	e
1367	- 200 mesh demineralized whole coal	f
1310	- 200 mesh raw whole coal	g
1311	- 200 mesh raw whole coal	h

TABLE C1 (contd.)

FILE CODES FOR ACTIVATION ENERGY DETERMINATION

AND PREDICTIVE MODEL DETERMINATION

SIU No.	Coal Description	File Code
1312	- 200 mesh raw whole coal	i
1332	- 200 mesh raw whole coal	j
1356	- 200 mesh raw whole coal	k
1365	- 200 mesh raw whole coal	l
1366	- 200 mesh raw whole coal	m
1367	- 200 mesh raw whole coal	n
1310	Micronized raw whole coal	o
1311	Micronized raw whole coal	p
1312	Micronized raw whole coal	q

[a] Coal 1365 (demineralized) had 2 vitrinite peaks. 1365a refers to the 1.270 density fraction. 1365b refers to 1.292 density fraction.

[b] Coal 1365 (raw) had 2 vitrinite peaks. 1365a refers to density fraction 13. 1365b refers to density fraction 16.

[c] Coal 1366 (raw) had 2 vitrinite peaks. 1366a refers to density fraction 11. 1366b refers to density fraction 16.

TABLE C2

ARRHENIUS COORDINATE DETERMINATION VALUES FOR DEMINERALIZED VITRINITE # 1356

Temperature T (^{o}C)	dW (%)	-dW/dt (%/min)	1/T * 1000 ($^{o}K^{-1}$)	k (sec^{-1})	log k	Temperature T (^{o}K)
400	100.40	.319	1.4858	.0031	-2.4996	673
425	98.74	1.199	1.4326	.0121	-1.9101	698
450	96.08	1.719	1.3831	.0178	-1.7300	723
475	92.85	2.079	1.3368	.0223	-1.6[illegible]	748
500	88.47	2.899	1.2936	.0327	-1.4313	773
5.5	81.57	4.64	1.2531	.0568	-1.1565	798
550	69.98	8.64	1.2150	.1252	-0.7408	823
575	45.83	14.96	1.1792	.3264	-0.1473	848
600	21.75	13.41	1.1454	.6166	0.4530	873
625	7.14	7.79	1.1135	1.0070	1.1497	898

Note: For this sample, sample weight = 4.7123 mg, moisture content = .38 %, and ash content = .62 %.

TABLE C3

RESULTS OF ACTIVATION ENERGY DETERMINATION

File Code[a]	E1 (kJ/mole)	E2 (kJ/mole)	E3 (kJ/mole)
1	123.04	66.99	277.5
2	114.84	70.18	251.55
3	539.11	53.59	120.31
4	114.84	61.25	237.88
5	225.85	57.42	241.64
6	126.32	65.93	331.59
7	103.36	57.42	259.76
8	[illegible]	76.57	218.74
9		80.81	267.94
A	220.11	58.62	179.44
B	207.35	53.59	231.81
C	122.5	68.9	237.88
D	312.62	53.59	174.65
E	118.03	68.9	200.97
F	164.6	61.67	196.87
G	215.76	63.8	226.95
H	195.23	78.69	229.68
I	380.07	46.48	193.97
J	239.25	63.8	174.65
K	223.33	34.69	272.75
L	103.9	48.72	165.08

TABLE C3 (contd.)

RESULTS OF ACTIVATION ENERGY DETERMINATION

File Code	E1	E2	E3
M	236.06	56.05	196.87
N	218.2	47.85	186.62
O	139.42	59.33	181.83
P	149.29	57.42	284.37
Q	145.46	65.93	273.43
R		68.9	315.81
S	156.95	62.89	253.61
T	133.98	49.76	174.99
U	133.98	63.8	218.74
V	312.62	45.94	187.92
W	226.49	57.42	262.49
X	111.01	57.42	186.62
Y	90.23	57.42	229.68
Z	237.34	45.94	124.41
a	122.5	80.81	237.88
b	150.39	63.16	229.68
c	271.79	78.69	263.18
d	545.49	59.33	253.61
e	179.92	78.69	196.19
g	92.97	57.42	205.76
h		58.7	224.9
i	140.36	95.7	280.72
j		57.42	248.82
k	153.12	59.22	210.54

TABLE C3 (contd.)

RESULTS OF ACTIVATION ENERGY DETERMINATION

File Code	E1	E2	E3
l		68.5	204.16
m	229.68	63.8	217.72
n	199.06	81.35	240.62
o	82.03	57.42	114.84
p	143.55	45.94	191.41

[a] File codes are defined in Table C1

TABLE C4

CORRELATION COMPARISON BETWEEN 3 POTENTIAL POLYNOMIAL REGRESSION CURVE FITS

Polynomial Regression Form To Fit 15 Data Points:	Coefficient of Correlation: (%)
$Y=(1/(EXP(b(0)+B(1)*(\ln(X))+B(2)*(\ln(X))^2+\ldots+B(M)*(\ln(X))^M))-273.15$	99.870456
$\ln(Y)=B(0)+B(1)*(\ln(1/X))+B(2)*(\ln(1/X))^2+\ldots+B(M)*(\ln(1/X))^M$	97.670553
$Y=B(0)+B(1)*\ln(X)+B(2)*(\ln(X))^2+B(3)*(\ln(X))^3\ldots+B(M)*(\ln(X))^M$	99.995296

TABLE C5

COMPARISON OF CORRELATION COEFFICIENTS FOR DEMINERALIZED MACERALS AND WHOLE COAL

Coal or Maceral Group	Correlation Coefficient (%)
Whole Coal	99.917102
Liptinites	99.995296
Inertinites	99.993362
Liptinites	99.987053

TABLE C6

CONSTANTS DETERMINED FOR POLYNOMIAL REGRESSION CURVE FITTING EQUATIONS

Equation Constant	Whole Coal (Demineralized)	Vitrinite (Demineralized)	Inertinite (Demineralized)	Liptinite (Demineralized)
B(0)	4.930016D+01	4.874737D+01	4.697985D+01	4.738757D+01
B(1)	-8.512131D+02	-7.017580D+02	-5.913940D+02	-5.360744D+02
B(2)	-2.090233D+03	-1.200535D+03	-1.004479D+03	-1.425747D+03
B(3)	8.587516D+04	4.378001D+04	2.646763D+04	1.923243D+04
B(4)	4.502262D+05	9.199225D+05	1.072220D+05	1.291162D+05
B(5)	-5.433726D+06	-2.060490D+06	-7.425970D+05	-2.296974D+05
B(6)	-4.022674D+07	-2.234495D+06	-4.201723D+06	-3.526911D+06
B(7)	8.228230D+07	4.962183D+07	5.299078D+06	-7.336148D+06
B(8)	1.186063D+09	1.543070D+07	5.946831D+07	3.207404D+06
B(9)	2.3[illegible]p+09	-4[illegible]4796D+09	8.490726D+07	[illegible]11D+07

Note: 'D' in the numbers indicates the constants determined are double precision.

Table C7. Coefficients for Empirical Fit of Maceral Burnoff Curves.

Sample Coefficient	1310 Vit.	1311 Vit.	1312 Vit.	1332 Vit.	1356 Vit.	1365 Vit.A	1365 Vit.B	1366 Vit.	1367 Vit.	1332 Lip.
B(0)	4.68 E+01	4.77 E+01	4.94 E+01	4.29 E+01	4.72 E+01	4.86 E+01	4.85 E+01	4.83 E+01	4.77 E+01	4.28 E+01
B(1)	-7.08 E+02	-7.18 E+02	-7.10 E+02	-6.04 E+02	-8.59 E+02	-7.03 E+02	-7.93 E+02	-7.35 E+02	-8.28 E+02	-5.02 E+02
B(2)	-2.91 E+03	-1.59 E+03	-1.22 E+03	-5.71 E+03	-1.95 E+03	-1.19 E+03	-2.52 E+03	-2.81 E+02	-1.52 E+03	-6.36 E+01
B(3)	5.14 E+04	5.01 E+04	4.26 E+04	3.37 E+04	8.27 E+04	4.41 E+04	7.52 E+04	7.75 E+04	6.53 E+04	2.67 E+04
B(4)	4.43 E+05	2.72 E+05	1.50 E+05	1.25 E+05	4.18 E+05	9.24 E+04	5.60 E+05	5.59 E+04	3.27 E+05	6.11 E+04
B(5)	-2.51 E+06	-2.65 E+06	-1.81 E+06	-1.07 E+06	-5.64 E+06	-2.08 E+06	-5.23 E+06	-9.81 E+06	-2.72 E+06	-1.13 E+06
B(6)	-2.83 E+07	-2.12 E+07	-7.24 E+06	-6.00 E+06	-4.00 E+07	-2.29 E+06	-5.55 E+07	-4.33 E+07	-2.34 E+07	-4.59 E+06
B(7)	2.21 E+07	3.69 E+07	2.98 E+07	7.56 E+06	1.16 E+08	5.00 E+07	7.40 E+07	4.19 E+08	-4.30 E+07	1.66 E+07
B(8)	6.95 E+08	6.19 E+08	1.26 E+08	8.94 E+07	1.43 E+09	1.69 E+07	1.95 E+09	3.60 E+09		1.14 E+08
B(9)	1.49 E+09	1.30 E+09		1.32 E+08	2.86 E+09	-4.59 E+08	4.85 E+09	7.35 E+09		1.60 E+08

General Model Form: $Y=B(0)+B(1)*\ln(X)+B(2)*(\ln X)^2+B(3)*(\ln X)^3 \ldots\ldots +B(M)*(\ln X)^M$

Sample Coefficient	1310 Int.	1311 Int.	1332 Int.	1356 Int.	1365 Int.	1366 Int.	1367 Int.
B(0)	4.44 E+01	4.80 E+01	4.69 E+01	4.03 E+01	4.64 E+01	4.73 E+01	4.87 E+01
B(1)	-6.24 E+02	-5.93 E+02	-5.91 E+02	-8.29 E+02	-6.28 E+02	-6.76 E+02	-7.05 E+02
B(2)	-2.00 E+03	-7.35 E+02	-9.94 E+02	1.43 E+03	6.02 E+02	-1.07 E+02	-5.33 E+02
B(3)	2.84 E+04	2.57 E+04	2.65 E+04	8.84 E+04	3.99 E+04	4.55 E+04	4.64 E+04
B(4)	2.26 E+05	6.92 E+04	1.06 E+05	-3.85 E+04	-2.98 E+04	2.20 E+04	9.79 E+04
B(5)	-4.30 E+05	-8.05 E+05	-7.49 E+05	-6.58 E+06	-2.29 E+06	-2.72 E+06	-2.55 E+06
B(6)	-7.67 E+06	-2.67 E+06	-4.20 E+06	-1.65 E+07	-3.47 E+06	-6.82 E+06	-1.04 E+07
B(7)	-1.43 E+07	9.96 E+06	5.40 E+06	1.67 E+08	6.00 E+07	6.59 E+07	5.20 E+07
B(8)	3.20 E+07	4.24 E+07	5.98 E+07	9.17 E+08	2.74 E+08	3.52 E+08	3.82 E+08
B(9)	8.71 E+07	2.41 E+07	8.53 E+07	1.28 E+09	3.43 E+08	4.78 E+08	6.14 E+08

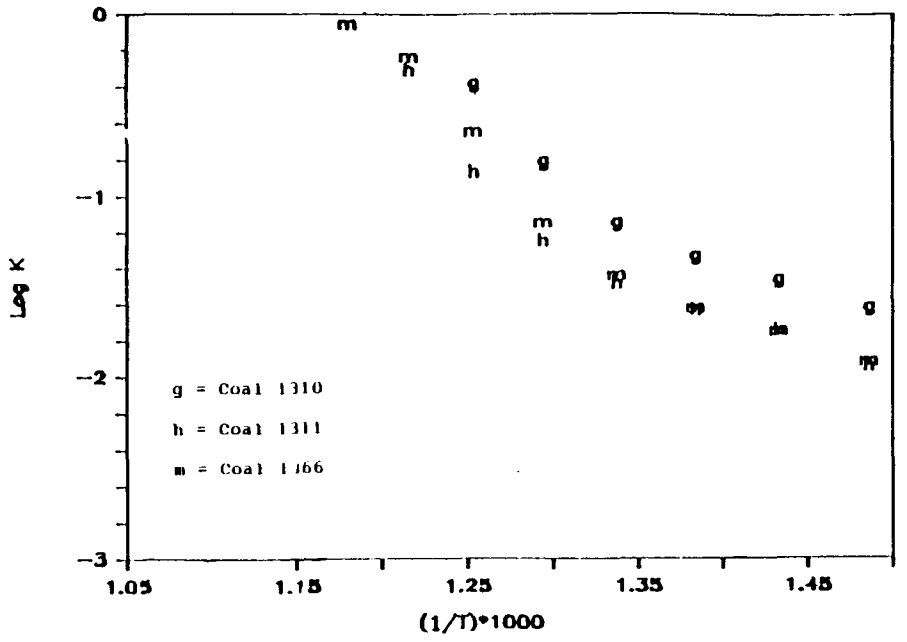

Figure C.1 Arrhenius Plot Used for Activation Energy Determination for Demineralized Vitrinite of Coal No. 1356.

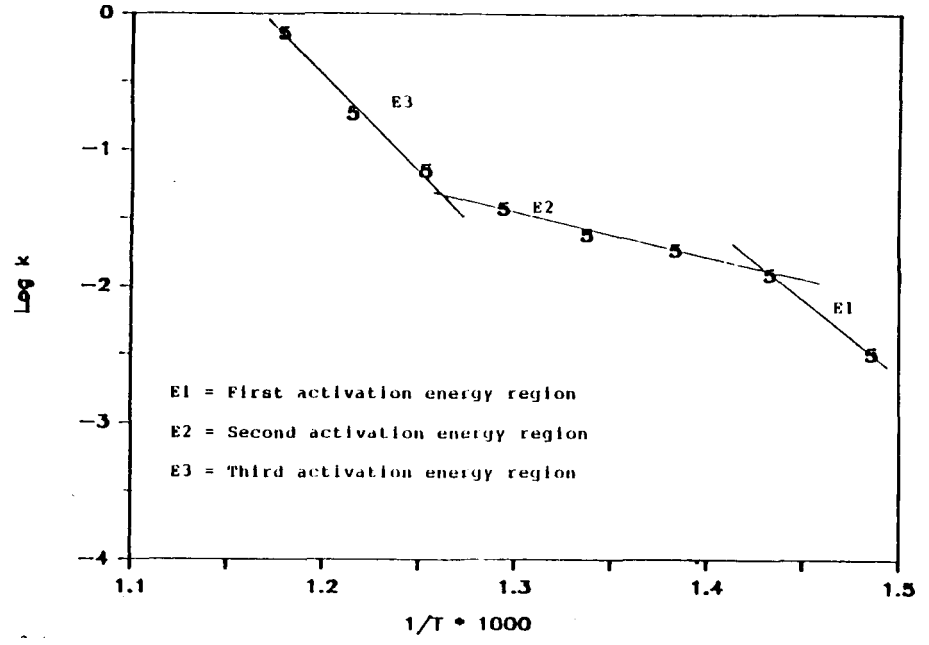

Figure C.2 Arrhenius Plot Comparison for 3 Raw Whole Coals, Illustrated by Coals 1310, 1311, and 1366.

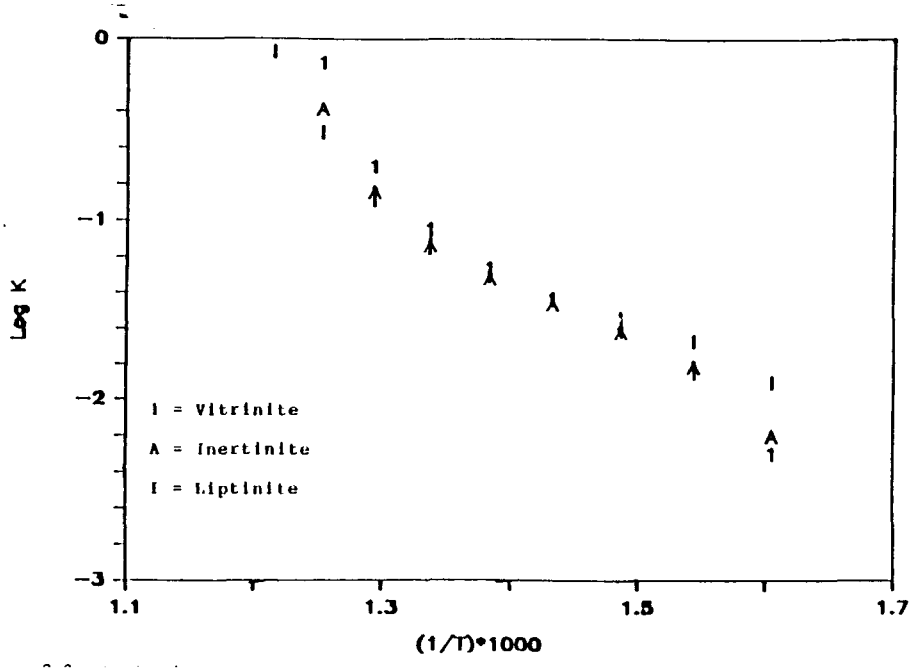

Figure C.3 Arrhenius Plot Comparison for the 3 Demineralized Maceral Groups for Coal No. 1310.

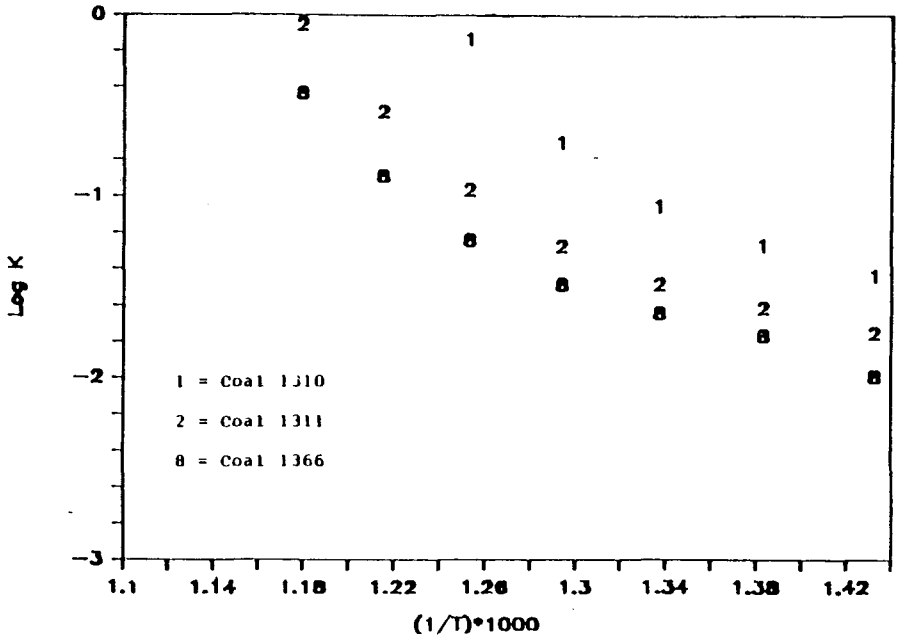

Figure C.4 Arrhenius Plot Comparison by Rank for Demineralized Vitrinites, Illustrated by Vitrinites from Coals 1310, 1311, and 1366.

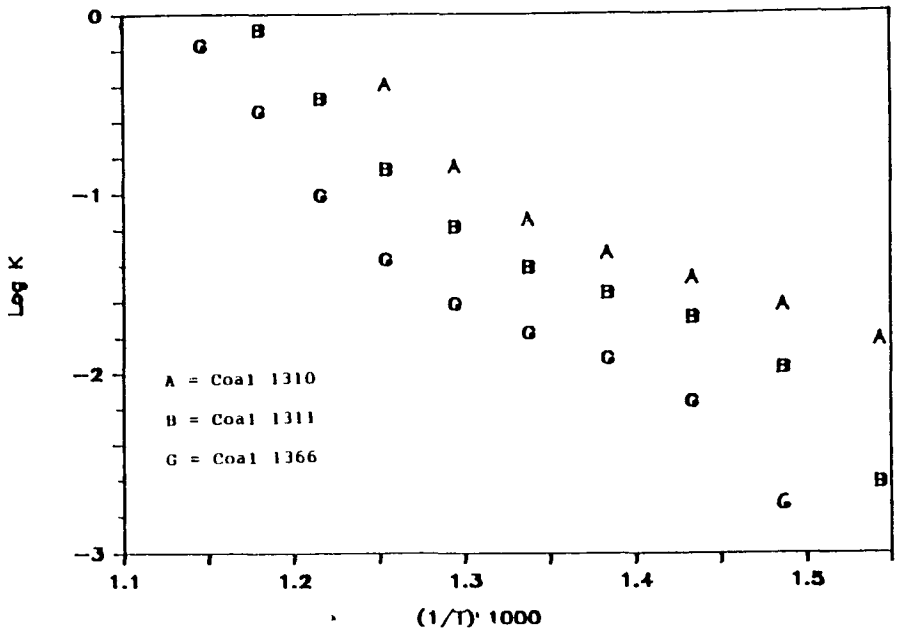

Figure C.5 Arrhenius Plot Comparison by Rank for Demineralized Inertinites, Illustrated by Inertinites from Coals 1310, 1311, and 1366.

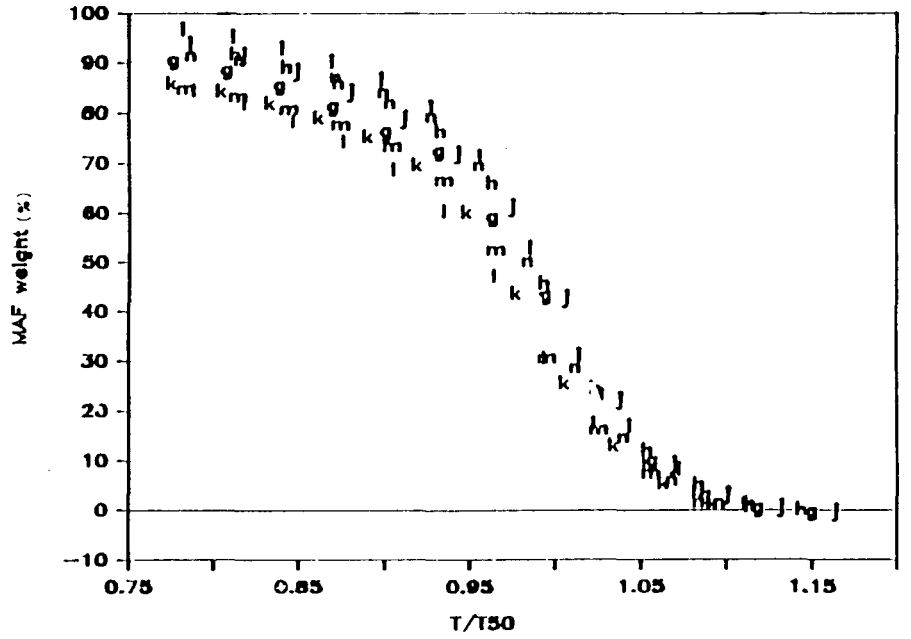

Figure C.6 Normalized Burnoff Curve Band for Raw Whole Coals.

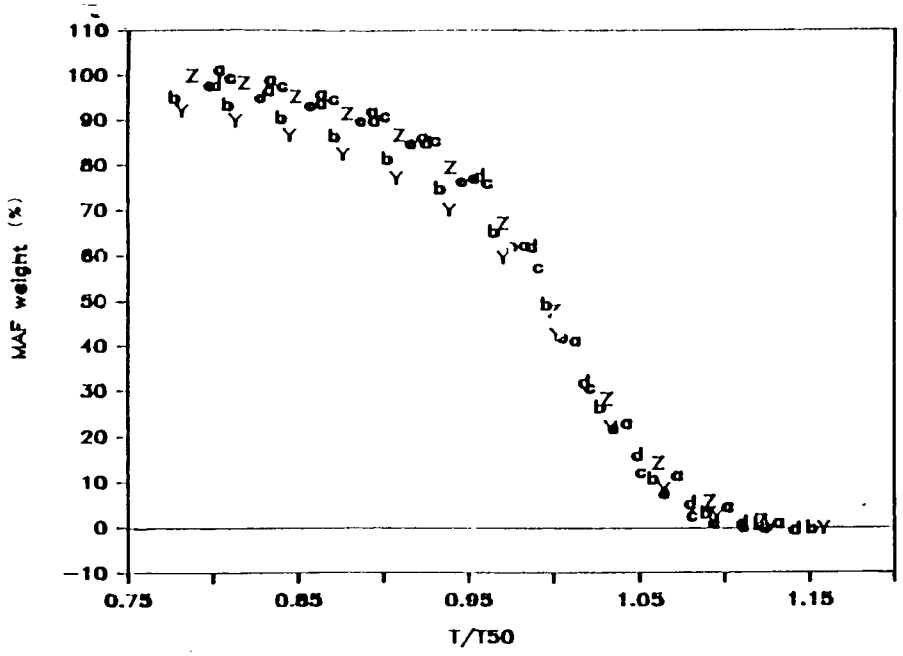

Figure C.7 Normalized Burnoff Curve Band for Demineralized Whole Coals.

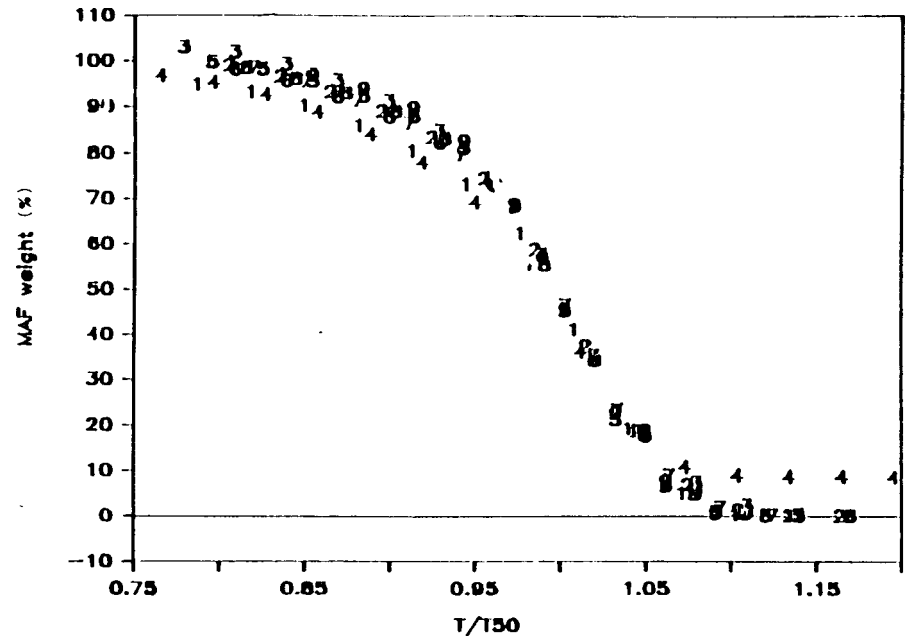

Figure C.8 Normalized Burnoff Curve Band for Demineralized Vitrinites.

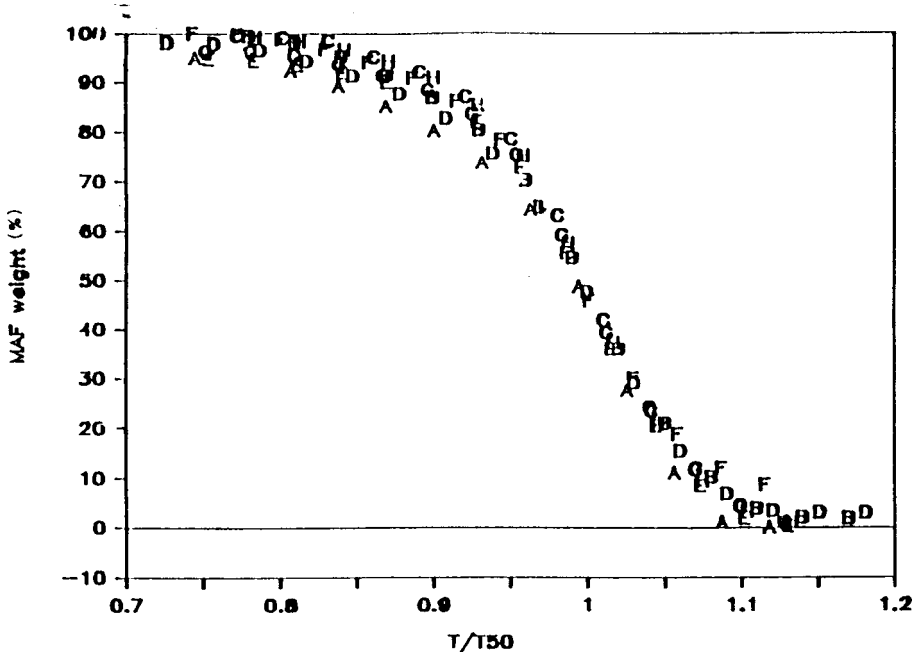

Figure C.9 Normalized Burnoff Curve Band for Demineralized Inertinites.

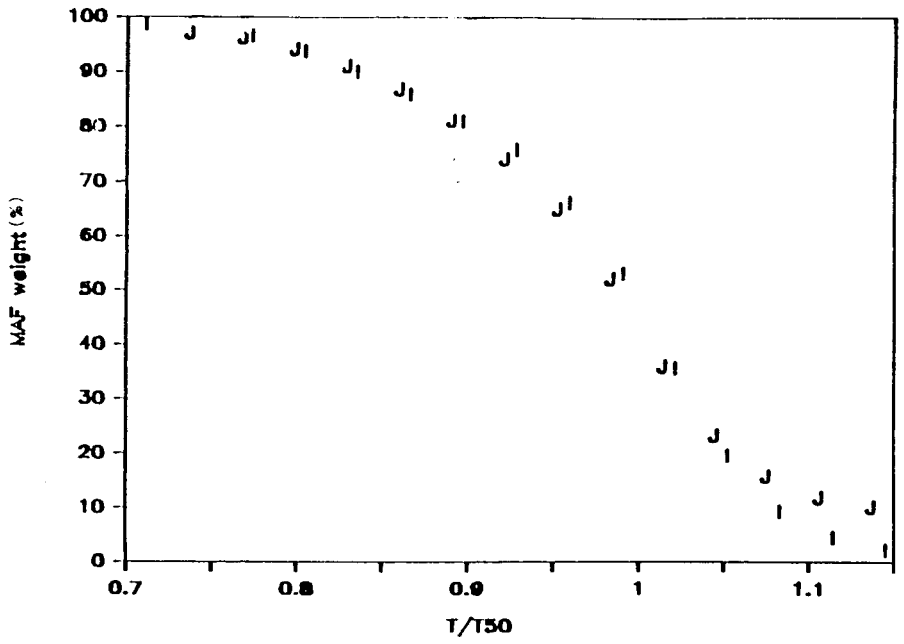

Figure C.10 Normalized Burnoff Curve Band for Demineralized Liptinites.

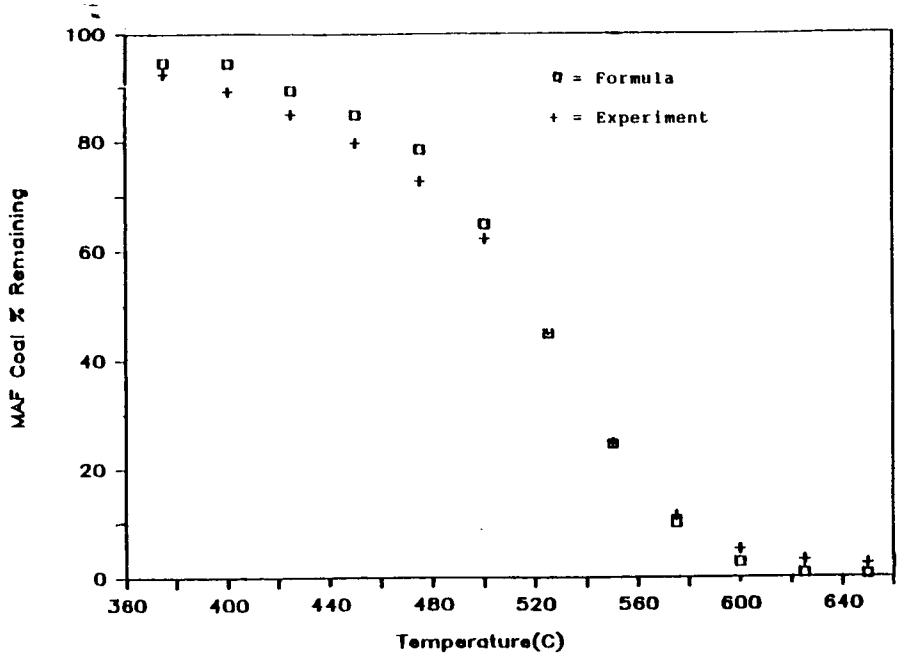

Figure C.11 Comparison of Burnoff Curves Predicted from Formula and Found by Experiment for Coal No. 1310.

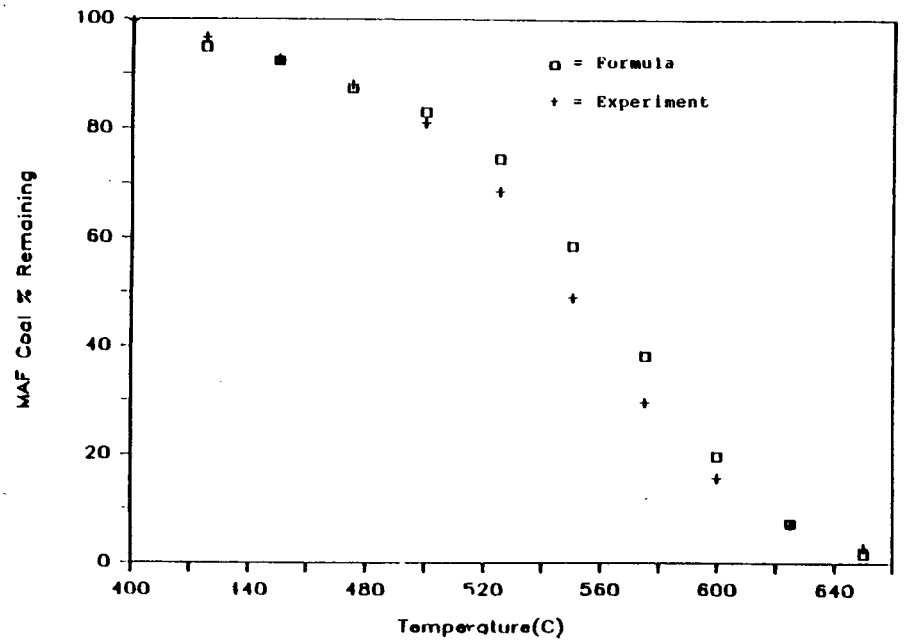

Figure C.12 Comparison of Burnoff Curves Predicted from Formula and Found by Experiment for Coal No. 1311.

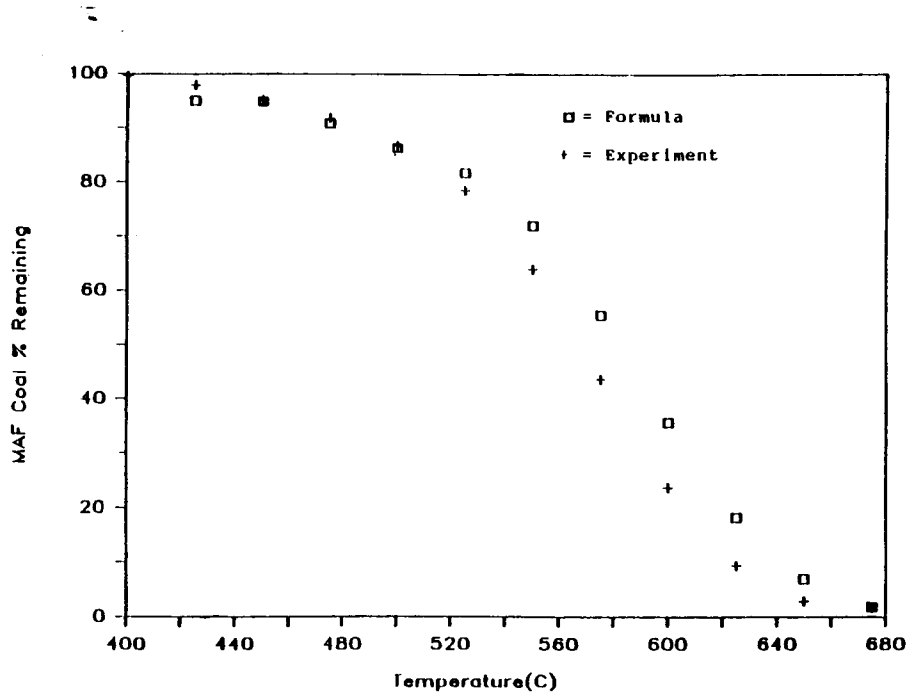

Figure C.13 Comparison of Burnoff Curves Predicted from Formula and Found by Experiment for Coal No. 1366.

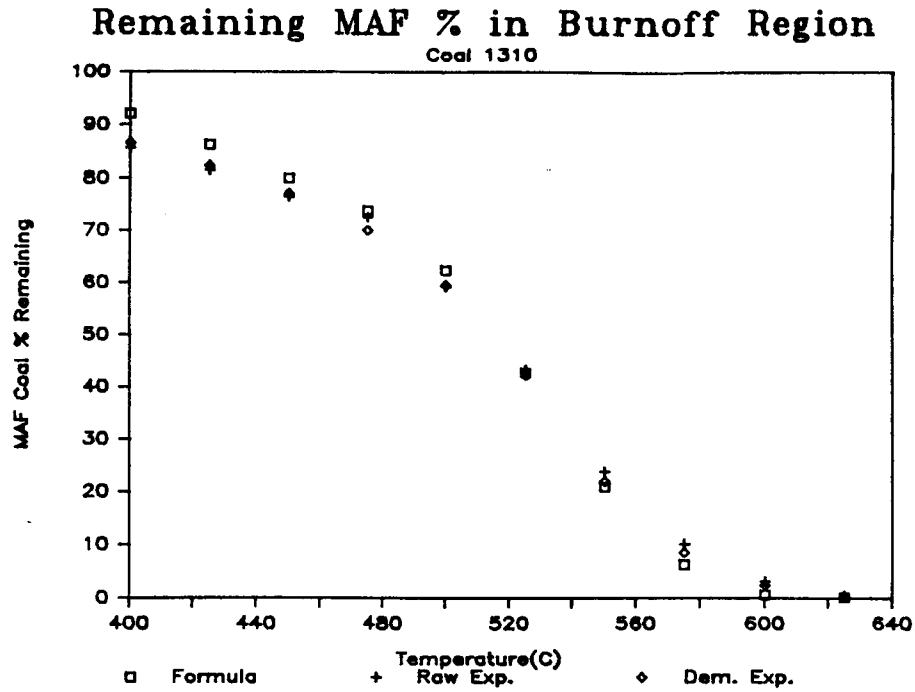

Figure C.14 Predicted and Experimental Burnoff Curves for SIU Coal 1310. Predicted Values Obtained from Model Fit of Normalized Burnoff Curve for Macerals Obtained from SIU 1310.

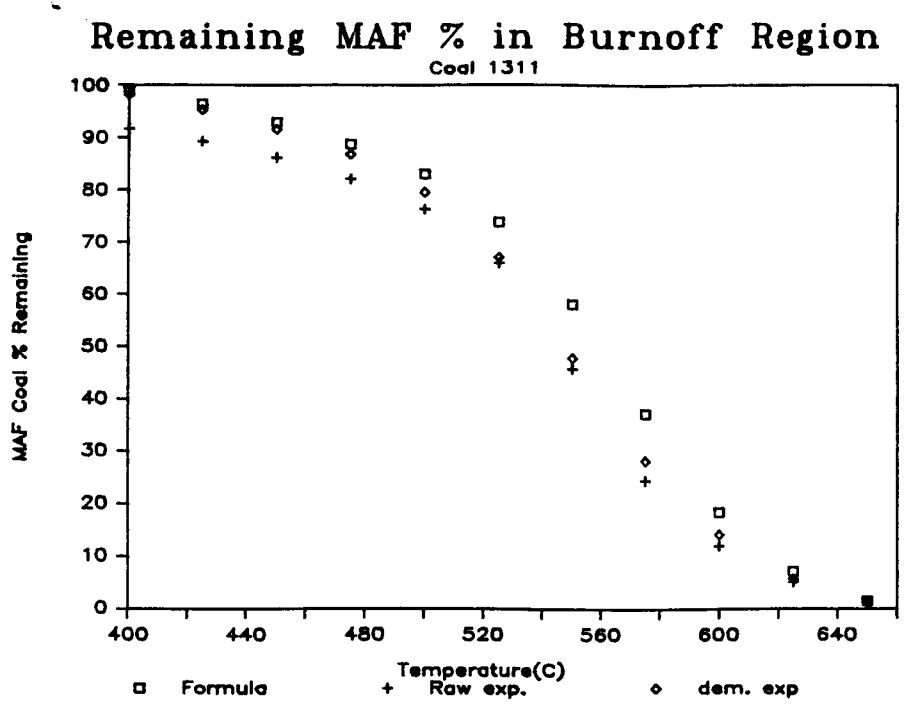

Figure C.15 Predicted and Experimental Burnoff Curves for SIU Coal 1311. Predicted Values Obtained from Model Fit of Normalized Burnoff Curve for Macerals Obtained from SIU 1311.

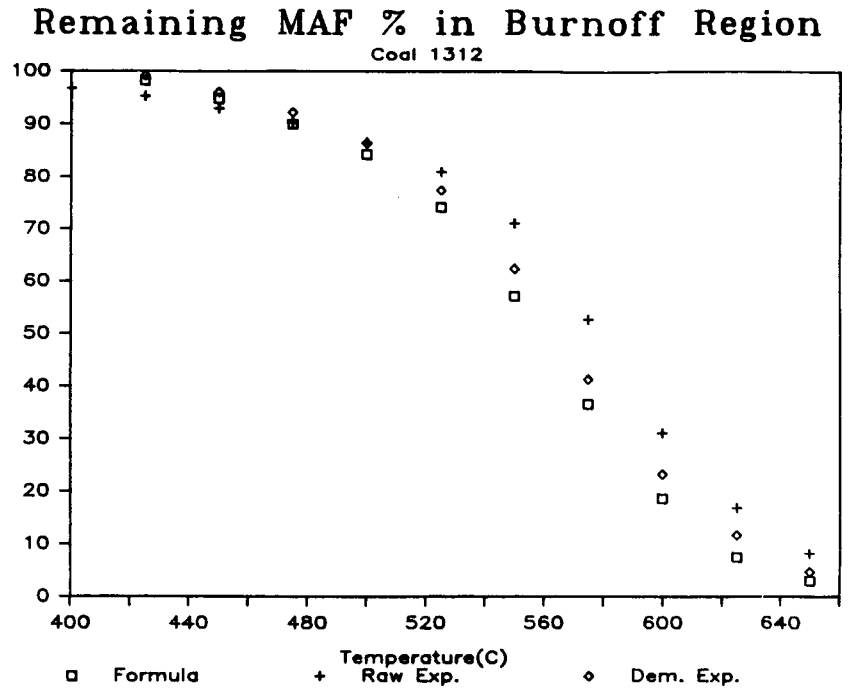

Figure C.16 Predicted and Experimental Burnoff Curves for SIU Coal 1312. Predicted Values Obtained from Model Fit of Normalized Burnoff Curve for Macerals Obtained from SIU 1312.

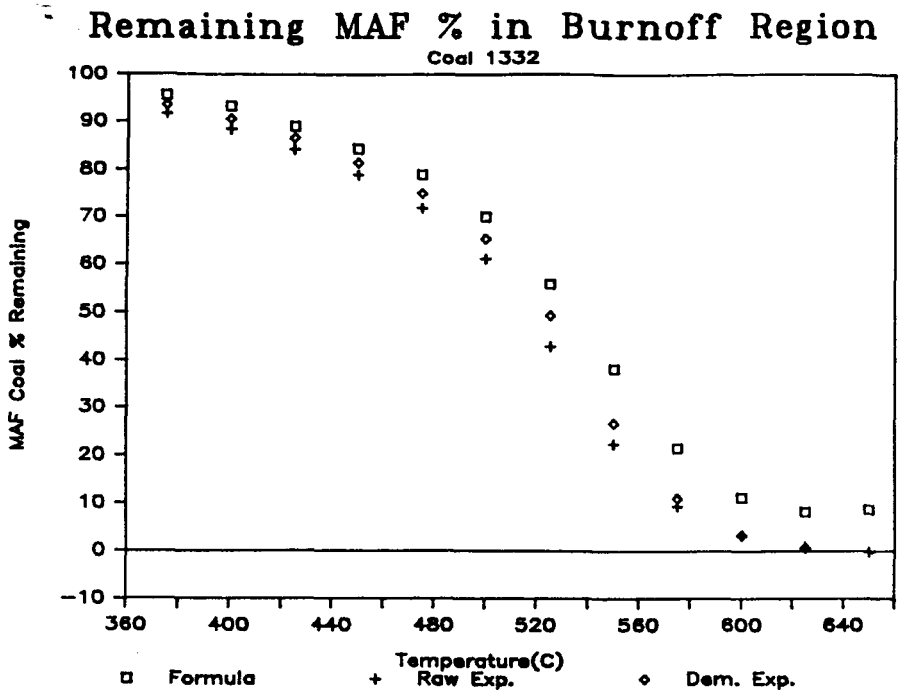

Figure C.17 Predicted and Experimental Burnoff Curves for SIU Coal 1332. Predicted Values Obtained from Model Fit of Normalized Burnoff Curve for Macerals Obtained from SIU 1332.

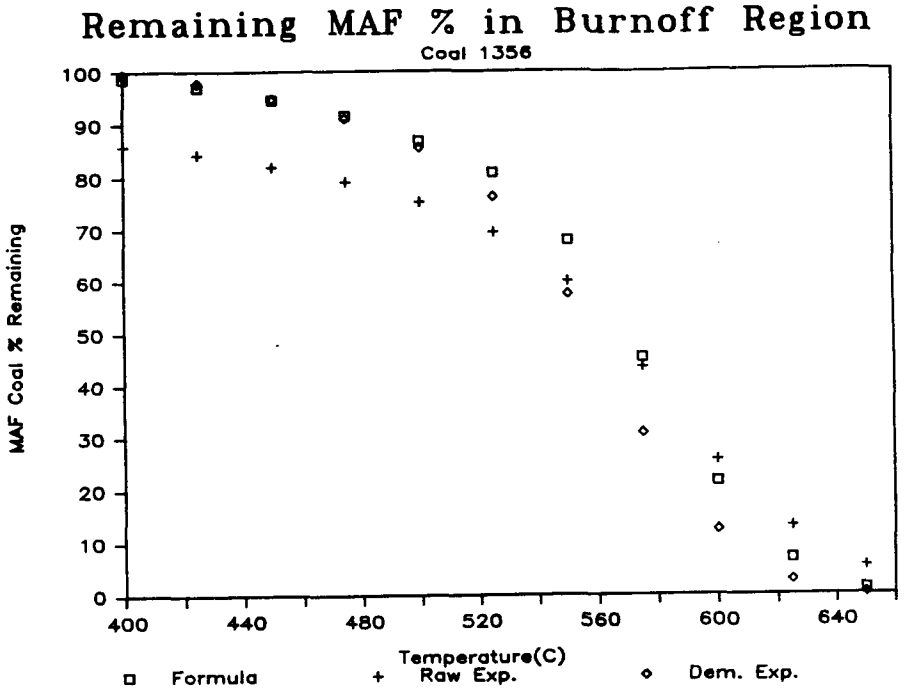

Figure C.18 Predicted and Experimental Burnoff Curves for SIU Coal 1356. Predicted Values Obtained from Model Fit of Normalized Burnoff Curve for Macerals Obtained from SIU 1356.

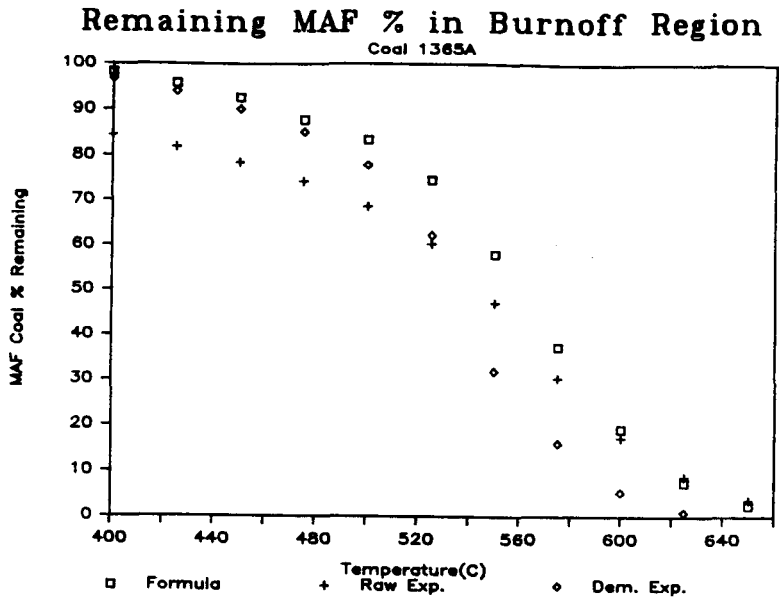

Figure C.19 Predicted and Experimental Burnoff Curves for SIU Coal 1365. Predicted Values Obtained from Model Fit of Normalized Burnoff Curve for Macerals Obtained from SIU 1365. The Data for the "A" Vitrinite Was Employed for the Model Values in this Figure.

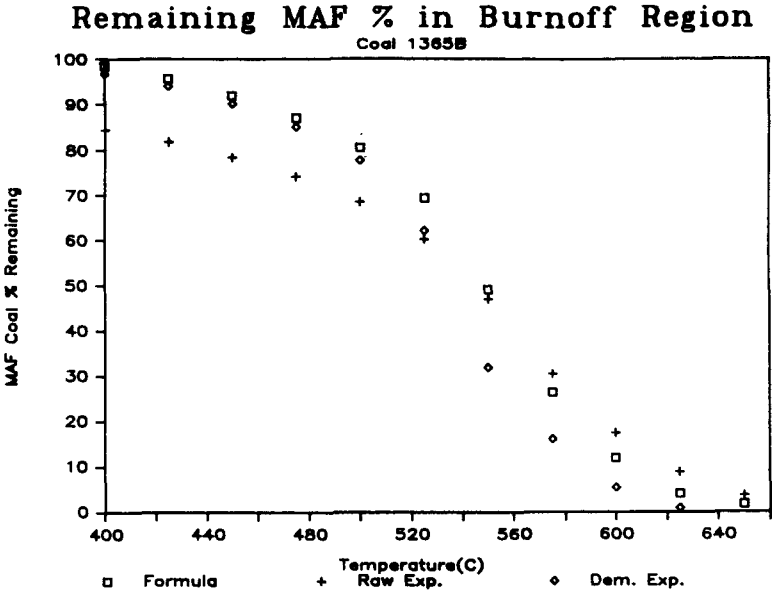

Figure C.20 Predicted and Experimental Burnoff Curves for SIU Coal 1365. Predicted Values Obtained from Model Fit of Normalized Burnoff Curve for Macerals Obtained from SIU 1365. The Data for the "B" Vitrinite Was Employed for the Model Values in the Figure.

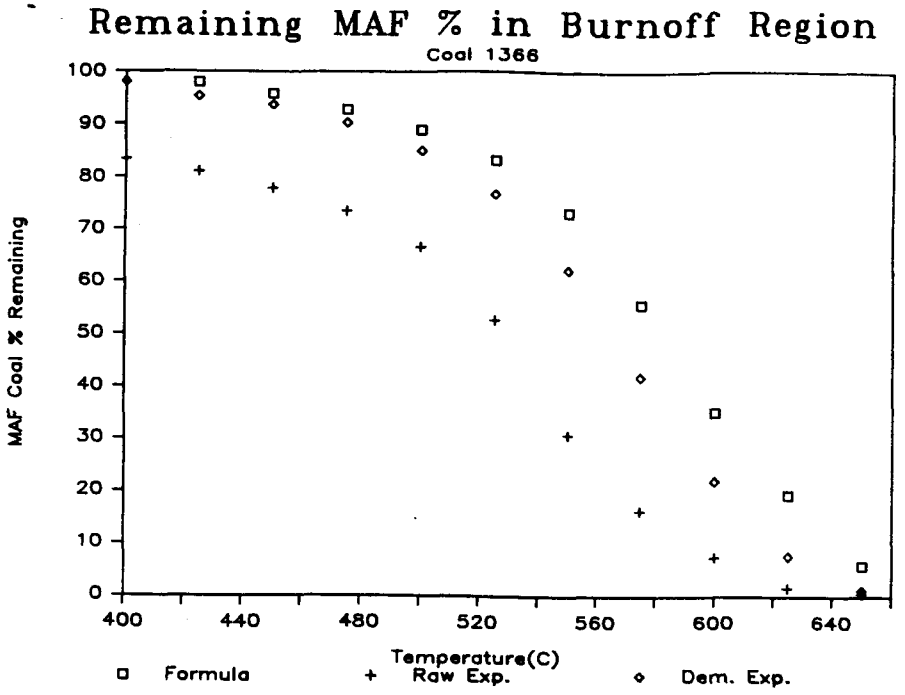

Figure C.21 Predicted and Experimental Burnoff Curves for SIU Coal 1366. Predicted Values Obtained from Model Fit of Normalized Burnoff Curve for Macerals Obtained from SIU 1366.

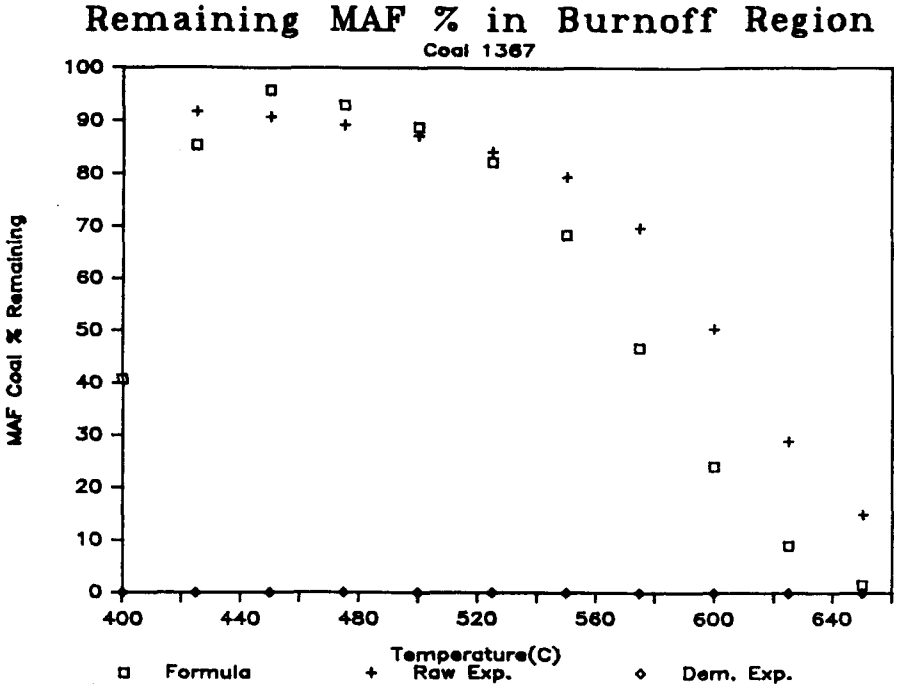

Figure C.22 Predicted and Experimental Burnoff Curves for SIU Coal 1367. Predicted Values Obtained from Model Fit of Normalized Burnoff Curve for Macerals Obtained from SIU 1367.